XN-NF-80-19(NP)(A)
VOLUME 1
SUPPLEMENT 3

XN-NF-80-19(NP)(A)
VOLUME 1
SUPPLEMENT 3
APPENDIX F

XN-NF-80-19(NP)(A)
SUPPLEMENT 4

ADVANCED NUCLEAR FUELS CORPORATION

ADVANCED NUCLEAR FUELS METHODOLOGY FOR BOILING WATER REACTORS

NOVEMBER 1990

A Siemens Company

ADVANCED NUCLEAR FUELS CORPORATION

XN-NF-80-19(NP)(A)
Volume 1
Supplement 3

XN-NF-80-19(NP)(A)
Volume 1
Supplement 3
Appendix F

XN-NF-80-19(NP)(A)
Supplement 4

Issue Date: 11/30/90

XN-NF-80-19(NP)(A) Volume 1 Supplement 3	ADVANCED NUCLEAR FUELS METHODOLOGY FOR BOILING WATER REACTORS: BENCHMARK RESULTS FOR THE CASMO-3G/MICROBURN-B CALCULATION METHODOLOGY
XN-NF-80-19(NP)(A) Volume 1 Supplement 3 Appendix F	ADVANCED NUCLEAR FUELS METHODOLOGY FOR BOILING WATER REACTORS: BENCHMARKING FOR THE CASMO-3G/MICROBURN-B CALCULATION METHODOLOGY
XN-NF-80-19(NP)(A) Supplement 4	NRC CORRESPONDENCE

UNITED STATES
NUCLEAR REGULATORY COMMISSION
WASHINGTON, D. C. 20555

Received
8/20/90

August 13, 1990

Mr. R. A. Copeland, Manager
Reload Licensing
Advanced Nuclear Fuels Corporation
P. O. Box 130
Richland, Washington 99352-0130

Dear Mr. Copeland:

SUBJECT: ACCEPTANCE FOR REFERENCING OF TOPICAL REPORT XN-NF-80-19(P), VOLUME 1, SUPPLEMENT 3, "ADVANCED NUCLEAR FUELS METHODOLOGY FOR BOILING WATER REACTORS; BENCHMARK RESULTS FOR THE CASMO-3G/MICROBURN-B CALCULATION METHODOLOGY"

The staff of the U.S. Nuclear Regulatory Commission (NRC) completed its review of Topical Report XN-NF-80-19(P), Volume 1, Supplement 3, "Advanced Nuclear Fuels Methodology for Boiling Water Reactors; Benchmark Results for the CASMO-3G/MICROBURN-B Calculation Methodology," submitted by Advanced Nuclear Fuels Corporation by letter dated March 8, 1989. It also reviewed the additional information submitted on December 22, 1989, and April 10, June 7, June 18, and July 20, 1990.

XN-NF-80-19(P), Volume 1, Supplement 3 presents the validation and verification of the CASMO-3G code for use as a physics core lattice analysis model. The code is to be used in the generation of reactor physics calculations required in the reload licensing analysis.

The topical report also provides the verification and benchmarking of the CASMO-3G/MICROBURN-B code, which is a multigroup transport theory calculation of the spatial flux and power distributions, cell multiplication, and isotopic depletion for two-dimensional BWR fuel assembly lattices. The topical report presents the results of the benchmarking of the ANF CASMO-3G/MICROBURN-B code system against measured operating data from six BWR plants: Chinshan Unit 1, Kuosheng Units 1 and 2, Quad Cities Unit 1, and Susquehanna Units 1 and 2. Calculation-to-measurement comparisons have been made for cold and hot eigenvalues and for traversing incore probe responses. ANF intends to use this code for reload design, steady-state licensing, and plant support applications. The new methodology introduces two improvements: (1) the number densities and burnup of key isotopes are evaluated on a nodal basis utilizing microscopic cross sections and (2) an improved coarse-mesh finite difference formulation is utilized in the solution of the full two-group diffusion theory representation.

We find the application of the CASMO-3G/MICROBURN-B code acceptable for use in reload analyses under the limitations delineated in the associated NRC technical evaluation. The evaluation defines the basis for acceptance of this topical report.

We do not intend to repeat our review of the matters found acceptable as described in XN-NF-80-19(P), Volume 1, Supplement 3, when the report appears as a reference in license applications, except to ensure that the material presented is applicable to the specific plant involved. Our acceptance applies only to the matters described in the application of XN-NF-80-19(P), Volume 1, Supplement 3.

In accordance with procedures established in NUREG-0390, we request that Advanced Nuclear Fuels Corporation publish accepted versions of this topical report, proprietary and non-proprietary, within three months of receipt of this letter. The accepted versions shall include an "A" (designating accepted) following the report identification symbol.

Should our criteria or regulations change so that our conclusions as to the acceptability of the report are invalidated, Advanced Nuclear Fuels Corporation and/or the applicants referencing the topical report will be expected to revise and resubmit their respective documentation, or submit justification for the continued effective applicability of the topical report without revision of their respective documentation.

Sincerely,

ACThadani

Ashok C. Thadani, Director
Division of Systems Technology
Office of Nuclear Reactor Regulation

Enclosure:
XN-NF-80-19(P), Volume 1,
Supplement 3, Evaluation

ENCLOSURE

SAFETY EVALUATION OF TOPICAL REPORT
XN-NF-80-19(P), VOLUME 1, SUPPLEMENT 3 (INCLUDING APPENDIX F)

1.0 INTRODUCTION

By letter dated March 8, 1989, Advanced Nuclear Fuels Corporation (ANF) submitted Topical Report XN-NF-80-19(P), Volume 1, Supplement 3, for NRC staff review. The report is the MICBURN-3/CASMO-3G/MICROBURN-B code package for steady-state analyses of boiling water reactor (BWR) cores (Refs. 1-4). This report presents the results of the benchmarking of this code system against measured data from six BWR plants: Chinshan Unit 1, Kuosheng Units 1 and 2, Quad Cities Unit 1, and Susquehanna Units 1 and 2. Additional information from Dresden Unit 2 was also included in Appendix F of Supplement 3.

The new code package is an extension of the currently approved code system which consists of the XFYRE bundle depletion code and the three-dimensional simulator code XTGBWR (Ref. 5). The new codes are intended for use as alternative fuel assembly depletion and simulator codes. All other ANF methods and procedures discussed in Reference 5 remain the same.

overview of the topical report is given in the next section. The technical evaluation is presented in Section 3, and the limitations are given in Section 4. Brookhaven National Laboratory was the staff contractor for this review. (Contract Number FIN No. A-3868).

2.0 SUMMARY OF TOPICAL REPORT

CASMO-3G and MICROBURN-B are the principal components of the ANF steady-state physics code package for use in the reload licensing analysis of BWRs operating with ANF fuel. ANF also intends to use the CASMO-3G/MICROBURN-B code system to model and analyze new fuel designs. CASMO-3G (Ref. 3) is a multigroup, two-dimensional transport theory code for fuel assembly burnup calculations. Cylindrical fuel rods, including fuel rods loaded with burnable absorbers, in a square pitch array with water gaps and cruciform control rods in the regions separating fuel assemblies can be calculated with CASMO-3G. CASMO-3G also provides macroscopic cross sections for the baffle/reflector region. Both a 70-group and a 40-group cross-section library are available. ANF uses the 40-group library for production calculations. Gamma detector responses are calculated using the gamma transport module of CASMO-3G.

MICROBURN-B is a three-dimensional, two-group, coarse-mesh diffusion theory, coupled neutronics/thermal-hydraulics BWR simulator code. The two principal areas of improvement over the earlier methodology (Ref. 2) are (1) the evaluation of the number densities of key isotopes on a nodal basis using microscopic cross sections and (2) the formulation of the coarse-mesh finite difference solution of the two-group diffusion equations. The code calculates a wide range of reactor parameters, including nodal powers, void and exposure distributions, core reactivity, core flow, in-core fission or gamma detector responses, and thermal limits. MICROBURN-B also calculates time-dependent and equilibrium xenon and samarium.

The neutronics verification of the MICBURN-3/CASMO-3G/MICROBURN-B code system was performed by comparing calculations with measured data from Chinshan Unit 1, Kuosheng Units 1 and 2, Quad Cities Unit 1, and Susquehanna Units 1 and 2. The measured operating data used in the validation were obtained throughout the cycle and consisted of hot eigenvalues and traversing incore probe (TIP) responses. In addition, cold eigenvalues were calculated at state points for which cold critical tests had been performed.

Fuel rod gamma scan measurements obtained from Quad Cities Unit 1 at the end of cycles 2, 3, and 4 (Refs. 5-7) were used in the validation of MICBURN-3/CASMO-3G. Calculated fuel rod powers were compared to the measured lanthanum -140 activity. The average relative standard deviation for all comparisons with the gamma scan measurements is 2.74 percent.

3.0 SUMMARY OF TECHNICAL EVALUATION

The evaluation of Supplement 3 to XN-NF-80-19(P) is based on (1) the MICBURN-3/CASMO-3G/MICROBURN-B calculations of the benchmark power distribution measurement data base, (2) the performance of both hot and cold models compared with measured data, and (3) the evaluation of the ANF responses to the questions raised in the course of the review (Refs. 9 and 10). The major issues raised during this review are summarized in the following sections.

3.1 Gamma TIP Detector Response Calculation

The TIP detector-to-power factors are calculated using CASMO-3G. The detector response is calculated as a function of the energy-dependent gamma flux, the detector sensitivity, and the fuel assembly power. In CASMO-3G, the detector sensitivity function is represented by a 10-group energy deposition cross section for iron. MICROBURN-B determines the gamma TIP response by averaging responses of the four adjacent assemblies. This method of calculating gamma TIP responses has been benchmarked against both Monte Carlo calculations and measured data in the Hatch plant (Refs. 4, 10 and 13). On the basis of the results of these benchmarks as well as the benchmarks presented in the topical report, the staff concludes that the uncertainty associated with the interpretation of the gamma detector response is comparable to, or less than, the uncertainty associated with the fission TIP detectors and the method of calculating gamma TIP responses is acceptable.

3.2 Radial and Axial Reflector Treatment

In the CASMO-3G/MICROBURN-B methodology, the leakage from the core is determined by the outer boundary conditions. MICROBURN-B calculates the leakage separately for each boundary node. A two-group, one-dimensional representation is used at the fuel-reflector node interface where node average fluxes and currents are evaluated. Two-group cross sections representing reflector regions in the top, bottom, and side reflector nodes are generated using the reflector calculation option of CASMO-3G.

The macroscopic cross sections for the reflector region have been found to be insensitive to fuel design, exposure, and void in the adjacent fuel region. Therefore, ANF uses a generic set of hot operating two-group reflector cross sections for the top, bottom, and side reflector nodes for all reactors. A different set of cold two-group reflector cross sections is used for cold critical calculations. The comparisons of the ANF calculated and measured power distributions include the modeling uncertainty resulting from the reflector treatment. Since this uncertainty has been incorporated in the MICROBURN-B uncertainty analysis, the staff concludes that the ANF method for modeling radial and axial reflectors is acceptable for application to reactors that contain fuel types similar to those used in the benchmarking.

3.3 Discontinuity Factors

Radial discontinuity factors, defined as the ratio of the assembly surface flux to the volume average flux, are generated by CASMO-3G and used in the three-dimensional calculation. When the reflector calculation is performed, flux discontinuity factors are calculated for each quadrant of the bundle and for the baffle/reflector regions. In the ANF CASMO-3G/MICROBURN-B methodology, the discontinuity factors for the fuel region are calculated for each lattice type as a function of voids and exposure and are input to MICROBURN-B. Because of axial enrichment variations (axial blankets), axially distributed gadolinia, and partially inserted control rods, a special treatment of axial internodal leakage has been included in MICROBURN-B. The methodology is based on an analytical two-group diffusion theory solution over an axial portion of the fuel assembly that includes three successive axial nodes. Two-group average fluxes, surface fluxes, and surface currents for the middle node of the three-node segment are calculated, and the values are used to determine axial discontinuity factors for the top and bottom surfaces of the node.

The use of discontinuity factors in the ANF methodology has been successfully validated by comparing power distribution calculations with measured data. The ANF implementation of the discontinuity factors is consistent with industry practice. The introduction of the discontinuity factors has contributed to the reduction of the overall nodal power uncertainty to about 3.6

percent. The use of discontinuity factors is therefore acceptable for application to fuel types similar to those included in the benchmarking.

3.4 Fundamental Mode Calculations

The infinite lattice results obtained from the transport calculation in CASMO-3G are adjusted using a fundamental mode buckling to account for the effects of nodal leakage. In CASMO-3G the correction can be made by applying diffusion theory or the B_1 approximation. In the diffusion theory method, CASMO-3G performs either (1) a normal eigenvalue (k_∞) calculation with zero buckling B^2, (2) a k_{eff} calculation with a user input value for B^2, or (3) a (k_{eff} = 1) buckling search. In the latter case, B^2 is equal to the material buckling.

Use of the B_1 approximation results in values of the diffusion coefficient that differ significantly from those derived from diffusion theory, and leads to power distributions that do not agree with the measured data. Since the application of the B_1 approximation results in an underprediction of the fast diffusion coefficient (in some cases by as much as about 7 percent), the staff concludes that the diffusion approximation is the recommended method for adjusting CASMO-3G transport calculations to include the effects of leakage.

3.5 TIP Sy etry Uncertainty

On the basis of the data presented in Supplement 3 of the topical report, the TIP uncertainty for the Chinshan Unit, Kuosheng Units 1 and 2, and Susquehanna Units 1 and 2 is determined to be a factor of about 2.5 times less than the uncertainty for Dresden Units 2 and 3 and Quad Cities Units 1 and 2 provided in Supplements 1 and 2. In response 27 (Ref. 10), ANF suggested two possible explanations for the observed improvement in the TIP symmetry in the new plants: (1) elimination of the channel bowing that was present in the D-lattice Dresden and Quad Cities plants and that resulted from a fast neutron fluence gradient between the wide and narrow water gaps and a heat treatment that resulted in a larger dimensional change with irradiation and (2) improved design of the TIP/LPRM system in the newer plants that reduced the geometrical variation in the neighborhood of the TIP detector. ANF also noted that in some Dresden and Quad Cities cycles, channel boxes were reused for a second lifetime; this reuse would further increase the bowing and TIP uncertainty. Although some or all of these effects may contribute to the observed asymmetries in the older plants, the extent to which these individual effects have been eliminated from specific C-lattice plants has not been determined quantitatively. Therefore, the reduced uncertainties observed in the Kuosheng, Chinshan, and Susquehanna plants may not be applied with confidence to other U.S. plants.

ANF has indicated in Reference 4 that the TIP asymmetry uncertainty value of 6.0 percent which was used in the currently approved XTGBWR (Ref. 5) methodology, will be used in determining the radial bundle power uncertainty for MICROBURN-B. With this change, we therefore find this method acceptable.

4.0 SUMMARY OF TECHNICAL POSITION AND LIMITATIONS

The NRC staff has reviewed in detail ANF Topical Report XN-NF-80-19(P), Volume 1, Supplement 3, and the benchmarking of the CASMO-3G/MICROBURN-B code system against operating data from Chinshan Unit 1, Kuosheng Units 1 and 2, Quad Cities Unit 1, and Susquehanna Units 1 and 2. This review included material provided in Supplement 3 as well as supporting information supplied in References 4, 10 and 13. Based of this review, the staff concludes that the ANF methodology is acceptable for performing reload analyses for BWR cores, subject to the following limitations:

(1) The currently approved TIP asymmetry uncertainty value of 6.0 percent should be used in determining the radial bundle power uncertainty (Section 3.5).

(2) The application of CASMO-3G/MICROBURN-B to fuel designs that differ significantly from those included in the Supplement 3 data base should be supported by additional code validation to ensure that the methodology and uncertainties are applicable (Sections 3.2 and 3.3).

5.0 REFERENCES

1. R. A. Copeland, ANF, letter to NRC, "Submittal of MICROBURN-B," March 8, 1989.

2. Advanced Nuclear Fuels Corporation, "MICROBURN-B: A Two-Group, Three-Dimensional BWR Nodal Simulator Code," ANF-88-101(P), Richland, Washington, dated July 1988.

3. Studsvik Energiteknik AB, "CASMO-3: A Fuel Assembly Burnup Program (Methodology)," Studsvik/NFA-86/8, Nykoping, Sweden, November 1986.

4. Letter from R. A. Copeland, ANF, to L. Lois, NRC, "TIP Asymmetry Uncertainty," July 20, 1990.

5. Exxon Nuclear Company, "Exxon Nuclear Methodology for Boiling Water Reactors Neutronic Methods for Design Analysis," XN-NF-80-19(P)(A), Volume 1, Supplements 1 and 2, Richland, Washington, March 1983.

6. Electric Power Research Institute, "Gamma Scan Measurements at the Quad Cities Nuclear Station Unit 1 Following Cycle 2," EPRI-NP-21114, Palo Alto, California, dated July 1976.

7. M. B. Cutrone and G. F. Valby, "Gamma Scan Measurements at Quad Cities Nuclear Power Station Unit 1 Following Cycle 2," EPRI NP-214, Electric Power Research Institute, July 1976.

8. D. W. Merth, and B. A. Zolotar, "Gamma Scan Measurements of Quad Cities Nuclear Power Station Unit 1 Following Cycle 3," EPRI NP-512, Electric Power Research Institute, July 1977.

9. R. C. Jones, NRC, letter to R. A. Copeland, ANF, "Request for Additional Information Regarding the Topical Report XN-NF-80-19(P), Vol. 1, Sup. 3," February 2, 1990.

10. R. A. Copeland, ANF, letter to R. C. Jones, NRC, "Responses to NRC Questions on CASMO-3G/MICROBURN-B," March 16, 1990; "D-Lattice CASMO-3G/MICROBURN-B Methods Verification" XN-NF-80-19(P), Supplement 3, Appendix F , April 9, 1990.

11. A. Ahlin et al., "Integral Transport Computation of In-Core Gamma Effects with CASMO/CPM," Transactions of the American Nuclear Society, 47, 434, 1984.

12. M. Edenius et al., "Benchmarking of the Gamma TIP Calculation in CASMO Against the Hatch BWR," Transactions American Nuclear Society, 49, 431 (1985).

13. R. A. Copeland, ANF, letter to L. Lois, NRC, "The Effect of Measured TIP Asymmetries on the Measured Assembly Power Uncertainty," June 29, 1990.

ADVANCED NUCLEAR FUELS CORPORATION

XN-NF-80-19(NP)(A)
Volume 1
Supplement 3
Issue Date: 2/1/89

ADVANCED NUCLEAR FUELS METHODOLOGY
FOR BOILING WATER REACTORS

BENCHMARK RESULTS FOR THE CASMO-3G/
MICROBURN-B CALCULATION METHODOLOGY

Prepared by:

31Jan89

O. C. Brown, Manager
BWR Neutronics
Neutronics & Fuel Management
Fuel Engineering & Technical Services

1/31/89

D. H. Timmons, Staff Engineer
Neutronics Development
Neutronics & Fuel Managemenet
Fuel Engineering & Technical Services

January 1989

ROCAEC REPORT DISCLAIMER

IMPORTANT NOTICE REGARDING CONTENTS AND USE OF THIS DOCUMENT

PLEASE READ CAREFULLY

This technical report was derived through research and development programs sponsored by Advanced Nuclear Fuels Corporation. It is bei[illegible]g submitted by Advanced Nuclear Fuels Corporation to the ROCAEC as p[illegible] of a technical contribution to facilitate safety analyses by lice[illegible] of the ROCAEC which utilize Advanced Nuclear Fuels Corr[illegible] fabricated reload fuel or other technical services provided by [illegible]ced Nuclear Fuels Corporation for light water power reactors and [illegible] true and correct to the best of Advanced Nuclear Fuels Cor[illegible]on's knowledge, information, and belief. The information containe[illegible] herein may be used by the ROCAEC in its review of this report, and under the terms of the respective agreements, by licensees or applicants before the ROCAEC which are customers of Advanced Nuclear Fuels Corporation in their demonstration of compliance with the ROCAEC's regulations.

Advanced Nuclear Fuels Corporation's warranties and representations concerning the subject matter of this document are those set forth in the agreement between Advanced Nuclear Fuels Corporation and the customer to which this document is issued. Accordingly, except as otherwise expressly provided in such agreement, neither Advanced Nuclear Fuels Corporation nor any person acting on its behalf:

A. Makes any warranty, or representation, express or implied, with respect to the accuracy, completeness, or usefulness of the information contained in this document, or that the use of any information, apparatus, method, or process disclosed in this document will not infringe privately owned rights, or

B. Assumes any liabilities with respect to the use of, or for damages resulting from the use of, any information, apparatus, method, or process disclosed in this document.

TABLE OF CONTENTS

TABLE OF CONTENTS (CONT.)

LIST OF TABLES

LIST OF TABLES (CONT.)

LIST OF FIGURES

LIST OF FIGURES (CONT.)

ADVANCED NUCLEAR FUELS METHODOLOGY FOR BOILING WATER REACTORS BENCHMARK RESULTS FOR THE CASMO-3G/ MICROBURN-B CALCULATION METHODOLOGY

1.0 INTRODUCTION

The use of XFYRE bundle depletion and XTGBWR reactor simulator codes in the neutronics methodology utilized by Advanced Nuclear Fuels Corporation (ANF) for boiling water reactors is documented in Reference 1. ANF plans to extend this methodology to include the use of an alternate fuel assembly depletion model, MICBURN-3/CASMO-3G and an alternate core simulator code, MICROBURN-B. All other methodology and procedures presented in Reference 1 remain unchanged. The new codes (MICBURN-3/CASMO-3G/MICROBURN-B) are described in detail in Reference 2 and are briefly summarized in Section 3.0.

Verification of the new code system consists of comparisons between calculated and measured fuel assembly and reactor parameters. Fuel rod gamma scan measurements of fuel from Quad Cities (large core BWR/3) Unit 1 Cycles 1 through 4 have been compared to MICBURN-3/CASMO-3G calculated fuel rod powers. These results are summarized in Section 4.1 The MICROBURN-B reactor core simulator code has been verified by comparing calculated versus measured reactor data. Quad Cities 1 end of Cycles 2 and 4 fuel assembly gamma scan measurements have been compared to MICROBURN-B calculated nodal powers. These results are summarized in Section 4.2.3. In addition, comparisons of measured and calculated traversing incore probe (TIP) data, as well as hot and cold critical eigenvalues, have been made for actual operating data for a small core BWR/4,5 (Chinshan), a large core BWR/6 (Kuosheng), and a large core BWR/4,5 (Susquehanna) reactor. Results for these reactors are summarized in Sections 4.2.1, 4.2.2, and 4.2.4, respectively.

A statistical evaluation has been performed to define the measured power distribution uncertainty associated with the new code system. This analysis is based on calculated results summarized in this report and is explained in detail in Section 5.0. The statistical evaluation methodology summarized in Section 5.0 is the same as the accepted statistical methodology defined in Reference 1. The measured power distribution uncertainties appropriate for the CASMO-3G/MICROBURN-B code system to be used in reload licensing applications are given in Table 2.1-1.

2.0 SUMMARY AND CONCLUSIONS

The new code system (CASMO-3G/MICROBURN-B) shows very good agreement with the measured performance parameters of the benchmark data summarized in this report. Specifically,

- Fuel rod gamma scan measurements for seven Quad Cities fuel assemblies were compared to CASMO-3G calculated local pin powers. The uncertainty of the calculated local power distribution for these assemblies is   which demonstrates excellent agreement (see Section 4.1).

- Fuel assembly gamma scan data for Quad Cities 1 fuel assemblies at the end of Cycles 2 and 4 were used to compare measured to MICROBURN-B calculated power distributions. Results of these calculations for both cycles show the radial and nodal power relative standard deviations (without peripheral assemblies included) to be less than   and   respectively (see Section 4.2.3).

- Overall predicted planar TIP response for the reactors in this report shows agreement with measured TIP data to be   (see Section 5.3.2).

- The calculated hot operating core k-eff is consistent between reactor types and shows little cycle exposure dependence (see Section 4.2).

- The calculated cold critical k-effs for both local and uniform cold criticals are consistent between reactor types (see Section 4.2).

In summary, the new code system accurately predicts the neutronic behavior of BWR reactors. Accuracy in calculating core power distributions is demonstrated in Table 2.1-1 which compares measured power distribution uncertainty between the existing codes (XFYRE/XTGBWR) as calculated in 1980 (Reference 1), and the new (CASMO-3G/MICROBURN-B) code system. As indicated in the table, the new codes, along with reduced TIP measurement uncertainty discussed in Section 5.3.1, provide a more precise prediction of core power distributions than the existing code system.

TABLE 2.1-1 MEASURED POWER DISTRIBUTION UNCERTAINTY SUMMARY

Type of Measured Power Distribution	Relative Standard Deviation, %	
	Existing Codes (Reference 1)	New Codes
Radial Bundle Power, P^n_{ij}		
Nodal Power, P^n_{ijk}		
Local Power, L_{ijk}		
Axial		
Radial Pin Power, P_{ij}		
Nodal Pin Power, P_{ijk}		

3.0 CASMO-3G/MICROBURN-B CALCULATION METHODOLOGY

Advanced Nuclear Fuels Corporation (ANF) has developed an improved boiling water reactor (BWR) nodal simulator code, MICROBURN-B. The new code represents a significant improvement over the previous core simulator XTGBWR in two principal areas. They are:

The number densities and burnup of key isotopes are evaluated on a nodal basis utilizing microscopic cross sections. This is the feature from which the name of the code is derived.

An improved coarse mesh finite differences formulation is utilized in the solution of the full two group diffusion theory representation of the reactor core.

Other important benefits arise directly from the introduction of these two improvements.

An additional significant extension to the ANF BWR methodology is the utilization of MICBURN-3/CASMO-3G, the bundle spectrum/depletion code system developed by Studsvik Energiteknik AB. This code system has been extensively evaluated by ANF and has been determined to be both flexible and accurate for providing the input constants required by MICROBURN-B. The major characteristics of these codes are summarized below. Additional details describing the codes are given in References 2 and 7.

3.1 Microscopic Burnup in Burnable Absorber Rods (MICBURN-3)

MICBURN-3 calculates the microscopic burnup in an absorber rod containing an initially homogeneously distributed burnable absorber. It generates effective cross sections as a function of the absorber number density to be used in CASMO-3G. ANF utilizes MICBURN-3 for the treatment of gadolinia, however the code can be used for any burnable neutron absorber. The input required for MICBURN-3 are data for geometry and material composition, and instructions for the choice of options in the calculations. Nuclear data are read from the CASMO-3G data library.

3.2 Fuel Assembly Burnup Code (CASMO-3G)

CASMO-3G is a multigroup two-dimensional transport theory code for burnup calculations on BWR and PWR assemblies or simple pin cells. The code handles a geometry consisting of cylindrical fuel rods of varying composition in a square pitch array with allowance for fuel rods loaded with burnable absorber, burnable absorber rods, cluster control rods, in-core instrument channels, water gaps, boron steel curtains and cruciform control rods in the regions separating fuel assemblies.

Significant features of CASMO-3G are the capability to handle four BWR bundle cases and a model for the generation of baffle/reflector data. The CASMO-3G version contains a gamma transport module to calculate gamma detector responses. Typical fuel storage rack geometries can also be handled.

Some important characteristics of CASMO-3G are:

- Nuclear data are collected in a library containing microscopic cross sections in 70 energy groups. Neutron energies cover the range 0 to 10 MeV. A library containing data in 40 energy groups is also available and is typically used in production calculations.
- CASMO-3G can accommodate non-symmetrical fuel bundles containing up to 19x19 rods. However, half-, quadrant- or octant-symmetry (mirror symmetry) can be utilized in calculations where applicable.
- Up to 12 energy groups are allowed in the two-dimensional transport theory calculation.

3.3 Reactor Simulator Code MICROBURN-B

MICROBURN-B is a three dimensional, two group, coarse mesh diffusion theory reactor simulator program for the analysis of BWR cores. The simulator code models the reactor core in three dimensional (X-Y-Z) geometry, and the reactor calculations can be performed in one-quarter, one-half, or full core geometry. The code calculates the reactor core reactivity, core flow distribution, nodal power distribution, reactor thermal limit values, and incore detector responses.

MICROBURN-B uses two group microscopic cross sections for key isotopes and calculates their number densities and burnup (microburn) at each node. The cross sections of the key isotopes are processed from CASMO-3G as functions of their number densities. The remaining isotopes are lumped into macroscopic cross sections that are functions of exposure and void fraction. The key isotopes are burned at each node in the three dimensional array at the void, control, and flux spectrum states appropriate for each burnup step. Void history and control history effects are thus automatically included, without the need for history correlations.

MICROBURN-B permits a more accurate treatment of plutonium than simulator codes which use only macroscopic cross sections. Since plutonium production depends strongly on the fast flux, while plutonium depletion depends primarily on the thermal flux, macroscopic cross sections cannot accurately treat plutonium at the simulator level even though both the fast and thermal flux groups might be treated by the simulator code. With macroscopic cross sections, the relative implicit changes in plutonium density relate to the fast to thermal flux ratio evaluated in the assembly burnup code (not the simulator code) at that exposure. Within the limits of two group theory, MICROBURN-B correctly treats plutonium at each node with the fast to thermal flux ratio as calculated by the simulator code itself.

For fuel management calculations, the code has a number of capabilities outlined in Reference 2, some of which include:

- Thermal hydraulic model including void feedback, subcooled boiling, and pressure drop flow calculations.
- Calculation of equilibrium and time dependent xenon and samarium.

- Nodally dependent Doppler broadening based on average LHGR of the node.
- Prediction of the TIP measurements for either fission or gamma detectors.

4.0 NEUTRONICS METHODS VERIFICATION

Section 4.0 presents the methods verification data for the MICBURN-3/CASMO-3G and MICROBURN-B calculation methods. Comparisons between calculations and measurements are presented for the Chinshan-1, Kuosheng-1, Kuosheng-2, Quad Cities-1, Susquehanna-1, and Susquehanna-2 reactors.

4.1 MICBURN-3 and CASMO-3G Verification (Quad Cities Gamma Scan Data

The Quad Cities-1 end of Cycle 2 (Reference 3), end of Cycle 3 (Reference 4), and end of Cycle 4 (Reference 5), fuel rod gamma scan measurements have been compared to the MICBURN-3/CASMO-3G calculated fuel rod powers and the results are shown in Figures 4.1-1 through 4.1-56. The Quad Cities gamma scan measurements were performed by removing fuel rods from the fuel assembly and measuring the La-140 activity as a function of core height. In that the tie rods and water rods were not gamma scanned, the measured and calculated powers appear as zero in Figures 4.1-1 through 4.1-56.

A total of seven bundles were measured at eight axial elevations each with three bundles in Cycles 2, three in Cycle 3, and one in Cycle 4. To perform the comparisons, the pin power distributions from CASMO-3G were converted to Ba-140 distributions. MICROBURN-B calculated exposure, instantaneous void, and void history distributions at EOC2, EOC3, and EOC4 were used in determining the Ba-140 distributions. The average relative standard deviation for all comparisons EPRI documents report a measurement uncertainty value of approximately 1.5%. Thus, the uncertainty of the calculated local power distribution is which shows good agreement between the measured and MICBURN-3/CASMO-3G calculated fuel rod powers.

4.2 MICROBURN-B Verification

The MICROBURN-B reactor core simulator code is verified by comparing the calculated and measured reactor parameters. The MICROBURN-B core-follow calculations for the Chinshan-1, Kuosheng-1, Kuosheng-2, Quad Cities-1, Susquehanna-1, and Susquehanna-2 reactors were calculated and compared to measured data. The hot operating k-eff values calculated by MICROBURN-B and the MICROBURN-B calculated startup cold critical k-eff values for these reactors are also summarized. The hot and cold critical data have not been corrected for reactivity biases associated with the effects of "crud", incore instrumentation, and fuel assembly spacers.

Measured and calculated traversing incore probe (TIP) data for the Chinshan-1, Kuosheng-1, Kuosheng-2, Quad Cities-1, Susquehanna-1 and Susquehanna-2 reactors have been compared and results are presented in Appendices A, B, D and E. The data shown is typical for beginning of cycle, middle of cycle, and end of cycle for each of the reactors. All MICROBURN-B calculations were performed with a full core model using 24 or 25 axial nodes.

The Quad Cities-1 end of Cycle 2 (Reference 3) and end of Cycle 4 (Reference 5) fuel assembly gamma scan measurements have been compared to MICROBURN-B calculated nodal powers. The calculated/measured results for Cycles 2 and 4 are shown in Appendix C. The measured data is La-140 activity. The MICROBURN-B calculated nodal powers were converted to La-140 activity for the comparisons.

4.2.1 Chinshan Unit 1 Cycles 5 through 9

CASMO-3G/MICROBURN-B core follow calculations have been performed for Chinshan 1 Cycles 1 through 9. TIP comparisons were performed for Cycles 5 through 8. Pertinent reactor core parameters at rated operating conditions for the Chinshan units are given in Table 4.2.1-1. Table 4.2.1-2 summarizes the GE and ANF fuel loaded in Cycles 3 through 9. ANF fuel was first loaded in Cycle 6. Results of measured versus calculated TIP comparisons and core k-eff (hot and cold) have been made for Cycles 5 through the beginning of Cycle 9. TIP comparisons are plotted and given in the following figures in Appendix A:

Chinshan 1 TIP Plots

Cycle	Figures
5	A-1 through A-3
6	A-4 through A-6
7	A-7 through A-9
8	A-10 through A-12

Tables 4.2.1-3 to 4.2.1-6 summarize the calculated k-eff and average voids versus cycle exposure for Cycles 5 through 8. Hot k-eff values are plotted versus core exposure for Cycles 5 through 8 in Figure 4.2.1-1. The cold k-critical values for Chinshan 1 Cycles 4 through 9 are summarized in Table 4.2.1-7. Table 4.2.1-8 summarizes results of multiple tests at the beginning of Cycle 9 for the initial and final loading patterns.

4.2.2 Kuosheng Units 1 and 2

Core follow calculations have been performed for Kuosheng Units 1 and 2 from Cycles 1 through 5. Table 4.2.2-1 summarizes reactor core parameters which define the units at rated operating condition. Table 4.2.2-2 lists GE and ANF fuel types loaded in Cycles 1 through 6 for Kuosheng 1 and Cycles 1 through 5 for Kuosheng 2. ANF fuel was first loaded in Cycle 4 of both units. Measured versus calculated TIP and core k-eff (hot and cold) comparisons have been made for both Kuosheng units. TIP comparisons for Kuosheng 1 Cycles 1 through 5 and Kuosheng 2 Cycles 4 and 5 are plotted in the following figures in Appendix B:

Kuosheng 1 and 2 TIP Plots

Unit	Cycle	Figures
KS1	1	B-1 through B-3
KS1	2	B-4 through B-6
KS1	3	B-7
KS1	4	B-8 through B-10
KS1	5	B-11 through B-13
KS2	4	B-14 through B-16
KS2	5	B-17 through B-19

Tables 4.2.2-3 to 4.2.2-9 summarize the calculated k-effs and average voids versus cycle exposure for the seven cycles. Hot k-eff values are plotted versus core exposure for the cycles for Kuosheng 1 and 2 in Figures 4.2.2-1 and 4.2.2-2, respectively. The cold k-critical values for Kuosheng 1 Cycles 2 through 6 and Kuosheng 2 Cycles 2 through 5 are summarized in Table 4.2.2-10. The eight cold critical tests for Kuosheng 1 Cycle 5 are defined in detail in Reference 6.

4.2.3 Quad Cities Unit 1 Cycles 1 through 4

Core follow calculations have been repeated for Quad Cities Unit 1 Cycles 1 through 4. Table 4.2.3-1 summarizes reactor core parameters which define the unit at rated operating conditions. Table 4.2.3-2 lists fuel types loaded in Cycles 1 through 4. Results of measured versus calculated TIP comparisons and core k-eff have been made. TIP comparisons for Quad Cities 1 Cycle 2 are plotted in the Figures D-1 through D-4 in Appendix D. Tables 4.2.3-3 to 4.2.3-6 summarize the calculated k-effs and average voids versus cycle exposure for the four cycles. Hot k-eff values are plotted versus core exposure for the cycles of Quad Cities 1 in Figure 4.2.3-1.

The Quad Cities-1 end of Cycle 2 (Reference 3) and end of Cycle 4 (Reference 5) fuel assembly gamma scan measurements have been compared to the MICROBURN-B calculated nodal powers. The calculated/measured nodal power results for Cycles 2 and 4 are shown in Appendix C. The assembly gamma scan results (without peripheral assemblies included) are presented in Figures 5.3.5-1 an 5.3.5-2. The measured data is La-140 activity. The XTGBWR calculated nodal powers were converted to La-140 activity for the comparisons. The comparisons show good agreement between the measured and calculated results. The relative standard deviations for the 2D assembly results are and for Cycles 2 and 4. The relative standard deviations for the 3D nodal results are and for Cycles 2 and 4.

4.2.4 Susquehanna Units 1 and 2

Core follow calculations have been performed for Susquehanna Units 1 and 2 for Cycles 1 through 4 in Unit 1 and for Cycles 1 through 3 in Unit 2. Table 4.2.4-1 summarizes reactor core parameters which define the units at rated operating conditions. Table 4.2.4-2 lists the fresh GE and ANF fuel types loaded in Cycles 1 through 4 for Susquehanna 1 and Cycles 1 through 3 for Susquehanna 2. ANF fuel was first loaded in Cycle 2 of both units. Results of measured versus calculated TIP comparisons and core k-eff (hot and cold) have been made for both of these units. TIP comparisons for Unit 1 Cycles 1 and 2 and Unit 2 Cycles 1 through 3 are plotted in the following figures in Appendix B:

Susquehanna 1 and 2 TIP Plots

Unit	Cycle	Figures
SQB	1	E-1
SQB	2	E-2
SQB	3	E-3
SQA	1	E-4
SQA	2	E-5
SQA	2	E-6

Tables 4.2.4-3 through 4.2.4-6 summarize the calculated k-eff and average voids versus cycle exposure for Unit 1 Cycles 1 through 4. The corresponding information for Unit 2 Cycles 1 through 3 is contained in Tables 4.2.4-8 through 4.2.4-10. Hot k-eff values are plotted versus core exposure for Susquehanna Units 1 and 2 in Figures 4.2.4-1 and 4.2.4-2, respectively. The cold k-critical values for Susquehanna 1 Cycles 1 through 4 and Susquehanna 2 Cycles 1 through 3 are summarized in Tables 4.2.2-7 and 4.2.2-11, respectively.

TABLE 4.2.1-1 CHINSHAN 1 AND 2 REACTOR CORE RATED PARAMETERS

Thermal Power, MWt	1775 (100% of rated)
Core Flow, Mlb/hr	53.0 (100% of rated)
Inlet Subcooling, Btu/lbm	22.3
Core Pressure, psia	1035
Total Assemblies in Core	408

TABLE 4.2.1-2 CHINSHAN 1 CYCLES 3 THROUGH 9 FUEL LOADING SUMMARY

Cycle	Cycle Energy, GWd	Fuel Type Loaded	Number Loaded
3	592	GE P8CRB284-8G3	28
		GE P8CRB284-2G3/4G2	84
4	366	GE P8CRB284-8G3	40
		GE P8CRB284-2G3/4G2	24
5	565	GE P8CRB284-8G3	28
		GE P8CRB284-6G3	84
6	704	ANF ANF8-314B-6G3	64
		ANF ANF8-314B-8G4	64
7	711	ANF ANF8-314B-6G3	76
		ANF ANF8-314B-8G4	56
8	674	ANF ANF8-314B-6G3	12
		ANF ANF8-314B-8G4	80
		ANF ANF8-300B-6G3	32
9	559*	ANF ANF8-314B-6G3	16
		ANF ANF8-314B-8G4	84
		ANF ANF8-300B-6G3	16
		ANF ANF8-300B-8G4	8

* Cycle currently in operation.

TABLE 4.2.1-3 MICROBURN-B CALCULATED K-EFF AND AVERAGE VOIDS FOR CHINSHAN 1 CYCLE 5

Cycle Exposure (MWd/MTU)	k-eff	Average Voids	Power MWt	Flow 10^6 lb/hr
86.4			1351.0	31.68
253.3			1770.0	52.33
395.5			1761.0	50.11
582.2			1775.0	52.89
710.0			1773.0	48.81
785.1			1763.0	52.47
928.1			1769.0	52.41
1064.1			1765.0	51.32
1156.1			1772.0	50.97
1344.5			1772.0	47.72
1475.5			1772.0	51.11
1698.7			1765.0	50.20
1848.2			1558.0	39.49
1961.2			1765.0	48.84
2088.2			1756.0	48.81
2267.3			1768.0	52.11
2427.5			1775.0	51.37
2593.5			1766.0	51.37
2756.8			1657.0	45.45
2918.0			1772.0	50.92
3107.3			1762.0	50.64
3273.0			1765.0	50.70
3413.1			1776.0	52.80
3618.8			1764.0	51.59
3785.1			1767.0	51.74
3963.8			1768.0	51.50
4152.0			1772.0	50.08
4341.9			1775.0	48.85
4508.4			1772.0	50.32
4674.3			1772.0	50.20
4864.1			1774.0	51.81
5009.3			1661.0	45.64
5168.3			1772.0	53.00
5311.0			1769.0	52.91
5477.7			1761.0	51.15
5572.9			1773.0	51.81

TABLE 4.2.1-3 MICROBURN-B CALCULATED K-EFF AND AVERAGE VOIDS FOR CHINSHAN 1 CYCLE 5 (CONTINUED)

Cycle Exposure (MWd/MTU)	k-eff	Average Voids	Power MWt	Flow 10^6 lb/hr
5673.2			1772.0	51.91
5801.8			1772.0	50.97
5939.7			1771.0	51.17
6124.8			1764.0	50.35
6290.9			1775.0	51.41
6457.4			1766.0	52.53
6643.6			1771.0	52.77
6781.0			1768.0	51.74
7009.7			1767.0	50.35
7247.7			1767.0	52.95
7247.7			1769.0	50.38
7408.5			1769.0	50.38
7593.6			1766.0	52.21

TABLE 4.2.1-4 MICROBURN-B CALCULATED K-EFF AND AVERAGE VOIDS FOR CHINSHAN 1 CYCLE 6

Cycle Exposure (MWd/MTU)	k-eff	Average Voids	Power MWt	Flow 10^6 lb/hr
440.9			1292.2	34.90
578.8			1771.3	50.49
741.4			1770.8	52.27
1187.4			1772.1	52.32
1740.9			1770.7	52.54
1942.7			1775.1	51.89
2164.2			1775.8	51.53
2398.9			1776.0	50.37
2563.5			1772.0	51.96
2681.7			1771.6	51.27
2847.1			1774.3	50.74
3036.0			1766.2	51.91
3199.8			1766.7	51.42
3362.7			1773.2	51.05
3526.0			1774.6	51.69
3739.6			1777.7	51.10
3906.1			1776.9	49.59
4016.6			1770.0	51.37
4183.6			1773.4	51.47
4352.4			1767.3	50.59
4682.5			1773.4	52.88
4810.1			1769.9	51.75
5030.1			1773.1	51.84
5343.1			1767.5	51.52
5507.9			1767.1	51.66
5664.9			1771.6	51.40
5859.1			1769.3	52.58
5952.3			1769.0	52.29
6139.3			1770.4	50.98
6280.4			1773.7	51.72
6463.9			1768.4	51.24
6619.1			1774.5	50.53
6941.7			1772.0	50.78
7130.1			1771.7	50.79
7269.8			1771.4	51.32
7425.9			1770.4	51.06

TABLE 4.2.1-4 MICROBURN-B CALCULATED K-EFF AND AVERAGE VOIDS FOR CHINSHAN 1 CYCLE 6 (CONTINUED)

Cycle Exposure (MWd/MTU)	k-eff	Average Voids	Power MWt	Flow 10^6 lb/hr
7587.1			1772.0	52.59
7836.9			1691.2	46.34
7933.3			1656.1	45.68
8079.5			1741.7	52.08
8211.7			1721.2	52.36
8369.9			1745.7	52.96
8473.1			1763.1	52.31
8638.6			1661.1	50.09
8732.5			1662.2	50.36
8951.7			1182.0	38.50
9093.5			1630.5	52.38
9051.0			1182.0	38.50
9192.8			1630.5	52.38
9337.9			1570.9	52.86
9452.0			1538.9	52.16
9574.5			1544.2	52.39
9660.6			1511.9	52.50

TABLE 4.2.1-5 MICROBURN-B CALCULATED K-EFF AND AVERAGE VOIDS FOR CHINSHAN 1 CYCLE 7

Cycle Exposure (MWd/MTU)	k-eff	Average Voids	Power MWt	Flow 10^6 lb/hr
177.8			1660.8	52.78
281.6			1764.0	52.14
584.7			1760.5	52.18
737.4			1771.5	52.17
975.1			1769.5	51.32
1179.2			1771.7	51.26
1327.2			1771.4	50.82
1479.1			1775.2	50.75
1479.1			1734.8	52.56
1655.7			1734.8	52.56
1798.1			1772.4	50.68
2061.8			1773.8	51.32
2262.0			1771.1	51.26
2411.8			1772.4	50.84
2559.8			1770.0	50.84
2718.5			1762.6	51.56
2989.0			1770.7	51.93
3140.5			1771.5	50.61
3290.6			1772.5	50.51
3475.8			1776.1	50.59
3665.4			1773.7	50.03
3760.8			1732.4	52.49
3911.5			1775.0	52.02
4049.7			1770.4	51.38
4259.7			1766.9	51.40
4442.1			1769.3	50.60
4660.3			1773.5	50.39
4777.8			1769.5	51.20
4966.5			1762.1	48.03
5100.2			1770.8	48.65
5198.5			1769.5	50.70
5448.9			1770.3	50.97
5577.8			1771.6	51.55
5775.0			1770.8	51.84
5920.7			1772.1	52.10
6053.4			1769.9	48.61
6193.7			1647.0	45.21
6333.8			1765.7	51.03

TABLE 4.2.1-5 MICROBURN-B CALCULATED K-EFF AND AVERAGE VOIDS FOR CHINSHAN 1 CYCLE 7 (CONTINUED)

Cycle Exposure (MWd/MTU)	k-eff	Average Voids	Power MWt	Flow 10^6 lb/hr
6499.7			1771.5	51.77
6710.8			1767.7	52.27
6858.9			1770.0	49.78
6976.1			1769.6	51.45
7136.0			1771.0	51.00
7351.8			1770.1	52.20
7521.0			1771.2	52.05
7641.4			1765.0	52.50
7815.4			1766.8	50.47
7989.4			1770.6	50.28
8204.9			1771.3	50.82
8428.9			1766.4	52.89
8505.0			1769.3	51.29
8705.8			1763.0	52.42
8841.4			1770.0	51.89
8957.2			1740.3	49.61
9136.5			1736.2	52.33
9292.6			1700.4	52.52
9568.6			1647.4	52.55
9693.9			1623.5	52.65
9774.0			1617.6	52.99
9774.0			1617.6	52.99

TABLE 4.2.1-6 MICROBURN-B CALCULATED K-EFF AND AVERAGE VOIDS FOR CHINSHAN 1 CYCLE 8

Cycle Exposure (MWd/MTU)	k-eff	Average Voids	Power MWt	Flow 10^6 lb/hr
189.0			1762.9	50.93
478.1			1770.3	51.14
625.8			1770.3	50.93
773.7			1768.9	50.56
995.4			1771.5	49.82
1165.9			1766.0	50.19
1[illegible]3.1			1769.5	51.46
1509.4			1771.6	50.61
1681.7			1770.0	49.82
1826.5			1774.0	50.24
1999.0			1771.8	50.93
2155.7			1753.3	52.74
2326.2			1772.8	51.46
2444.8			1772.9	51.04
2638.4			1772.1	50.03
2786.0			1772.6	49.93
3211.3			1773.8	51.41
3382.9			1774.3	51.36
3600.7			1770.5	50.93
3797.8			1772.4	50.93
4016.5			1771.2	50.46
4135.8			1773.9	52.26
4281.6			1773.3	50.19
4478.2			1773.7	50.03
4600.9			1773.5	51.52
4748.9			1770.8	50.61
4945.9			1773.3	51.73
5108.5			1765.4	51.94
5244.7			1773.1	52.47
5297.0			1766.8	51.36
5441.5			1773.2	50.93
5509.6			1767.0	49.93
5804.9			1767.4	51.25
6026.9			1770.6	51.46
6263.2			1774.4	50.40
6558.9			1766.0	52.31
6682.0			1771.9	51.89

TABLE 4.2.1-6 MICROBURN-B CALCULATED K-EFF AND AVERAGE VOIDS FOR CHINSHAN 1 CYCLE 8 (CONTINUED)

Cycle Exposure (MWd/MTU)	k-eff	Average Voids	Power MWt	Flow 10^6 lb/hr
6934.3			1769.6	52.20
7092.0			1771.6	51.62
7336.6			1765.0	51.14
7552.2			1772.9	50.77
7894.5			1771.1	50.61
8042.0			1770.8	51.57
8262.3			1715.1	53.12
8374.6			1751.6	52.66
8531.2			1730.7	52.99
8661.3			1725.9	52.86
8852.6			1692.7	52.59
9009.9			1665.9	52.58
9164.1			1075.6	26.44
9252.3			1243.5	32.20
9348.8			1248.5	33.55
9348.8			1248.5	33.55

TABLE 4.2.1-7 CHINSHAN 1 CYCLES 4 THROUGH 9
COLD CRITICAL EIGENVALUES

Case	Cycle	k-critical
1	BOC4	
2	BOC5	
3	MOC5	
4	BOC6	
5	BOC7	
6	BOC8	
7	BOC9 (Final Loading)	(mean of 8 tests
8	(Initial Loading)	(mean of 8 tests

TABLE 4.2.1-8 CHINSHAN 1 CYCLE 9
COLD CRITICAL EIGENVALUES

(Final Loading Pattern)

Case	k-critical
1	
2	
3	
4	
5	
6	
7	
8	

Mean k-critical =

Standard Deviation =

(Initial Loading Pattern)

Retest Case	k-critical
1	
2	
3	
4	
5	
6	
7	
8	

Mean k-critical =

Standard Deviation =

TABLE 4.2.2-1 KUOSHENG 1 AND 2 REACTOR CORE RATED PARAMETERS

Thermal Power, MWt	2894 (100% of rated)
Core Flow, Mlb/hr	84.5 (100% of rated)
Inlet Subcooling, Btu/lbm	23.05
Core Pressure, psia	1055
Total Assemblies in Core	624

TABLE 4.2.2-2 KUOSHENG 1 AND 2 FUEL LOADING SUMMARY

Unit	Cycle	Cycle Energy, GWd	Fuel Type Loaded	Number Loaded
1	1	1195.2	GE P8S1B219-4GZ GE P8S1B176-4GZ GE P8S1B071-NOG	360 188 76
	2	902.8	GE P8CRB284-6G3	212
	3	834.9	GE P8CRB284-6G3	156
	4	1190	ANF ANF8-315B-8G4	216
	5	896	ANF ANF8-315B-8G4 ANF ANF8-315B-6G4	96 96
	6	1192	ANF ANF8-315B-8G4 ANF ANF8-315B-6G3	168 24
2	1	1170	GE P8S1B219-4GZ GE P8S1B176-4GZ GE P8S1B071-NOG	360 188 76
	2	856	GE P8SRB284-6G3	212
	3	821	GE P8SRB284-6G3	156
	4	1289	ANF ANF8-315B-8G4	184
	5	1180*	ANF ANF8-315B-8G4 ANF ANF8-315B-6G4	48 200

* Cycle currently in operation.

TABLE 4.2.2-3 MICROBURN-B CALCULATED K-EFF AND AVERAGE VOIDS FOR KUOSHENG 1 CYCLE 1

Cycle Exposure (MWd/MTU)	K-eff	Average Voids	Power MWt	Flow 10^6 lb/hr
0.0			2154.0	59.30
693.0			2154.0	59.30
914.6			2879.0	84.66
1210.6			2841.0	84.48
1743.9			2871.0	82.86
1861.1			2756.0	78.46
2147.7			2728.0	77.26
2185.3			2860.0	84.25
2648.1			2874.0	79.93
2648.1			2878.0	81.85
3007.8			2871.0	80.04
3188.7			2819.0	78.35
3301.5			1869.0	44.08
3561.9			2410.0	64.82
3793.4			2717.0	78.05
3838.6			2717.0	78.05
4062.8			2851.0	83.35
4299.0			2889.0	81.09
4374.3			2889.0	81.09
4603.5			2893.0	82.86
4870.4			2692.0	72.64
5053.3			2893.0	81.51
5244.7			2891.0	80.46
5500.3			2886.0	81.17
5570.6			2886.0	81.17
5661.2			2848.0	82.44
5713.9			2882.0	79.93
5935.7			2604.0	67.08
6114.7			2895.0	83.20
6324.2			2753.0	74.74
6488.3			2767.0	84.25
6653.0			2756.0	81.09
6727.1			2286.0	67.49
6899.4			2738.0	75.81
7009.7			2789.0	75.46
7200.2			2885.0	84.40
7373.6			2871.0	77.19
7556.1			2343.0	57.19
7655.4			2385.0	83.95

TABLE 4.2.2-3 MICROBURN-B CALCULATED K-EFF AND AVERAGE VOIDS FOR KUOSHENG 1 CYCLE 1 (CONT.)

Cycle Exposure (MWd/MTU)	k-eff	Average Voids	Power MWt	Flow 10^6 lb/hr
7931.7			2890.0	83.95
8107.2			2890.0	83.20
8338.7			2747.0	74.33
8464.4			2898.0	82.16
8810.4			2884.0	84.48
8868.7			2811.0	84.59
8981.7			2740.0	79.85
9315.3			2879.0	84.25
9625.2			2733.0	77.75
9737.2			2880.0	84.32
10502.8			2357.0	73.65

TABLE 4.2.2-4 MICROBURN-B CALCULATED K-EFF AND AVERAGE VOIDS FOR KUOSHENG 1 CYCLE 2

Cycle Exposure (MWd/MTU)	k-eff	Average Voids	Power MWt	Flow 10^6 lb/hr
0.0			2865.0	83.99
119.3			2865.0	83.99
260.9			2887.0	82.49
387.3			2874.0	84.50
511.2			2837.0	81.61
686.9			2880.0	82.41
812.7			2897.0	81.54
972.0			2891.0	81.61
1149.8			2893.0	80.48
1251.4			2894.0	79.83
1418.3			2878.0	78.20
1568.5			2893.0	81.54
1689.7			2808.0	75.46
1788.4			2817.0	79.41
1962.1			2658.0	68.47
2135.4			2814.0	75.16
2135.4			2895.0	84.27
2188.2			2895.0	84.27
2378.4			2895.0	82.98
2488.0			2894.0	79.78
2593.2			1527.0	44.53
2782.3			2173.0	50.36
2937.0			2249.0	59.56
3055.3			2694.0	73.53
3199.3			2887.0	81.35
3300.2			2894.0	81.65
3427.2			2894.0	81.05
3578.0			2226.0	56.44
3764.3			2892.0	78.03
3917.3			2248.0	54.29
4037.1			2390.0	62.33
4159.3			2894.0	78.94
4306.5			2893.0	82.13
4382.8			2891.0	82.56
4556.5			2892.0	81.50
4759.8			2891.0	82.36
4931.4			2895.0	77.84
5129.0			2891.0	81.35

TABLE 4.2.2-4 MICROBURN-B CALCULATED K-EFF AND AVERAGE VOIDS FOR KUOSHENG 1 CYCLE 2 (CONT.)

Cycle Exposure (MWd/MTU)	k-eff	Average Voids	Power MWt	Flow 10^6 lb/hr
5299.2			2893.0	81.65
5477.8			2888.0	82.94
5580.5			2894.0	82.37
5858.0			2896.0	80.18
6031.7			2894.0	81.16
6166.7			2891.0	81.65
6342.9			2894.0	81.16
6505.4			2894.0	81.65
6652.0			2891.0	83.28
6652.0			2663.0	66.25
6828.7			2633.0	66.25
6989.7			2888.0	78.73
7154.1			2886.0	78.48
7309.8			2850.0	82.33
7493.4			2806.0	84.22
7657.0			2755.0	80.60
7825.6			2755.0	84.56
7941.3			2536.0	80.18

TABLE 4.2.2-5 MICROBURN-B CALCULATED K-EFF AND AVERAGE VOIDS FOR KUOSHENG 1 CYCLE 3

Cycle Exposure (MWd/MTU)	k-eff	Average Voids	Power MWt	Flow 10^6 lb/hr
0.0			2870.0	84.17
176.5			2870.0	84.17
392.5			2790.0	79.17
618.7			2890.0	83.75
872.7			2892.0	80.31
1112.8			2894.0	81.52
1301.6			2894.0	80.04
1454.3			2892.0	79.29
1655.7			2889.0	78.19
1858.9			2885.0	77.32
2001.9			2765.0	72.96
2215.4			2494.0	67.70
2345.2			2315.0	57.90
2503.9			2888.0	83.22
2743.0			2802.0	78.53
2827.2			2891.0	81.78
2917.6			2817.0	75.50
3125.3			2769.0	75.20
3283.1			2738.0	75.92
3442.5			2731.0	74.14
3610.8			2836.0	79.78
3786.5			2872.0	82.35
3887.6			2883.0	81.41
4065.6			2889.0	81.96
4242.8			2888.0	81.19
4343.7			2887.0	82.60
4469.0			2892.0	80.70
4622.2			2891.0	82.19
4811.1			2893.0	83.00
5033.0			2891.0	81.15
5210.3			2890.0	81.71
5388.2			2887.0	83.23
5535.1			2894.0	80.11
5631.5			2884.0	79.32
5777.7			2885.0	73.10
5977.9			2886.0	75.55
6180.9			2886.0	80.82
6296.6			2890.0	80.63

TABLE 4.2.2-5 MICROBURN-B CALCULATED K-EFF AND AVERAGE VOIDS FOR KUOSHENG 1 CYCLE 3 (CONT.)

Cycle Exposure (MWd/MTU)	k-eff	Average Voids	Power MWt	Flow 10^6 lb/hr
6463.6			2879.0	77.70
6622.6			2890.0	84.12
6723.1			2796.0	90.70
6909.0			2893.0	82.45
7053.6			2876.0	87.16
7202.8			2854.0	87.97
7301.1			2751.0	84.86
7345.6			2751.0	84.86

TABLE 4.2.2-6 MICROBURN-B CALCULATED K-EFF AND AVERAGE VOIDS FOR KUOSHENG 1 CYCLE 4

Cycle Exposure (MWd/MTU)	k-eff	Average Voids	Power MWt	Flow 10^6 lb/hr
0.0			2875.8	82.20
185.2			2875.8	82.20
346.2			2878.1	85.20
512.7			2886.4	81.40
742.6			2883.8	81.80
948.1			2890.3	80.10
1076.5			2891.2	78.70
1178.0			2892.2	79.40
1368.4			2889.5	77.50
1394.0			2395.1	57.40
1531.0			2388.6	70.60
1787.0			2889.0	72.80
1995.6			2879.7	74.40
2210.4			2891.9	71.90
2400.6			2884.3	70.80
2602.7			2889.3	73.70
2801.2			2891.1	71.70
2973.4			2874.8	69.04
3144.2			2890.6	76.24
3323.6			2892.0	74.72
3503.0			2892.5	72.95
3821.4			2892.5	70.55
4026.8			2889.3	70.33
4195.0			2880.2	70.15
4436.4			2889.1	66.74
4604.2			2882.6	68.63
4752.5			2795.4	66.01
4923.7			2257.3	50.58
5103.1			2608.1	61.25
5352.5			2891.2	71.32
5546.9			2880.8	70.26
5722.2			2334.7	71.56
5893.7			2882.3	73.17
6069.6			2545.6	59.99
6283.1			2889.2	74.24
6459.6			2886.2	74.50
6617.0			2888.4	73.13
6743.2			2679.8	70.05

TABLE 4.2.2-6 MICROBURN-B CALCULATED K-EFF AND AVERAGE VOIDS FOR KUOSHENG 1 CYCLE 4 (CONT.)

Cycle Exposure (MWd/MTU)	k-eff	Average Voids	Power MWt	Flow 10^6 lb/hr
6864.9			2885.1	80.08
7033.7			2885.2	77.48
7213.2			2890.5	81.90
7366.3			2887.8	82.65
7621.9			2883.7	82.57
7747.6			2887.8	81.46
7926.8			2885.6	83.25
8142.5			2484.6	60.82
8344.3			2884.0	80.33
8446.9			2885.3	81.93
8702.5			2884.7	83.41
8906.5			2876.7	84.17
9200.9			2886.7	80.97
9329.0			2888.5	82.98
9507.4			2882.4	82.47
9678.4			1891.7	45.77
9833.5			2888.4	79.47
10012.6			2884.5	82.34
10182.2			2885.1	82.27
10359.3			2886.4	81.35
10587.7			2889.7	86.23

TABLE 4.2.2-7 MICROBURN-B CALCULATED K-EFF AND AVERAGE VOIDS FOR KUOSHENG 1 CYCLE 5

Cycle Exposure (MWd/MTU)	k-eff	Average Voids	Power MWt	Flow 10^6 lb/hr
0.0			1180.4	32.02
12.9			1180.4	32.02
46.9			2352.4	51.
71.5			2803.1	64.72
123.4			2889.7	74.95
227.9			2892.1	76.32
357.9			2891.1	77.39
539.4			2890.4	76.62
688.9			2889.4	75.85
1103.2			2806.0	74.07
1223.9			2885.4	74.60
1378.1			2888.3	74.18
1623.7			2705.3	68.20
1674.7			2870.9	78.52
1803.5			2886.1	78.60
1971.1			2886.1	78.15
2073.5			2893.4	79.46
2230.1			2881.8	79.16
2333.3			2887.7	78.96
2384.7			2883.2	78.35
2488.0			2888.2	78.60
2565.7			2888.1	79.83
2824.5			2886.1	76.63
3050.5			2891.6	78.99
3284.1			2891.9	78.62
3438.8			2828.2	75.02
3542.0			2877.2	77.57
3696.7			2890.4	77.25
3800.3			2893.6	76.83
4033.2			2869.1	72.94
4232.4			2866.8	71.90
4432.3			2890.5	74.91
4624.1			2616.3	61.50
4827.9			2891.3	72.24

TABLE 4.2.2-7 MICROBURN-B CALCULATED K-EFF AND AVERAGE VOIDS FOR KUOSHENG 1 CYCLE 5 (CONT.)

Cycle Exposure (MWd/MTU)	k-eff	Average Voids	Power MWt	Flow 10^6 lb/hr
4983.4			2887.9	72.43
5227.2			2882.5	74.49
5472.4			2889.2	73.98
5809.5			2888.2	74.23
6031.6			2887.3	75.87
6210.8			2885.5	75.84
6471.0			2884.5	76.54
6755.5			2888.2	77.33
6937.0			2886.5	78.73
7017.9			2271.2	55.98
7214.4			2890.3	80.04
7399.4			2888.1	78.56
7606.9			2885.5	80.82
7866.1			2880.3	77.94
8071.9			2885.4	79.09
8277.2			2885.1	81.45
8473.5			2882.3	83.83

TABLE 4.2.2-8 MICROBURN-B CALCULATED K-EFF AND AVERAGE VOIDS FOR KUOSHENG 2 CYCLE 4

Cycle Exposure (MWd/MTU)	k-eff	Average Voids	Power MWt	Flow 10^6 lb/hr
289.8			2887.9	72.06
575.5			2892.4	77.59
751.6			2860.6	72.67
1105.3			2887.1	75.05
1341.9			2889.2	73.35
1749.4			2890.9	76.88
2029.4			2892.5	75.46
2250.2			2890.6	76.04
2937.4			2886.9	68.49
3402.9			2887.6	74.85
3782.8			2891.5	72.80
4013.0			2887.2	71.83
4171.6			2880.1	77.97
4451.0			2882.9	76.84
4915.8			2889.8	70.91
5143.3			2888.3	69.64
5249.5			2887.9	77.43
5758.1			2886.7	73.62
6033.4			2881.6	74.[illegible]6
6263.7			2892.9	78.09
6591.3			2889.3	77.88
6743.2			2889.0	84.10
7135.1			2885.9	82.72
7386.5			2887.4	79.81
7615.0			2886.0	84.55
7925.5			2893.0	85.28
8116.2			2876.6	84.35
8690.7			2882.8	81.58
8881.3			2888.0	86.40
9150.4			2828.1	78.60
9349.9			2889.7	81.11
9681.0			2853.0	87.71
9847.9			2876.9	85.87
10148.3			2761.3	87.60
10245.6			2735.6	88.36
10293.5			2719.4	88.18
10410.8			2819.5	88.65
10795.0			2659.1	87.47
10945.2			2619.5	88.19
11150.7			2535.4	88.16

TABLE 4.2.2-9 MICROBURN-B CALCULATED K-EFF AND AVERAGE VOIDS FOR KUOSHENG 2 CYCLE 5

Cycle Exposure (MWd/MTU)	k-eff	Average Voids	Power MWt	Flow 10^6 lb/hr
0.0			2575.2	64.84
57.7			2575.2	64.84
102.4			2261.2	50.34
177.3			2882.0	76.68
342.0			2882.0	76.68
711.8			2127.2	48.37
817.6			2873.9	72.88
869.5			2891.1	76.00
1172.9			2868.0	76.22
1224.8			2888.6	79.72
1510.9			2890.8	77.44
1640.3			2888.5	71.52
1718.2			2888.7	73.47
1911.9			2825.0	70.47
1964.3			2882.6	77.39
2016.9			2885.8	75.76
2198.8			2829.5	72.65
2250.7			2885.4	78.31
2406.6			2886.9	76.91
2536.2			2891.4	76.03
2582.6			2888.8	74.87
2831.0			2882.3	73.[illegible]
3200.0			2882.3	[illegible]
3226.3			2889.0	74.28
3408.0			2887.4	73.39
3589.7			2887.1	71.99
3821.2			2885.3	69.89
4063.1			2877.7	73.59
4298.0			2877.7	73.59
4323.0			2644.8	73.66
4518.9			2726.3	65.93
4644.0			2881.0	76.33
4888.7			2575.5	65.99
4939.8			2885.2	78.66
5018.0			2885.2	78.66
5109.0			1513.5	42.04
5237.5			2878.2	76.52
5323.8			2889.0	76.53
5704.8			2890.4	76.59

TABLE 4.2.2-10 KUOSHENG 1 AND 2 CYCLES 2 THROUGH 6
COLD CRITICAL EIGENVALUES

Case	Unit	Cycle	k-critical
1	1	BOC2	
2	1	BOC3	
3	1	BOC4	
4	1	BOC5	
5	2	BOC2	
6	2	BOC3	
7	2	BOC4	
8	2	BOC5	
9	1	BOC6 SEQ1	
10	1	BOC6 SEQ2	
11	1	BOC6 SEQ3	
12	1	BOC6 SEQ4	
13	1	BOC6 SEQ5	
14	1	BOC6 SEQ6	
15	1	BOC6 SEQ7	
16	1	BOC6 SEQ8	
Mean k-critical (Cases 9-16)			
Standard Deviation (Cases 9-16)			
17	2	MOC5 SEQ1	
18	2	MOC5 SEQ2	

TABLE 4.2.3-1 QUAD CITIES 1 REACTOR CORE RATED PARAMETERS

Thermal Power, MWt	2511 (100% of rated)
Core Flow, Mlb/hr	98.0 (100% of rated)
Total Assemblies in Core	724

TABLE 4.2.3-2 QUAD CITIES 1 CYCLES 1 THROUGH 4 FUEL LOADING SUMMARY

Cycle	Cycle Energy, GWd	Fuel Type Loaded	Number Loaded
1	1124	GE 7x7 2.12 w/o U-235	724
2	897	GE 7x7 2.30 w/o U-235	23
		GE 8x8 2.50 w/o U-235	36
3	616	GE 8x8 2.50 w/o U-235	104
		GE 8x8 2.62 w/o U-235	52
4	1066	GE 8x8 2.50 w/o U-235	183

TABLE 4.2.3-3 MICROBURN-B CALCULATED K-EFF AND AVERAGE VOIDS
FOR QUAD CITIES 1 CYCLE 1

Cycle Exposure (MWd/MTU)	k-eff	Average Voids	Power MWt	Flow 10^6 lb/hr
712.1			2235	99.61
881.9			2240	94.65
1470.6			2197	97.58
2238.9			2450	97.97
3190.2			2414	95.30
3836.2			2197	94.84
4074.3			2320	94.72
4736.8			2377	92.93
5301.6			2337	90.95
6031.3			2014	73.50
6558.2			2225	97.89
6807.3			2210	94.14
7397.0			2267	95.62
7659.4			2187	97.73
8060.2			2203	95.94

TABLE 4.2.3-4 MICROBURN-B CALCULATED K-EFF AND AVERAGE VOIDS FOR QUAD CITIES 1 CYCLE 2

Cycle Exposure (MWd/MTU)	k-eff	Average Voids	Power MWt	Flow 10^6 lb/hr
677.0			2286	88.01
1502.5			2412	97.42
1855.2			2500	96.68
2886.9			2463	97.23
5609.5			1829	93.87
5911.5			1713	94.10
6324.5			1547	95.70
6454.5			1487	94.90

TABLE 4.2.3-5 MICROBURN-B CALCULATED K-EFF AND AVERAGE VOIDS FOR QUAD CITIES 1 CYCLE 3

Cycle Exposure (MWd/MTU)	k-eff	Average Voids	Power MWt	Flow 10^6 lb/hr
445.3			2441	96.30
1989.6			2423	98.20
2783.2			2445	98.40
3753.2			2190	97.60
4221.7			2126	96.80

TABLE 4.2.3-6 MICROBURN-B CALCULATED K-EFF AND AVERAGE VOIDS FOR QUAD CITIES 1 CYCLE 4

Cycle Exposure (MWd/MTU)	k-eff	Average Voids	Power MWt	Flow 10^6 lb/hr
412.4			2416	95.70
849.6			2103	78.67
1498.0			2462	98.94
1944.1			2438	97.89
2365.5			2454	99.09
2731.0			2468	97.96
3277.9			2482	97.38
3839.4			2495	98.59
4347.4			1890	61.95
4733.9			2217	89.06
5173.3			2387	97.38
5471.1			2442	97.54
5824.5			2283	92.88
6043.1			2023	81.32
6559.6			2053	97.62
6846.3			1456	55.16
6983.8			1242	41.05
7656.6			1342	75.27
7843.2			1342	75.27

TABLE 4.2.4-1 SUSQUEHANNA UNITS 1 AND 2 REACTOR CORE RATED PARAMETERS

Thermal Power, MWt	3293 (100% of rated)
Core Flow, Mlb/hr	100.0 (100% of rated)
Inlet Subcooling, Btu/lbm	24.0
Core Pressure, psia	1005
Total Assemblies in Core	764

TABLE 4.2.4-2 SUSQUEHANNA UNITS 1 AND 2 FUEL LOADINGS SUMMARY

Unit 1

Cycle	Cycle Energy, GWd	Fuel Type Loaded	Number Loaded
1	1624.9	GE P8CRB711-NGD GE P8CRB176-3GZ GE P8CRB219-3GZ	92 240 432
2	743.7	ANF82-273B-5G2	192
3	1390.3	ANF82-289B-6G4	296
4	1543*	ANF92-331B-9G4 (9x9 Fuel)	240

Unit 2

Cycle	Cycle Energy, GWd	Fuel Type Loaded	Number Loaded
1	1688	GE P8CRB711-NGD GE P8CRB176-3GZ GE P8CRB219-3GZ	92 240 432
2	1504	ANF92-331B-7G4 (9x9 Fuel)	324
3	1289*	ANF92-333B-9G4 (9x9 Fuel) ANF92-333B-10G5 (9x9 Fuel)	140 96

* Cycle currently operating.

TABLE 4.2.4-3 MICROBURN-B CALCULATED K-EFF AND AVERAGE VOIDS FOR SUSQUEHANNA 1 CYCLE 1

Cycle Exposure (MWd/MTU)	k-eff	Average Voids	Power MWt	Flow 10^6 lb/hr
73.8			644.5	40.00
173.5			1307.6	43.00
221.0			1435.5	53.75
311.7			1435.5	53.75
353.8			2186.0	89.86
609.8			2271.0	60.00
737.6			2717.0	75.62
835.5			3209.0	97.50
990.6			3240.0	101.87
1274.4			2360.0	67.03
1319.1			3281.0	97.11
1490.3			3278.5	99.61
1602.4			3293.6	98.83
2050.2			3291.8	97.11
2073.1			3290.0	96.88
2305.4			1966.8	57.11
2512.1			3294.9	95.08
2743.9			3286.0	93.83
2907.9			3293.9	98.13
2975.0			3293.9	98.13
3144.9			3291.0	95.86
3400.2			3287.9	97.58
3869.2			3294.8	95.63
4013.2			3290.7	97.03
4194.2			3289.1	96.88
4342.0			3292.7	97.11
4539.6			3289.1	96.88
4717.0			3289.8	98.13
4988.6			3291.5	98.13
5107.8			3287.5	98.75
5186.9			1837.3	54.38
5416.5			3294.1	98.13
5627.0			3294.8	98.75
5834.2			3286.8	98.75
5995.4			3291.4	98.13
6251.7			3288.3	98.13
6413.7			3268.3	96.25
6552.5			3285.7	98.75

TABLE 4.2.4-3 MICROBURN-B CALCULATED K-EFF AND AVERAGE VOIDS FOR SUSQUEHANNA 1 CYCLE 1 (CONT.)

Cycle Exposure (MWd/MTU)	k-eff	Average voids	Power MWt	Flow 10^6 lb/hr
6724.4			3283.1	97.50
6884.8			3282.3	96.25
7000.5			3285.4	98.75
7110.5			3297.5	96.25
7236.9			3276.4	94.38
7387.6			3287.2	93.75
7505.8			3281.3	96.25
7638.4			3279.3	94.45
7840.9			3259.5	96.88
7991.6			3290.9	93.75
8165.7			3300.6	94.38
8342.5			3291.8	95.70
8482.3			3288.0	96.25
8603.5			3283.9	99.38
8818.3			3290.2	95.63
8968.5			3283.3	98.28
9116.8			3286.6	98.67
9242.3			3283.8	91.25
9383.6			3209.7	100.00
9617.0			3295.5	95.00
9703.3			3288.6	92.50
9773.7			3298.1	99.38
9910.0			3279.3	96.33
10045.2			3283.6	89.38
10139.1			3282.0	94.38
10287.4			3279.6	96.25
10392.1			3288.6	95.78
10571.5			3284.6	92.50
10663.6			3290.3	95.63
10768.6			3284.0	100.00
10932.6			3202.3	100.00
11081.9			3059.3	100.00
11152.0			2991.0	100.00
11257.2			2897.0	100.00
11329.4			2833.5	99.38
11464.0			2776.2	99.38
11542.2			2714.2	99.45
11616.4			2668.8	100.00

TABLE 4.2.4-4 MICROBURN-B CALCULATED K-EFF AND AVERAGE VOIDS FOR SUSQUEHANNA 1 CYCLE 2

Cycle Exposure (MWd/MTU)	k-eff	Average Voids	Power MWt	Flow 10^6 lb/hr
90.7			2720.9	80.67
197.0			3279.6	94.08
274.3			3282.3	98.83
380.8			3288.9	99.41
623.5			3291.3	97.12
791.2			3290.1	94.98
962.6			3293.6	93.12
1143.1			3294.3	95.18
1247.8			3292.0	97.28
1403.4			3289.9	94.87
1527.7			3293.0	98.47
1684.7			3292.5	96.87
1802.5			3293.2	95.22
1922.1			3294.5	97.04
2027.0			3295.0	96.28
2240.1			3289.0	96.86
2415.5			3287.3	96.97
2619.7			3293.5	95.72
2786.4			3285.7	95.53
2951.7			3291.9	95.98
3039.3			3298.8	96.72
3150.4			3298.8	96.72
3320.8			3294.2	96.56
3473.9			3291.8	96.28
3660.9			3285.0	97.55
3871.4			3289.0	90.23
3957.6			3288.5	97.41
4076.7			3283.8	99.25
4333.2			3288.6	94.88
4503.4			3288.6	94.88
4637.0			3290.3	98.80
4897.5			3283.8	99.25
4944.2			3285.9	96.80
5358.6			3293.0	99.50

TABLE 4.2.4-5 MICROBURN-B CALCULATED K-EFF AND AVERAGE VOIDS FOR SUSQUEHANNA 1 CYCLE 3

Cycle Exposure (MWd/MTU)	k-eff	Average Voids	Power MWt	Flow 10^6 lb/hr
208.0			3291.1	96.93
449.0			3291.5	97.50
592.0			3293.8	96.20
630.0			3293.8	96.20
787.4			3290.5	98.10
964.5			3288.7	97.80
1070.0			3292.3	94.96
1290.8			3295.1	96.10
1459.3			3294.7	95.70
1579.1			3290.7	94.20
1674.8			3292.0	94.20
1796.3			3292.5	94.40
1963.9			3289.6	93.20
2120.4			3293.8	97.40
2288.6			3292.4	97.60
2480.6			3292.8	95.20
2619.0			3291.6	93.60
2782.5			3292.5	95.30
2949.8			3292.4	93.90
3117.5			3290.9	96.80
3334.6			3292.0	96.18
3525.6			3291.1	94.80
3809.3			3291.0	96.20
4069.7			3293.6	95.63
4189.2			3292.6	94.30
4334.0			3289.0	92.50
4550.6			3293.0	93.70
4597.2			3293.0	93.70
4752.3			3290.0	97.08
4921.9			3292.7	97.00
5114.7			3292.6	95.79
5210.8			3290.3	95.40
5379.0			3291.6	93.90
5522.4			3293.7	92.90
5731.9			3291.4	97.59
5852.2			3292.2	96.10
5996.1			3292.3	95.90
6116.0			3292.0	95.70

TABLE 4.2.4-5 MICROBURN-B CALCULATED K-EFF AND AVERAGE VOIDS FOR SUSQUEHANNA 1 CYCLE 3 (CONT.)

Cycle Exposure (MWd/MTU)	k-eff	Average Voids	Power MWt	Flow 10^6 lb/hr
6284.8			3289.2	95.56
6452.7			3291.6	95.20
6768.0			3292.7	95.52
6848.2			3289.8	94.40
7014.5			3289.8	94.40
7374.7			3290.5	94.90
7495.0			3293.4	96.75
7711.8			3290.3	96.88
7831.3			3288.6	94.40
7951.4			3289.4	96.90
8134.7			3294.4	93.80
8231.2			3290.5	97.20
8519.3			3289.3	96.60
8680.0			3291.9	96.55
8849.9			3293.4	97.70
9041.2			3291.4	97.10
9159.9			3290.2	98.30
9371.0			3290.4	91.80
9491.1			3294.0	95.20
9633.1			3291.9	90.16
9657.8			3290.1	94.09
9899.3			3292.1	97.90
10115.3			3291.9	98.40

TABLE 4.2.4-6 MICROBURN-B CALCULATED K-EFF AND AVERAGE VOIDS FOR SUSQUEHANNA 1 CYCLE 4

Cycle Exposure (MWd/MTU)	k-eff	Average Voids	Power MWt	Flow 10^6 lb/hr
279.5			3292.4	97.67
430.7			3293.7	96.40
688.5			3294.1	95.00
884.5			3291.0	95.60
1032.0			3292.8	95.00
1155.4			3292.9	96.88
1443.5			3291.7	97.00
1640.0			3293.6	95.40
1908.0			3293.6	95.40
2027.6			3294.0	97.00
2329.9			3291.7	96.40
2623.3			3291.9	95.50
2820.2			3291.6	93.80
3067.0			3284.4	91.00
3232.3			3289.0	94.98
3404.3			3294.4	96.00
3576.3			3293.0	94.30
3822.8			3293.6	93.70
3931.6			3289.6	97.60
4078.0			3290.6	98.00
4344.4			3292.7	96.50
4538.4			3293.0	96.10
4710.8			3289.6	94.00
4956.2			3292.6	92.70
5268.0			3292.8	94.50
5366.1			3240.7	91.50
5463.5			3294.6	95.50
5709.7			3290.8	94.40
5883.3			3290.8	93.70
6078.1			3291.1	93.70
6284.6			3291.3	94.23
6551.5			3292.7	96.20
6738.1			3291.5	97.10
7130.8			3291.5	97.10
7301.8			3292.1	96.77
7522.4			3292.1	96.77
7763.1			3293.5	92.47

TABLE 4.2.4-7 SUSQUEHANNA 1 CYCLES 1 THROUGH 3
COLD CRITICAL EIGENVALUES

Case	Cycle	k-critical
1	BOC1	
2	BOC1	
3	BOC1	
4	BOC1	
5	BOC1	
6	MOC1	
7	MOC1	
8	MOC1	
9	MOC1	
10	MOC1	
11	MOC1	
12	BOC2	
13	BOC2	
14	BOC2	
15	BOC2	
16	BOC2	
17	BOC3	
18	MOC3	
19	MOC3	
20	MOC3	
21	MOC3	
22	MOC3	
23	BOC4	

TABLE 4.2.4-8 MICROBURN-B CALCULATED K-EFF AND AVERAGE VOIDS FOR SUSQUEHANNA 2 CYCLE 1

Cycle Exposure (MWd/MTU)	k-eff	Average Voids	Power MWt	Flow 10^6 lb/hr
158.0			1363.5	46.17
180.3			1363.5	46.17
275.2			1612.1	96.17
455.3			2313.1	97.27
585.8			2632.4	72.11
768.0			3292.5	96.72
847.0			2121.5	55.86
893.6			2121.5	55.86
976.0			3287.8	92.73
1114.3			3287.8	92.73
1227.8			2592.9	66.80
1331.3			2592.9	66.80
1453.9			3289.9	95.39
1625.9			3293.0	96.56
1730.1			3289.3	97.42
1919.0			3296.3	95.47
2101.3			3293.3	97.11
2273.3			3292.9	95.55
2402.2			3292.9	93.98
2481.3			3284.8	97.42
2629.1			3283.2	97.58
2778.7			3288.1	96.88
2883.2			3288.2	96.64
3062.0			3291.3	95.70
3231.6			3288.0	94.84
3405.9			3286.4	95.23
3604.5			3298.9	96.48
3722.5			3296.8	96.41
3903.1			3285.2	93.44
4137.1			3284.4	93.98
4308.7			3105.5	87.03
4416.8			2955.0	73.67
4552.4			3290.9	95.86
4764.5			3289.0	95.94
4902.8			3294.4	95.70
5094.9			3290.8	97.56
5278.9			3293.1	93.38
5434.6			3291.0	97.03

TABLE 4.2.4-8 MICROBURN-B CALCULATED K-EFF AND AVERAGE VOIDS FOR SUSQUEHANNA 2 CYCLE 1 (CONT.)

Cycle Exposure (MWd/MTU)	k-eff	Average Voids	Power MWt	Flow 10^6 lb/hr
5599.9			3286.7	97.50
5756.8			3292.3	98.52
5941.6			3293.5	98.05
6106.3			3289.7	96.56
6271.0			3291.7	98.05
6433.2			3291.7	98.36
6621.5			3294.0	95.86
6857.7			3232.3	96.80
7081.3			3286.9	97.04
7198.9			3288.8	94.38
7363.7			3294.2	97.03
7498.3			3293.9	93.68
7630.6			2676.5	70.78
7810.9			3292.3	95.79
8001.1			3284.4	96.80
8188.1			3288.7	96.10
8361.1			3285.4	92.97
8390.0			3285.4	92.97
8469.4			3288.0	98.36
8654.6			3294.0	95.32
8787.1			3291.7	96.91
8971.3			3289.4	95.08
9112.5			3295.2	99.22
9275.0			3288.3	94.61
9463.4			3288.5	99.06
9594.2			3293.1	96.33
9758.7			3252.8	99.61
9896.3			3298.0	93.83
10108.0			3261.6	99.46
10266.8			3273.8	99.77
10426.3			3286.0	97.97
10614.1			3242.0	99.77
10704.5			3279.3	95.88
10915.4			3295.3	99.14
11076.3			3163.0	99.77
11264.2			3048.5	99.84
11346.8			3015.7	99.61
11493.9			2879.[illegible]	99.46

TABLE 4.2.4-8 MICROBURN-B CALCULATED K-EFF AND AVERAGE VOIDS FOR SUSQUEHANNA 2 CYCLE 1 (CONT.)

Cycle Exposure (MWd/MTU)	k-eff	Average Voids	Power MWt	Flow 10^6 lb/hr
11574.6			2806.7	99.85
11707.2			2684.9	99.85
11799.7			2620.0	100.00
11922.2			2555.9	99.93
12028.4			2437.8	99.46
12113.3			2373.2	99.93

TABLE 4.2.4-9 MICROBURN-B CALCULATED K-EFF AND AVERAGE VOIDS FOR SUSQUEHANNA 2 CYCLE 2

Cycle Exposure (MWd/MTU)	k-eff	Average Voids	Power MWt	Flow 10^6 lb/hr
156.6			3096.1	86.30
358.2			3291.1	96.40
534.5			3291.4	96.58
678.6			3291.7	94.80
893.7			3293.4	96.20
919.0			3290.0	96.80
1034.4			3290.0	96.80
1218.7			3293.0	95.50
1385.3			3292.9	97.70
1574.1			3291.1	95.90
1788.0			3290.8	95.90
1973.6			3291.6	95.50
2133.3			3290.8	95.30
2325.2			3290.7	95.10
2470.4			3292.5	94.90
2590.1			3291.9	95.00
2774.6			3292.2	98.10
2893.2			3291.6	95.60
3135.5			3294.6	95.80
3279.0			3291.7	96.60
3447.0			3291.7	[illegible].10
3622.4			3292.6	93.60
3795.5			3284.2	94.80
3873.7			3291.0	94.70
4034.1			3293.4	98.80
4200.3			3293.7	96.80
4371.3			3291.2	94.90
4539.0			3292.1	95.90
4707.2			3291.3	94.20
4844.3			3292.9	96.20
5093.8			3296.4	94.90
5235.2			3295.4	96.20
5382.2			3290.5	95.30
5526.6			3286.7	94.50
5670.9			3293.3	94.00
5829.3			3290.2	95.60
6021.9			3291.9	96.30
6214.5			3292.6	96.60

TABLE 4.2.4-9 MICROBURN-B CALCULATED K-EFF AND AVERAGE VOIDS FOR SUSQUEHANNA 2 CYCLE 2 (CONT.)

Cycle Exposure (MWd/MTU)	k-eff	Average Voids	Power MWt	Flow 10^6 lb/hr
6390.7			3292.5	96.70
6575.5			3292.9	97.30
6815.2			3290.0	98.40
7014.0			3293.5	94.10
7163.7			3291.5	96.40
7331.6			3288.9	97.40
7474.0			3286.4	97.10
7593.3			3286.3	91.20
7761.9			3290.9	94.10
7976.2			3289.8	96.90
8170.8			3291.0	97.20
8314.9			3292.1	96.40
8484.2			3292.3	96.70
8627.3			3292.1	95.20
8856.7			3084.8	91.30
9005.5			3289.5	96.00
9173.4			3292.0	98.10
9340.9			3290.9	94.80
9496.3			3290.1	98.20
9674.9			3290.3	93.70
9842.9			3289.6	98.20
10008.5			3291.9	93.70
10201.7			3293.9	99.30
10341.5			3292.6	96.80
10504.9			3289.0	94.40
10673.8			3290.1	100.10
10822.5			3180.8	99.70
10929.6			2012.2	48.30
10991.6			2008.8	61.00

TABLE 4.2.4-10 MICROBURN-B CALCULATED K-EFF AND AVERAGE VOIDS FOR SUSQUEHANNA 2 CYCLE 3

Cycle Exposure (MWd/MTU)	k-eff	Average Voids	Power MWt	Flow 10^6 lb/hr
189.1			3290.4	91.00
374.0			3294.6	98.10
481.7			3292.3	98.40
608.4			3292.3	98.30
747.2			3290.6	97.60
920.4			3293.8	96.60
1093.9			3292.1	97.20
1440.4			3290.3	94.30
1621.9			3292.3	92.90
1842.3			3292.3	93.00
1972.7			3293.2	94.90
2178.0			3292.9	95.80
2337.5			3294.7	94.40
2544.5			3296.0	95.50
2722.8			3294.2	95.90
2894.6			3292.5	94.60
3052.9			3293.1	96.70
3201.4			3293.3	96.00
3362.3			3293.5	96.40
3547.9			3293.0	95.00
3694.3			3293.4	97.00
3855.3			3292.5	95.40
4029.8			3291.4	95.10
4226.7			3295.5	94.10
4410.7			3295.7	95.60

TABLE 4.2.4-11 SUSQUEHANNA 2 CYCLES 1 THROUGH 3
COLD CRITICAL EIGENVALUES

Case	Cycle	k-critical
1	BOC1	
2	BOC1	
3	BOC1	
4	BOC1	
5	BOC1	
6	MOC1	
7	MOC1	
8	MOC1	
9	EOC1	
10	BOC2	
11	BOC2	
12	MOC2	
13	MOC2	
14	BOC3	
15	BOC3	

Pages 62 - 124 (Figures 4.1-1 - 4.2.4-2) have been deleted.

5.0 MEASURED POWER DISTRIBUTION UNCERTAINTY

The information presented below is intended to supplement Section 6 of the Reference 1 report XN-NF-80-19(P) "Exxon Nuclear Methodology for Boiling Water Reactors", Volume 1, "Neutronics Methods for Design and Analysis", Supplement 2. Section 6 of the referenced report described the ENC methodology for measuring the power distribution in a BWR reactor and the procedure by which the uncertainty associated with the measurement of a BWR power distribution would be determined using the XTGBWR core simulator code. In this report the same accepted procedure, employed to determine the uncertainties in the measured power distribution using the MICROBURN-B core simulator code, is presented and the measured power distribution uncertainties which result from application of this methodology to the data base are given.

The data base from which the values of the individual uncertainties are estimated consists of TIP (Traversing Incore Probe) system measurements and gamma scan measurements. The TIP system measurements are taken from 16 reactor cycles: Chinshan Unit 1, Cycles 5, 6, 7, 8; Kuosheng Unit 1, Cycles 1, 2, 3, 4, 5; Kuosheng Unit 2, Cycles 4, 5; Susquehanna Unit 1, Cycles 1, 2; Susquehanna Unit 2, Cycles 1, 2, 3. The gamma scan measurements were performed at the Quad Cities Unit 1 reactor at the end of Cycles 2, 3, and 4. Eighth core gamma scan measurements made at the end of Cycles 2 and 4. A total of seven UO_2 bundles were gamma scanned on a pin by pin basis.

The following sections reviews the accepted formulation and presents the results of the uncertainty analysis in detail. A detailed description of the measured power distribution determination procedure is given in Section 5.1. A derivation of the uncertainties associated with this determination of the measured power distribution is presented in Section 5.2. The quantification of the measurement uncertainties in terms of the primary sources of uncertainty is detailed in Sections 5.3.1 to 5.3.5 and the specification of the power distribution measurement uncertainty is presented in Section 5.3.6.

5.1 Measured Power Distribution Determination

Reactor measured power distributions are combinations of measured reactor data and computer calculated data. The measured reactor power distribution data include the fixed local power range monitor (LPRM) in-core detector data and the traversing in-core probe (TIP) detector data. The LPRM data are and the traversing in-core probe (TIP) detector data. The LPRM data are electric current readings proportional to the neutron flux level at four axial elevations in a number of radial locations. The radial locations are distributed in a uniform lattice throughout the core. The LPRM detectors are fission chambers using U-235 as the fissionable isotope. The LPRM detectors are intercalibrated utilizing the TIP data. The TIP system consists of a number of movable fission chamber detectors (about 1" long) which can each enter a number of the radial locations at which the fixed LPRM detectors are located. The movable TIP detectors are all capable of entering one of the radial positions to allow intercalibration of the TIP system. Figure 5.1-1 is a drawing of an in-core instrument tube which contains both the four LPRM detectors and the TIP tube. Figure 5.1-2 depicts typical radial locations for both fixed and movable in-core detectors in a BWR core. Each radial location contains the equipment shown in Figure 5.1-1.

The computer calculated data include the relative core nodal power distribution, the in-core detector response distribution, and the local peaking factors for the fuel rods. The predicted relative nodal power and detector response distributions are calculated with MICROBURN-B reactor simulator code described in Reference 2. The MICROBURN-B code is a three dimensional two group diffusion theory reactor simulator program. The code uses large mesh sizes to perform full core nodal power calculations with time dependent xenon and samarium.

The local peaking factors are calculated by the CASMO-3G code described in Reference 7. The CASMO-3G code is a bundle depletion model that performs a microscopic depletion of each fuel rod in the fuel assembly.

The synthesis of the measured power distribution can be viewed to occur in two phases. Phase I consists of the fixed LPRM in-core detector calibration. Phase II consists of combining the individual fixed LPRM in-core detector distribution measurements with MICROBURN-B calculated data to produce the measured power distribution. An outline of the procedure is presented here.

Pages 129 -132 have been deleted.

5.2 <u>Derivation of the Uncertainty in the Measured Power Distribution</u>

The uncertainty in the measured power distribution is derived based upon the definition of the measured power distribution

Pages 134 - 137 have been deleted.

5.3 Estimation of Uncertainty

The uncertainties,

are determined by comparison to measured data. The measured data consists of distributions of TIP detector responses plus gamma scan measurements of bundles and pins. The majority of the data consists of TIP distributions.

5.3.1 Synthesized TIP Distribution

utilizes measured and calculated data. The measured data consists of a relative distribution of fixed in-core detector response, F_{ijk}'. The fixed detectors are located at four axial elevations in each of a number of radial locations as shown in Figure 5.1-2. The fixed detector responses are calibrated to TIP system measurements at regular intervals and are adjusted for the reduction in sensitivity to the neutron flux as a function of burnup between calibrations to the TIP system.

The uncertainty in the synthesized TIP distribution is composed of three sources: the uncertainty due to the TIP system which is acquired through the calibration process, the uncertainty associated with the fixed in-core detector response itself, and the uncertainty added by the interpolation procedure which utilizes the calculated data.

The data base used to define the TIP measurement uncertainty is summarized in Table 5.3.1-1. Data were utilized from a number of cycles in five reactors: Chinshan Unit 1, Cycles 5 to 8; Kuosheng Unit 1, Cycles 1 to 5; Kuosheng Unit 2, Cycles 4 and 5; Susquehanna Unit 1, Cycles 1 and 2; Susquehanna Unit 2, Cycles 1 to 3.

The uncertainty in the LPRM detector response has been previously determined by General Electric in Reference 8. A value for δLPRM of 3.4% is reported in Section 3.1.2.2 of Reference 8. This is the value which will be used in this analysis.

The last term in the determination of the uncertainty in the synthesized TIP distribution is the synthesis procedure uncertainty. The synthesis procedure uncertainty is that portion of the uncertainty due to interpolation between LPRM axial locations. The synthesis uncertainty can be determined by measuring the TIP distribution and then creating a synthesized TIP distribution which uses the TIP distribution

5.3.2 Calculated TIP Uncertainty

The uncertainty in the calculated TIP response distribution can be determined by comparison to measured TIP distributions. The relative standard deviation in the calculated TIP distribution can be determined as follows:

The measured data base used to evaluate the calculated TIP distribution uncertainty is summarized in Table 5.1. The data were taken from full core TIP measurements at five reactors: Chinshan Unit 1, Cycles 5 to 8; Kuosheng Unit 1, Cycles 1 to 5; Kuosheng Unit 2, Cycles 4 and 5; Susquehanna Unit 1, Cycles 1 and 2; Susquehanna Unit 2, Cycles 1 to 3.

5.3.3 Calculated Power Distributions

The uncertainty in the calculated power distribution will be determined

Comparisons of the calculated power distributions to measured power distributions are presented in Section 5.3.5.

Pages 149 - 151 have been deleted.

5.3.4 Calculated Local Power Uncertainty

The pin power distribution is determined by multiplying the nodal power, B_{ijk}, by a local power distribution factor, L_{ijk}. Local factors for each fuel type are calculated by the CASMO-3G code and input to the MICROBURN-B code as a function of exposure, void, and control state (controlled or uncontrolled). MICROBURN-B interpolates among the input data to determine a value for the particular exposure, void and control state at node ijk.

The uncertainty in local peaking factors are determined by comparing the calculated pin powers to the pin-by-pin gamma scans of bundles which have been irradiated in a reactor. To perform the comparisons, the pin by pin power distributions from CASMO-3G must be converted to Ba-140 distributions, since the gamma scans measure Ba-140 distributions rather than power distributions.

5.3.5 Bundle Gamma Scan Comparisons

The correlation coefficients in the equation of Section 5.3.3 are determined from two gamma scan measurements. The gamma scan measurements measure the relative La-140 activity in irradiated bundles which is proportional to the power distribution of the bundles prior to shutdown. The gamma scan measurements utilized were performed at the Quad Cities Unit 1 reactor following Cycles 2 and 4. The Cycle 2 results are reported in Reference 9. The Cycle 4 results were taken from a draft copy of the results was obtained from EPRI.

To compare the MICROBURN-B calculated power distributions to the gamma scan results, Cycles 1, 2, 3 and 4 were modeled and depleted with the MICROBURN-B model. The power distributions obtained from these calculations were then converted to Ba-140 distributions for comparison to the gamma scan results. The conversion method from calculated power distributions to calculated Ba-140 distributions is detailed in Reference 9.

The comparisons of the calculated and measured bundle power distribution at the end of Cycles 2 and 4 are shown in Figures 5.3.5-1 and 5.3.5-2, respectively. The comparison and normalization of the relative distributions excludes all mixed oxide bundles and all bundles on the core periphery. The figures show only those bundles in an 1/8 core for simplicity in presentation. The exterior bundles were excluded since these bundles are of low power and therefore, not important from a safety standpoint. Inclusion of the edge bundles does not affect the resultant correlation coefficient or the relative standard deviations to a significant degree.

The comparisons shown in Figures 5.3.5-1 and 5.3.5-2 indicate that the agreement between the measured and calculated bundle power distributions is quite good. The largest deviations occur in the low power bundles near the core edge. The largest deviation in the core interior is 5.3%; the difference occurs in the Cycle 2 comparison. The relative standard deviations for the comparisons are as follows: two dimensional comparison, Cycle 2 - 1.98%; Cycle 4 - 2.00%; nodal distribution, Cycle 2 - Cycle 4 - The calculations appear better radially than axially.

S = relative standard deviation for bundle or nodal comparisons

$dx_n;dy_n$ = differences between calculated and measured bundle or nodal power for radially adjacent bundles or nodes.

5.3.6 Summary of the Measured Power Distribution Uncertainty

The measured power distribution uncertainty is derived in Section 5.2 based upon the formulation of the measured power distribution.

Pages 157 - 160 have been deleted.

TABLE 5.3.1-1 DATA BASE SUMMARY

Component	Data Source	No. of Two Dimensional Data Points	No. of Nodal/ Planar Data Points
TIP System	Reactor measurements: Chinshan Unit 1, Cycles 5,6,8 Kuosheng Unit 1, Cycles 1,2,3,4,5 Kuosheng Unit 2, Cycles 4,5 Susquehanna Unit 1, Cycles 1,2 Susquehanna Unit 2, Cycles 1,2,3		
LPRM	Report NEDO-20340 - June 1974		
TIP and Power Calculation, TIP Synthesis	Reactor measurements and MICROBURN-B calculations of the following: Chinshan Unit 1, Cycles 5,6,7,8 Kuosheng Unit 1, Cycles 1,2,3,4,5 Kuosheng Unit 2, Cycles 4,5 Susquehanna Unit 1, Cycles 1,2 Susquehanna Unit 2, Cycles 1.2,3		
Local Power within a Bundle	CASMO-3G calculations and gamma scan measurements for Quad Cities Unit 1, EOC 2,3,4, a total of 7 bundles in the three cycles		
Calculated Bundle Power, Correlation Coefficient	The above gamma scan data for bundles		

TABLE 5.3.1-2 TIP SYMMETRY UNCERTAINTY SUMMARY

			TIP Distribution Uncertainty (Relative Standard Deviations %)		
REACTOR	CYCLE	DATE	2D-BUNDLE	3D-NODAL	3D-PLANAR
CS1	5	03 25 83			
CS1	5	05 26 83			
CS1	5	06 22 83			
CS1	5	07 12 83			
CS1	5	09 02 83			
CS1	6	03 02 84			
CS1	6	04 17 84			
CS1	6	05 30 84			
CS1	6	07 11 84			
CS1	6	07 23 84			
CS1	6	08 23 84			
CS1	6	10 12 84			
CS1	6	11 08 84			
CS1	6	01 10 85			
CS1	6	02 06 85			
CS1	8	10 09 86			
CS1	8	12 26 86			
CS1	8	03 25 87			
CS1	8	06 30 87			
KS1	1	02 11 82			
KS1	1	09 07 82			
KS1	1	10 21 82			
KS1	2	10 13 83			
KS1	3	12 01 84			
KS1	4	12 21 85			
KS1	4	03 05 86			
KS1	4	06 04 86			
KS1	5	10 24 87			
KS2	4	10 23 86			
KS2	4	01 15 87			
KS2	4	04 08 87			
KS2	5	02 03 88			
KS2	5	04 25 88			
SQA	1	02 07 83			
SQA	1	08 10 83			
SQA	1	08 17 83			
SQA	1	12 02 83			
SQA	1	04 03 84			
SQA	1	04 12 84			

TABLE 5.3.1-2 TIP SYMMETRY UNCERTAINTY SUMMARY (CONT.)

			TIP Distribution Uncertainty (Relative Standard Deviations %)		
REACTOR	CYCLE	DATE	2D-BUNDLE	3D-NODAL	3D-PLANAR
SQA	1	05 31 84			
SQA	1	06 08 84			
SQA	1	06 25 84			
SQA	1	08 24 84			
SQA	1	09 04 84			
SQA	1	12 21 84			
SQA	2	07 19 85			
SQA	2	09 11 85			
SQA	2	09 27 85			
SQA	2	10 23 85			
SQA	2	01 14 86			
SQB	1	01 16 85			
SQB	1	04 04 85			
SQB	1	04 15 85			
SQB	1	08 02 85			
SQB	1	08 12 85			
SQB	1	08 20 85			
SQB	1	09 09 85			
SQB	2	02 05 87			
SQB	2	05 07 87			
SQB	2	08 21 87			
SQB	2	09 08 87			
SQB	3	07 18 88			
SQB	3	07 28 88			
SQB	3	09 22 88			
SQB	3	10 07 88			
SIGMA*					
NUM**					

* SIGMA = Average Relative Standard Deviation

** NUM = Number of Data Points Utilized in the Estimate

TABLE 5.3.6-1 MEASURED POWER DISTRIBUTION UNCERTAINTY COMPONENTS

Uncertainty Component	Relative Standard Deviation %

TABLE 5.3.6-1 MEASURED POWER DISTRIBUTION UNCERTAINTY COMPONENTS (CONT.)

Uncertainty Component	Relative Standard Deviation %

1

IMAGE EVALUATION TEST TARGET (MT-3)

150mm

6"

1

IMAGE EVALUATION TEST TARGET (MT-3)

150mm

6"

TABLE 5.3.5-2 MEASURED POWER DISTRIBUTION UNCERTAINTY

Type of Measured Power Distribution	Relative Standard Deviation %

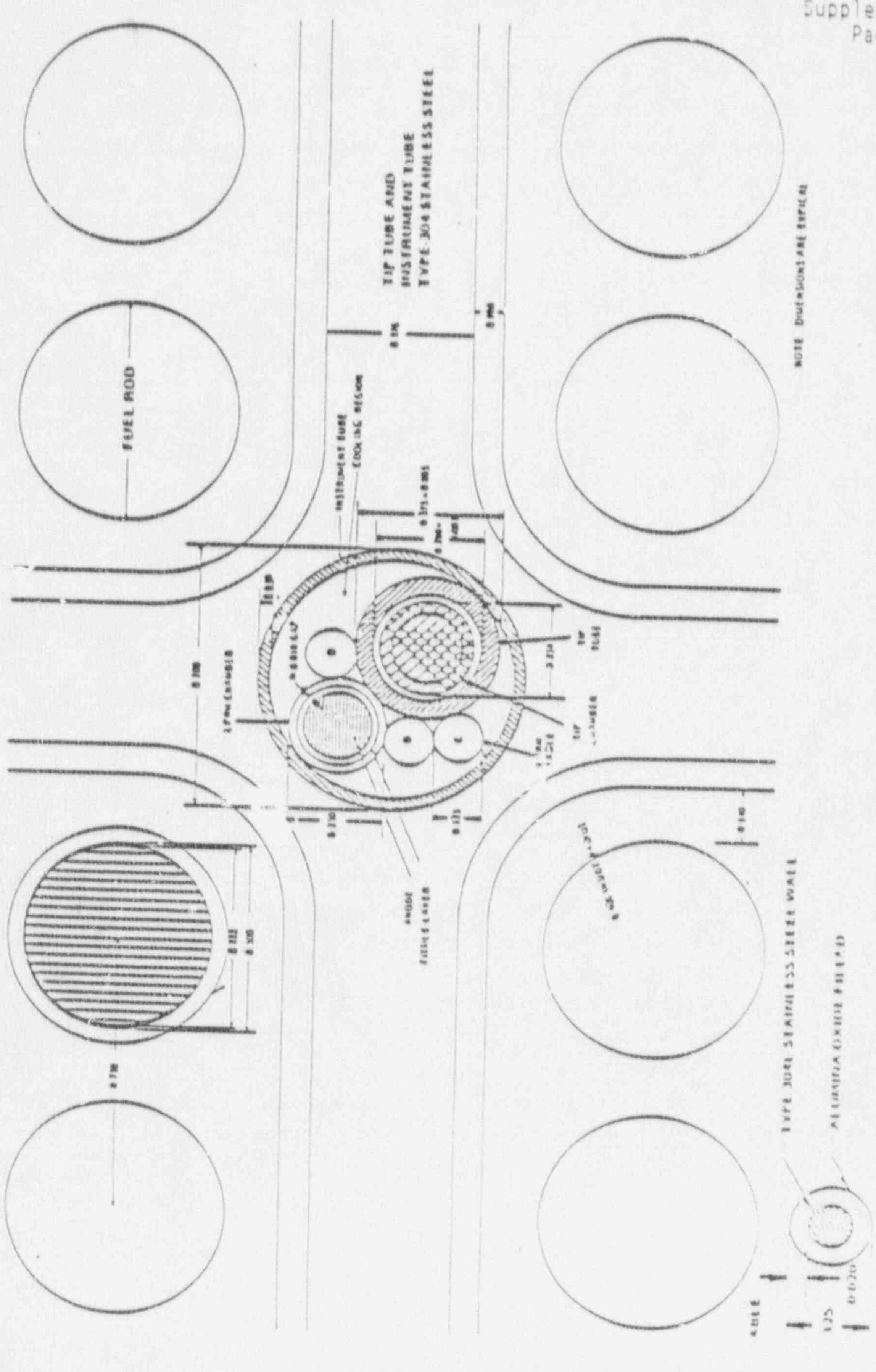

FIGURE 5.1.1 LPRM IN CORE ASSEMBLY CROSS SECTION

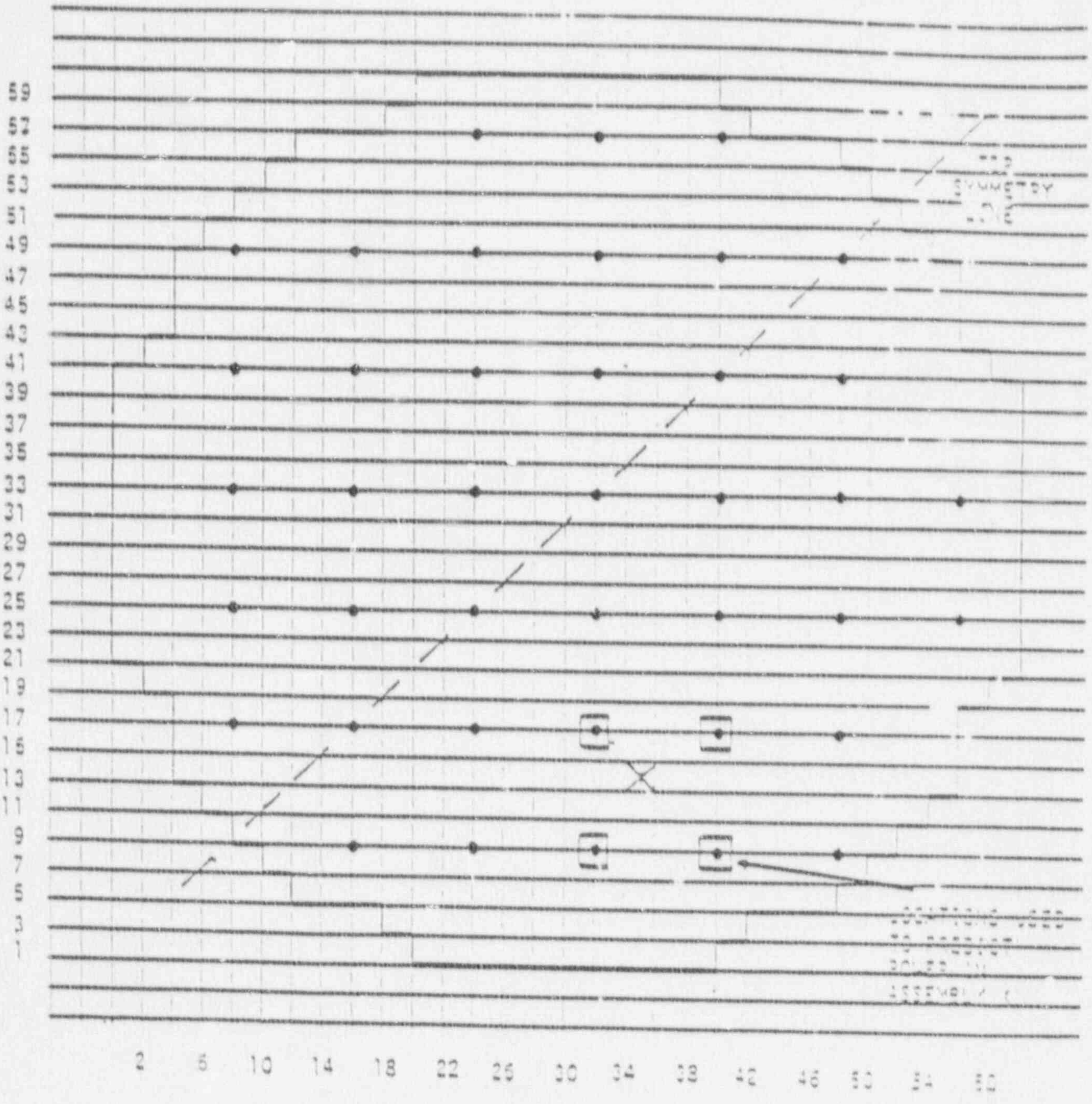

FIGURE 5.1-2 BWR TYPICAL INSTRUMENT LOCATIONS

Pages 169 - 176 (Figures 5.3.1-1 - 5.3.1-5, 5.3.2-1 - 5.3.2-2, and 5.3.4-1) have been deleted.

FIGURE 5.3.5-1 QUAD CITIES 1 LOC 2 ASSEMBLY GAMMA SCAN RESULTS
COMPARISON OF MEASURED AND CALCULATED BA 140 DISTRIBUTION

FIGURE 5.3.5-2 QUAD CITIES 1 EOC4 ASSEMBLY GAMMA SCAN RESULTS
COMPARISON OF MEASURED AND CALCULATED BA-140 DISTRIBUTION

6.0 REFERENCES

1. XN-NF-80-19(P)(A), Volume 1, Supplements 1 and 2, Exxon Nuclear Methodology for Boiling Water Reactors Neutronic Methods for Design Analysis, Exxon Nuclear Company, Richland, Washington 99352, March 1983.

2. ANF-88-101(P), MICROBURN-B: A Two-Group, Three Dimensional BWR Nodal Simulator Code, Advanced Nuclear Fuels Corporation, Richland, Washington 99352, July 1988.

3. M. B. Cutrone and G. F. Valby, Gamma Scan Measurements at Quad Cities Nuclear Power Station Unit 1 Following Cycle 2, EPRI NP-214, July 1976.

4. D. W. Merth and B. A. Zolotar, Gamma Scan Measurements of Quad Cities Nuclear Power Station Unit 1 Following Cycle 3, EPRI NP-512, July 1977.

5. Personal Communication from B. A. Zolotar (EPRI) to J. S. Holm (ENC), February 1981.

6. ANF-88-175(P), Kuosheng 1 Cycle 6 Startup and Operations Report, Advanced Nuclear Fuels Corporation, Richland, Washington 99352, November 1988.

7. Studsvik/NFA-86/8, CASMO-3: A Fuel Assembly Burnup Program (Methodology), Studsvik Energiteknik AB, Nyköping, Sweden, November 1986.

8. NEDO-20340, Process Computer Performance Evaluation Accuracy, J. F. Carew, General Electric Company, June 1974.

9. EPRI-NP-21114, Gamma Scan Measurements at the Quad Cities Nuclear Station Unit 1 Following Cycle 2, Electric Power Research Institute, Palo Alto, California, July 1976.

Appendices A-1 - E-25 (Figures A-1 - E-6) have been deleted.

ADVANCED NUCLEAR FUELS CORPORATION

XN-NF-80-19(NP)(A)
Volume 1
Supplement 3
Appendix F
Issue Date: 04/09/90

ADVANCED NUCLEAR FUELS METHODOLOGY FOR BOILING WATER REACTORS

BENCHMARKING FOR THE CASMO-3G/ MICROBURN-B CALCULATION METHODOLOGY

APPENDIX F

D-LATTICE CASMO-3G/MICROBURN-B METHODS VERIFICATION

Prepared by: J. L. Maryott

APPENDIX F

D-LATTICE CASMO-3G/MICROBURN-B METHODS VERIFICATION

F.1 INTRODUCTION

Calculations have been performed for the Dresden 2 and 3 D-lattice BWR reactors using the ANF CASMO-3G/MICROBURN-B methods presented in XN-NF-80-19(P) Volume 1, Supplement 3. The MICROBURN-B reactor core simulator code is verified for D-lattice plants by comparing calculated reactor parameter to the measured reactor parameters. The hot operating k-eff values and the startup critical cold k-eff values calculated by MICROBURN-B are summarized for the last four cycles of reactor operation.

Measured and calculated traversing incore probe (TIP) data for the Dresden 2 and 3 reactors have been compared and uncertainty analysis performed. The data shown is typical for beginning of cycle, middle of cycle, and end of cycle for each of the reactors. All MICROBURN-B calculations were performed with a full core model using 24 axial nodes.

F.2 DRESDEN 2 CYCLE 9 THROUGH 12

CASMO-3G/MICROBURN-B core follow calculations have been performed for Dresden 2. Pertinent reactor core parameters at rated operating conditions for the Dresden units are given in Table F-1. Table F-2 summarizes the fuel loaded in Dresden 2 Cycles 9 through 12. Results of measured versus calculated TIP comparisons and core k-eff have been made for the Dresden 2 cycles loaded with ANF fuel. TIP comparisons for Dresden 2 are plotted in Figures F-3 through F-122.

Tables F-3 to F-6 summarize the calculated hot operating k-eff and average voids versus cycle exposure for Cycles 9 through 12. Hot k-eff values are plotted versus core exposure for Cycles 9 through 12 in Figure F-1. The cold k-critical values for Dresden 2 are summarized in Table F-7.

F.3 DRESDEN 3 CYCLE 8 THROUGH 11

CASMO-3G/MICROBURN-B core follow calculations have been performed for Dresden 3. Table F-8 summarizes the ANF fuel loaded in Dresden 3 Cycles 8 through 11. Results of measured versus calculated TIP comparisons and core k-eff have been made for Cycle 8 through 11. Tip comparisons for Dresden 3 are plotted in Figures F-123 through F-242.

Tables F-9 to F-12 summarize the calculated hot operating k-eff and average voids versus cycle exposure for Cycles 8 through 11. Hot k-eff values are plotted versus core exposure for Cycles 8 through 11 in Figure F-2. The cold k-critical values for Dresden 3 are summarized in Table F-13.

F.4 UNCERTAINTY ANALYSIS FOR D-LATTICE PLANTS

The results of an uncertainty analysis using the D-lattice data presented herein is shown in Table F-14. The methods used to perform the analysis are discussed in Section 5.0 of XN-NF-80-19(P) Volume 1, Supplement 3.

F.5 SUMMARY

Core follow calculations for the D-lattice Dresden plants show good agreement. The calculated hot critical eigenvalues plotted in Figures F-1 and F-2 are consistent between cycles. Cold critical eigenvalues are similar to the hot critical eigenvalues and are consistent from cycle to cycle. Comparisons of measured and calculated TIP data are good. In summary, the CASMO-3G/MICROBURN-B code system accurately predicts the neutronic behavior of the D-lattice plants.

Pages F-3 - F-261 (Tables F-1 - F-14 and Figures F-1 - F-242) have been deleted.

ADVANCED NUCLEAR FUELS CORPORATION

XN-NF-80-19(NP)(A)
Supplement 4

Issue Date: 11/30/90

NRC CORRESPONDENCE

ADVANCED NUCLEAR FUELS CORPORATION

2101 HORN RAPIDS ROAD, PO BOX 130, RICHLAND, WA 99352-0130
(509) 375-8100 TELEX 15-2878

RAC:022:90
March 16, 1990

Mr. R. C. Jones, Chief
Reactor Systems Branch
Division of Engineering and System Technology
Office of Nuclear Reactor Regulation
U. S. Nuclear Regulatory Commission
Washington, D.C. 20555

Dear Mr. Jones:

Subject: Responses to NRC questions on CASMO-3G/MICROBURN-B

Reference 1: Letter, R. C. Jones (NRC) to R. A. Copeland (ANF), "Request for Additional Information Regarding the Topical Report XN-NF-80-19 (P), Supplement 3," dated February 2, 1990.

Reference 2: Letter L. A. Nielsen (ANF) to L. Lois (NRC), "Draft Responses to NRC question on CASMO-3G/MICROBURN-B," dated February 23, 1990.

Reference 3: Meeting L. A. Nielsen (ANF) and L. Lois (NRC), "Draft Responses to NRC question on CASMO-3G/MICROBURN-B," February 15, 1990.

Reference 4: Letter, R. A. Copeland (ANF) to Director NRR (NRC), "Submittal of MICROBURN-B," dated March 8, 1989 (RAC:010:89).

Attached are the ANF responses to the 34 items of additional information on CASMO-3G/MICROBURN-B requested in the Reference 1 letter. The 32 draft responses previously transmitted (Reference 2) are unchanged. Confirming our conversation in the February 15 meeting (Reference 3), ANF is intending to use CASMO-3G/MICROBURN-B to perform licensing calculations for "C" and "D" lattice plants and for plants using Fission and/or Gamma TIPs. Additional information showing detailed analyses of "D" lattice plants are being transmitted under separate cover.

The information in the attached responses is proprietary to ANF. The affidavit submitted with the transmittal of the original submittal, Reference 4, provides the necessary information as required by 10 CFR 2.790(b) to support the withholding of the attached from public disclosure.

Please contact Larry Nielsen on (509) 375-8358 if you have additional questions or need more information.

Sincerely,

Bob Copeland

R. A. Copeland
Manager, Reload Licensing

/skm
cc: Dr. L. Lois (USNRC)
Enclosures

ATTACHMENT

RESPONSES TO NRC QUESTIONS ON CASMO-3G/MICROBURN-B

CONTRIBUTORS: OC BROWN
GR CORRELL
RG GRUMMER
ALB HO
CW LINDENMEIER
JW MARYOTT
LA NIELSEN
DH TIMMONS
TA WELLS

March 1990

NRC QUESTIONS ON CASMO-3G/MICROBURN-B

Reference: XN-NF-80-19(P), Vol. 1, Supplement 3, "Advanced Nuclear Fuels Methodology for Boiling Water, Benchmark Results For the CASMO-3G/MICROBURN-B Calculation Methodology," February 1989.

1. What are the uncertainties in the CASMO-3G/MICROBURN-B calculated input to ANF Licensing Safety Analyses (e.g., DOPPLER coefficient, moderator temperature coefficient, delayed neutron fraction, shutdown margin, etc.)?

Reference: ANF-913(P), Vol. 1, Supplements 1, 2, and 3, "COTRANSA2: A Computer Program for Boiling Water Reactor Transient Analyses," May 18, 1988.

ANSWER: ANF performs licensing safety analyses with the COTRANSA2 (Ref) transient analysis code. The input from the CASMO-3G/MICROBURN-B code to COTRANSA2 includes best estimate core average cross sections (axially dependent), Doppler coefficient, delayed neutron fraction, core flow, and moderator density coefficient. Use of these and other best estimate system parameters have been verified by analyzing and comparing results against the Turbine Trip test measurements performed at Peach Bottom. Additional Comparisons to analytical results from other models were made by performing an analysis of the NRC Licensing Basis Transient.

Uncertainties associated with shutdown margin and the critical eigenvalues are addressed in Questions 14 and 15 attached herein.

2. Will CASMO-3G be used to calculate TIP detector-to-power factors for gamma TIPs? If so, provide verification for this application. Also, how is the gamma flux related to the bundle power in this case?

ANSWER: Yes, the standard CASMO-3G treatment of gamma TIPs is used. See Section 12 of STUDSVIK/NFA-86/8. In this treatment the detector response is calculated from:

Studsvik has benchmarked this approach against both Monte Carlo calculations and against Hatch data as reported in Transactions ANS, Vol. 47, p. 434, Washington, November 1984 and Transactions ANS, Vol. 49, p. 431, Boston, June 1985 (Attachment 3). It is concluded that gamma detector calculations using the integral transport theory model (COXY) in CASMO yield accurate results.

3. Will CASMO-3G/MICROBURN-B be applied to new fuel designs (lattice geometry, water holes, enrichment, Gd zoning, etc.) which are outside the range of the Supplement 3 verification data base? Provide justification for these applications.

ANSWER: The CASMO-3G/MICROBURN-B code package will be used to model and analyze advanced fuel designs. The benchmark calculations performed for CASMO-3G/MICROBURN-B in Supplement 3 show that the codes can handle a wide variety of fuel design differences. The benchmark calculations which show good agreement with measurements were performed using only mechanical design input parameters.

4. To what plants will the CASMO-3G/MICROBURN-B methods be applied, and how does the Chinshan 1, Kuosheng 1 and 2, and Susquehanna 1 and 2 data base support these applications?

ANSWER: The CASMO-3G/MICROBURN-B code system will be applied to GE BWR/2, BWR/3, BWR/4, BWR/5 and BWR/6 class plants in the United States.

5. What is the recommended method (diffusion theory or the B-1 approximation) for calculating the fundamental mode solution used to modify the infinite lattice results to account for leakage effects in CASMO-3G? Provide justification for the selection of this option.

Pages 7-9 have been deleted.

6. Provide details of the thermal-hydraulic model used in the MICROBURN-B calculations.

Reference 1: XN-NF-80-19(P)(A) Vol. 1, and Supplements 1 and 2, "Neutronics Methods for Design and Analysis," April 1982.

Reference 2: XN-NF-79-59(P)(A), "Methodology for Calculation of Pressure Drop in BWR Fuel Assemblies," November 1983.

ANSWER: ANF's existing NRC approved BWR thermal hydraulics methodology is used in MICROBURN-B. Thus, the thermal hydraulics model is identical to that used in the NRC approved XTGBWR calculations. This methodology is described in References 1 and 2.

7. Are radial and/or axial flux discontinuity factors used in CASMO-3G\MICROBURN-B? If so, provide a discussion of the determination and application of these factors. Were the factors determined by comparison with the measured data in the verification data base?

Reference: ANF-88-101(P), "MICROBURN-B: A Two Group, Three Dimensional BWR Nodal Simulator Code," July 1988.

8. How are the radial and axial reflectors treated in MICROBURN-B? Are the reflectors modeled explicitly or implicitly via a boundary condition? Do the reflector parameters vary during a fuel cycle or from cycle to cycle?

ANSWER: The treatment of boundary conditions in MICROBURN-B is described in Section 3.2.2 of ANF-88-101(P).

9. What other changes have been introduced with MICROBURN-B, in addition to the explicit calculation of isotopics and the use of CASMO-3G?

ANSWER: A summary of the core simulator improvements is presented in Sections 2.0-2.3 of ANF-88-101(P). The principal model enhancements, in addition to nodal depletion of key isotopes and the use of CASMO-3G,

10. Since control-history is no longer used in MICROBURN-B, how is the effect of control-history on the bundle pin-wise power distribution and on the detector response-to-power factors accounted for?

ANSWER: The node dependent reactivity effects due to control-history (as well as void-history, Doppler-history, and boundary-spectral-history) are determined by the nodal depletion model. The effect of control-history on the bundle pin-wise power distribution is treated in MICROBURN-B by the formulation utilized in XTGBWR.

11. Provide typical comparisons of CASMO-3G/MICROBURN-B and XFYRE/XTGBWR predictions of the safety analysis input parameters.

ANSWER: Table 2 presents comparisons of the pressure coefficient, Doppler coefficient, and delayed neutron fraction for a reload cycle of a BWR/6 licensing analysis with the XFYRE/XTGBWR and CASMO-3G/MICROBURN-B code systems.

TABLE 2 TYPICAL COMPARISON OF NEUTRONICS
INPUT TO LICENSING ANALYSIS

12. How do the CASMO-3G/MICROBURN-B procedures/models for the hot and cold calculations differ ((e.g.), libraries, thermal-hydraulic parameters, etc.)?

ANSWER: The CASMO-3G cross-section library contains absorption, fission, nu-fission, transport and P0 scattering cross sections (and for hydrogen, deuterium and oxygen also P1-scattering cross sections, which are used only in the B_1 fundamental mode calculation). Data are tabulated as function of temperature when needed. For U-235, U-236, U-238 and Pu-239 shielded resonance integrals versus potential background cross section and temperature are tabulated. The library also contains yield values for fission products and decay constants. For temperatures other than those present in the table, cross-section are determined by interpolation. Saturated water densities at the specified temperature are used for cold (<500°F) calculations. Thermal hydraulic feedback is not present for cold conditions.

13. Have any plant or cycle specific normalizations been used in the CASMO-3G/MICROBURN-B calculations to improve agreement with the measurement data? If so, will the calculational uncertainties increase for plants or cycles where this data s not available?

ANSWER: No. There are no plant or cycle specific adjustable parameters in the CASMO-3G/MICROBURN-B calculations.

14. Why are the mean and standard deviation only calculated for certain sets of cold critical measurements?

15. How do the MICROBURN-B and XTGBWR predictions of hot and cold critical measurements compare (i.e., mean and standard deviation)?

ANSWER: In general, MICROBURN-B provides a better prediction for both cold and hot conditions. The following comparisons between the MICROBURN-B and XTGBWR critical eigenvalues for Kuosheng Units 1 and 2 are provided.

TABLE 3: KUOSHENG UNITS 1 AND 2
HOT CRITICAL EIGENVALVUES

MICROBURN-B	XTGBWR

16. In the CASMO-3G calculations, are four bundles or just a single fuel bundle modeled?

17. The comparisons of the Quad Cities-1 gamma scan and CASMO-3G pin-wise power distributions indicate a systematic (nonconservative) underprediction of the highest powered pin. Also, the largest calculation-to-measurement differences tend to occur at low instantaneous voids (VI=0.0). Therefore, discuss the effect of biases in the CASMO-3G predictions at the most limiting locations and how are they accounted for in the determination of the Safety Limit MCPR?

ANSWER: For most of the reported measured gamma scan data, the maximum measured local power value varies from rod to rod in adjacent axial planes and varies across the diagonal line of symmetry in a given axial plan. The random location of the maximum measured rod power in the assembly is an indication of measurement uncertainties rather than an indication of a calculation problem. The local power uncertainty used in the ANF MCPR safety limit calculations is the value calculated from the reported results with no correction due to measurement errors or flux tilt effects.

The critical heat flux tests performed by ANF for boiling water reactors shows the critical heat flux to occur close to the top of the fuel assembly where the void fraction is high; thus the uncertainty in the local peaking at low instantaneous void is less important.

18. Have comparisons of CASMO-3G to the XMC Monte Carlo code (or other independent calculations benchmark) been made, as were included in Supplement 2 for XFYRE? If so, how does the standard deviation for the comparisons compare with the standard deviation inferred from the Quad Cities-1 gamma scan?

19. What is causing the increase in the k_{eff} bias with fuel exposure (e.g., Figures 4.2.1-1 and 4.2.4-2)and how is this accounted for in the licensing analyses?

20. Do the CASMO-3G/MICROBURN-B calculational uncertainties and biases increase at the high exposures expected for high burnup fuel?

ANSWER: No high burnup trends in the calculational uncertainties and biases have been observed. If gross reactivity biases which are a function of fuel burnup were to be present, they would be apparent in the reactor eigenvalue versus cycle exposure plots (Figures 4.2.1-1 through 4.2.4-2 in XN-NF-80-19(P), Volume 1, Supplement 3). These data show a significant consistency which is independent of reactor size, fuel design, operating philosophy, and cycle number. Of particular importance is the fact that the reactor eigenvalue at the end of each cycle is very consistent, independent of whether the calculations are for first-cycle cores (low average discharge exposure), or for fourth-cycle cores (high average discharge exposure).

If calculational uncertainties were increasing with fuel exposure, this trend would be apparent from the comparisons of measured and calculated TIPs. However, the results presented in Appendices A, B, D, and E show that end-of-cycle TIP comparisons are as good as, or better than, corresponding beginning-of-cycle and middle-of-cycle TIP comparisons. Again, these observations are true for high exposure cores, as well as low exposure cores.

21. Are the TIPs used in the verification data-base comparisons (Appendices A, B, D, and E) fission or gamma TIPs.

ANSWER: All TIP results reported in XN-NF-80-19(P), Volume 1, Supplement 3 are for fission TIPs.

22. Have any statepoint comparisons been deleted from either the k_{eff} critical or the power distribution verification data-base? If so, provide justification for the deletion or include the statepoints in the data-base.

ANSWER: In addition to those TIP data mentioned in Question 27, there are some k_{eff} critical and TIP data which were excluded from the data-base. The operating conditions of these data points were evaluated during the data-base collection. The points were excluded whenever the operating conditions were not at equilibrium or the recorded operating conditions were questionable.

23. Have the cold critical eigenvalues been corrected for temperature and reactor period? If not, what are the corrected eigenvalues and corresponding standard deviations?

ANSWER: All cold critical eigenvalues in Supplement 3 have been corrected for temperature and reactor period. In addition reactor downtime at the time of the test is also taken into account.

24. In Figure B-15, what is causing the large overprediction of the nodal peaking factor (1.8 vs. 1.4) at XTG location (18,24)?

ANSWER: The results presented in Figure B-15 are a comparison of measured and predicted TIPs for Kuosheng Unit 2, Cycle 4. This is one of the few comparisons for the CASMO-3G/MICROBURN-B methodology verification calculations in which the TIP discrepancies are this large. In fact, this is the worst comparison observed for the verification data base. Although the TIP discrepencies appear larger than expected, it should be noted that the standard deviation of the differences between measured and predicted TIPs for this case is less than twice the average standard deviation for the entire data base This TIP set has been included in the data base for the uncertainty analysis. Therefore, it's contribution has been included in the computation of the uncertainty components which are to be used for determining the core operational safety limits.

25. Are the recommended ANF CASMO-3G/MICROBURN calculation procedures (selection of code options, numerical convergence and mesh, thermal and hydraulic correlations, geometrical modeling, etc.) the same as used in calculating the verification data-base? If not, what is the effect of these differences on the inferred calculational uncertainties?

ANSWER: The recommended calculation procedures for performing neutronic analyses are the same that were used in generating the verification data-base.

26. Why was the Dresden Cycle 2 and 3 and Quad Cities 1 and 2 TIP data used in XN-NF-80-19(P) Supplements 1 and 2 excluded from the power distribution measurement data-base of Supplement 3?

ANSWER: The MICROBURN-B calculations for the methodology verification data base were chosen to represent a variety of reactor sizes and types and to be as recent as possible. The data for reactor cycles in operation prior to 1982 were considered as not being representative of current practices in fuel design, core loading, and operating strategy. The exception to this approach of choosing the verification data base was Quad Cities Unit 1. The QC1 calculations were performed to provide comparisons between gamma scan measurements and predictions.

TABLE 4

MEASURED POWER DISTRIBUTION UNCERTAINTY SUMMARY

27. Why is the TIP symmetry for the Chinshan 1, Kuosheng 1 and 2, and Susquehanna 1 and 2 plants used in Supplement 3 a factor of 2.5 times less than the TIP symmetry for the Dresden 2 and 3 and Quad Cities 1 and 2 plants used in Supplements 1 and 2?

28. The large difference between the verification data of Supplement 3 (Chinshan 1, Kuosheng 1 and 2, and Susquehanna 1 and 2) and the verification data of Supplements 1 and 2 (Dresden 2 and 3 and Quad

Cities 1 and 2) indicate a basic difference between these plants. This difference suggests that the data should not be combined statistically and the power distribution measurement uncertainty should be determined separately for these plants. Please discuss this apparent plant dependence of the power distribution measurement uncertainties, especially with respect to their use in the determination of the MCPR safety limit.

ANSWER: Table 4 included in the response to Question 26 confirms your observation. There appears to be a systematic difference between C Lattice plants (Supplement 3) and D Lattice plants. Therefore, ANF proposes to use a different set of uncertainty components for the evaluation of the MCPR safety limit for D Lattice plants.

29. Since Quad Cities 1 Cycles 1-4 have been calculated with CASMO-3G/MICROBURN-B, why haven't they been included in the verification comparisons?

ANSWER: The Quad Cities 1 calculations were performed primarily to utilize the gamma scan measurements (Figures 4.1-1 through 4.1-56 and Appendix C). The measured vs. predicted TIP comparisons (Appendix D) were included only for illustrative purposes. It was recognized at the time Supplement 3 was prepared that the large TIP asymmetries associated with Quad Cities 1 preclude their inclusion in the statistical uncertainty analysis data base.

Subsequent CASMO-3G/MICROBURN-B calculations for recent cycles of Dresden 2 and 3 have been combined with the Quad Cities 1 calculations in a supplementary D Lattice uncertainty analysis. The results are presented in Table 4 in the response to Question 26. The TIP asymmetries observed in the Dresden 2 and 3 data are comparable to those observed in the Quad Cities 1 data, so it was concluded that statistical combination of the data sets is acceptable.

30. The MICROBURN-B nodal power calculated using Equation (5.1) requires the measured detector distribution. How does MICROBURN-B calculate the power distribution when measurement data is not available, and what is the uncertainty associated with this calculation?

(5.2)).

31. If MICROBURN-B will be used with gamma detectors, what is the measurement uncertainty associated with Equation (5.1) in this case?

From EPRI NP-540

Table 1
HATCH 1 TIP TEST ASYMΛ ETRY RESULTS

		Nodes 3-22				A			
Data Set	Data	String Mean Ratio	String Standard Deviation (%)	Nodal Mean Ratio	Nodal Standard Deviation (%)	String Mean Ratio	String Standard Deviation (%)	dal an tio	Nodal Standard Deviation (%)
1	T	0.992	6.57	0.994	8.07	0.993	6.26	98	8.46
	G	0.980	2.77	0.980	5.48	0.981	2.64	30	6.29
	F	1.031	9.92	1.023	12.30	1.038	10.60	30	17.20
2	T	0.990	6.79	0.990	8.20	0.990	6.57	12	8.72
	G	0.996	2.54	0.995	5.78	0.996	2.29	15	6.40
	F	1.003	4.65	1.012	12.12	1.006	4.89	6	26.35
3	T	0.994	6.93	0.995	8.35	0.994	6.65	8	8.63
	G	0.997	2.33	0.995	5.32	0.997	2.28	8	6.26
	F	1.052	12.03	1.058	17.40	1.061	12.85	5	23.80
Av	T	0.992	6.76	0.993	8.21	0.992	6.49	)	8.60
	G	0.991	2.54	0.990	5.53	0.991	2.40		6.32
	F	1.017	7.28	1.017	12.21	1.022	7.75		21.78

Note: In this analysis the sample size for the string ratios consists of 13 symmetric pairs sizes for nodal calculations are 260 and 312.

32. In Equation (5.1) how are the Wkk' determined? If they were determined using the data in the verification data-base, will the power distribution measurement uncertainty be larger for plants not included in the data-base?

ANSWER: The Wkk' are weighting factors used in synthesizing the "measured TIP response", from the LPRM detector measurements and the predicted TIP response.

33. Provide a flow chart showing the complete set of individual CASMO-3G depletion calculations performed for a typical fuel assemble. Identify all branch calculations.

ANSWER: Details of the depletion steps are dependent upon the fuel design. Typically, fine time steps (500 MWd MTU) are used where the gadolinia has a major influence on neutronic behavior. Depletions steps are increased to 2500 MWd/MTU near end of life.

Branch calculations are performed to generate controlled cross-sections, as well as cold cross-sections. Table 5 shows a typical matrix of restart calculations. Doppler restart calculations are also performed at the indicated exposures. Both controlled and uncontrolled solutions may be performed, if required.

TABLE 5 TYPICAL RESTART SOLUTION MATRIX

34. Provide a list of the isotopes for which microscopic cross sections are used to calculate the nodal burnup. How are the fission products treated? Identify the remaining isotopes which are lumped into macroscopic cross sections as a function of exposure and void fraction.

PERFORMANCE OF GADOLINIA BURNABLE ABSORBER ASSEMBLIES AT BURNUPS UP TO 50,000 MWD/MTU

FB Skogen/A Hilton O'Leary
Advanced Nuclear Fuels Corporation
2101 Horn Rapids Road
Richland, Washington 99352

KE Karcher
Carolina Power & Light Company
411 Fayetteville Street
Raleigh, North Carolina 27602

INTRODUCTION

The utilization of gadolinia as a burnable absorber has become a standard fuel design feature applied by Advanced Nuclear Fuels Corporation (ANF) in the design of reload cores for pressurized water reactors (PWRs). The use of gadolinia-bearing fuel reduces beginning-of-cycle boron requirements, allows low radial leakage fuel management and extended operating cycles, and provides significant flexibility in fuel cycle designs relative to other burnable absorber alternatives. Gadolinia is the preferred burnable absorber because it requires no encapsulating hardware not otherwise provided for the fuel and has a reduced end-of-cycle residual reactivity penalty relative to boron burnable absorbers thereby leading to enhanced fuel cycle economics. Since no special storage and handling of gadolinia-bearing fuel is required either during reactor refueling outages or following discharge of the fuel, more economical plant operation is obtained. By incorporating the absorber directly into the fuel rods, all control rod positions are kept available and the average linear heat generation rate is not impacted. The design flexibility offered by gadolinia is further enhanced by the ANF removable upper tie plate which, when combined with the relatively short lead time required to fabricate gadolinia-bearing fuel rods, can permit design adjustments to be made after assembly fabrication has been completed.

ANF has achieved predictable neutronic performance and excellent fuel integrity in its supply of gadolinia-bearing fuel for light water reactors, including nine domestic and foreign PWRs, where gadolinia-bearing fuel rods have been routinely incorporated. Fuel rods with concentrations of up to 10 w/o gadolinia continue to be successfully utilized in low radial leakage and extended operating cycle fuel management schemes. In order to illustrate the attributes of the gadolinia burnable absorber, the HB Robinson (HBR) Unit 2 reactor has been chosen for more detailed discussion in a subsequent section. ANF and Carolina Power and Light Company (CP&L) have recently initiated the utilization of gadolinia concentrations up to 10 w/o in HBR Unit 2. The Cycle 9 core of HBR Unit 2 is also a good example of how the gadolinia design features can be utilized to optimize a cycle design even after the fuel has been fully fabricated.

IRRADIATION EXPERIENCE

Nearly 37,000 of ANF's gadolinia-bearing fuel rods in about 6,400 assemblies have been irradiated in twenty-five (25) reactors: 9 PWRs and 16 BWRs. The initial loading of ANF gadolinia-bearing fuel in a PWR core occurred at Palisades in 1978 and consisted of four pins of 1 w/o gadolinia in each of eight assemblies. As experience was gained in the manufacture of gadolinia-bearing fuel rods, and as operational data was acquired to benchmark the physics models, the quantities of gadolinia incorporated into reload batches, as well as the gadolinia concentrations, were increased. A total of about 5,300 gadolinia-bearing rods are or have been irradiated in PWRs. Table 1 gives an overview of ANF's gadolinia burnable absorber experience in PWRs. No fuel failures occurred in any of the gadolinia-bearing rods. A maximum assembly exposure of about 50,000 MWd/MTU has been achieved in Tihange-1 in a joint cooperative program with SEMO Exploitation in Belgium for monitoring the performance of lead assemblies initially loaded with 6 w/o gadolinia. Peak gadolinia-assembly exposures exceeding 43,000 MWd/MTU have been achieved in gadolinia-bearing reload batches with an average reload discharge exposure of about 40,000 MWd/MTU.

The use of gadolinia has not impacted the accuracy of current predictions for cycle length, and radial and axial power distributions. Calculated and measured assembly average powers typically agree within 3%. Predicted and measured soluble critical boron concentrations typically agree to within 30 ppm. (Examples are given in a subsequent section for HB Robinson Unit 2). Refinements to the calcula-

TABLE 1 ADVANCED NUCLEAR FUELS
GADOLINIA-BEARING FUEL ROD EXPERIENCE
IN PRESSURIZED WATER REACTORS

Gadolinia Concentration	No. of Gadolinia-Bearing Fuel Rods	No. of Gadolinia-Bearing Assemblies	Maximum Assembly Burnup, MWd/MTU
2.0 w/o	432	108	42,000
4.0 w/o	3,912	501	43,100
6.0 w/o	192	24	14,900
8.0 w/o	672	72	50,000
10.0 w/o	64	12	32,700
Total	5,272	717	

tional tools continue to be made. The evolution of the gadolinia calculational methodology has led to the adoption (by ANF) of the CASMO/MICBURN code package for the determination of the depletion characteristics of PWR fuel designs. The CASMO code in conjunction with the ANF core simulator code XTGPWR has been extensively benchmarked against operating data for several PWRs operating with significantly different fuel cycle scenarios.

FUEL ROD PERFORMANCE

The physical behavior of the gadolinia-bearing fuel has been monitored through a number of programs that include both poolside and hot-cell examinations. The absorber fuel has been examined over a range of burnup levels by performing poolside examinations both during reactor refueling outages and after fuel discharge, and by withdrawing rods for hot-cell examinations at intermediate exposures as well as at discharge. Electricite' de France (EdF), Rheinisch-Westfalisches Elektrizitatswerk (RWE), Intercom, and ANF are participating in a cooperative program to study the behavior of 4 and 8 w/o gadolinia burnable absorber fuel in two European reactors (Biblis A and Tihange-1).

Eight w/o gadolinia-bearing fuel rods at Tihange-1 have been inspected at poolside along with non-absorber fuel after one and three cycles of operation at assembly average burnups of about 13,200 and 37,000 MWd/MTU, respectively. The exposure history of both the UO_2 and gadolinia-bearing fuel rods is given in Table 2. The fuel rods inspected at poolside were in excellent condition after both one and three cycles of irradiation. Some of the gadolinia-bearing and regular fuel rods were removed at these outages and shipped to a hot-cell laboratory where they have been sectioned and examined.

Results of the hot cell examinations on the gadolinia-bearing rods show no redistribution of gadolinia in the pellets. The pellet cracking patterns are similar to the standard UO_2 pellets as are changes in pellet density. Gadolinia isotopic concentrations, along with burnup and uranium/plutonium isotopics, have been measured radially in pellets at different axial locations and hence, at different burnups. Analytical modelling of the gadolinia-bearing fuel is in excellent agreement with the measured isotopic concentrations for the gadolinia isotopes (155, 156, 157, and 158). Figures 1 through 4 show comparisons for the four gadolinia isotopes measured at an equivalent assembly average exposure level of about 9,500 MWd/MTU. The analytical modelling is performed with MICBURN.

TABLE 2 TIHANGE-1 EXPOSURE HISTORIES

	Urania Rods		Gadolinia Rods		
	LHGR W/cm	Exposure MWd/MTU	LHGR W/cm	Exposure MWd/MTU	Fluence $x10^{21}$ n/cm^2
Cycle 7					
Peak Rod	307	14.4	158	5.5	
Average Rod	267	12.7	155	5.3	1.94
Cycle 8					
Peak Rod	284	27.9	182	13.9	
Average Rod	267	25.6	168	13.8	4.00
Cycle 9					
Peak Rod	228	38.3	165	21.4	
Average Rod	221	35.8	162	21.2	5.76

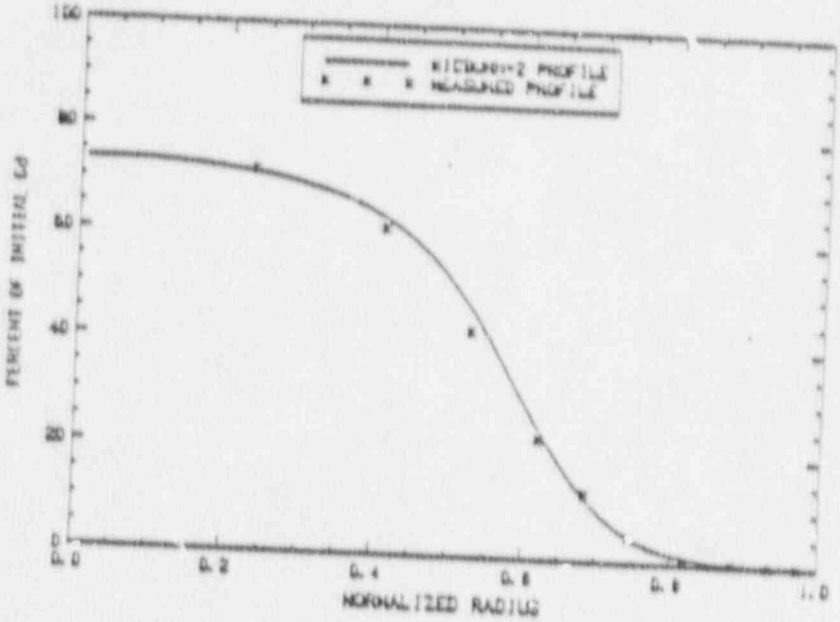

FIGURE 1 CALCULATED VERSUS MEASURED Gd-155 RADIAL PROFILE

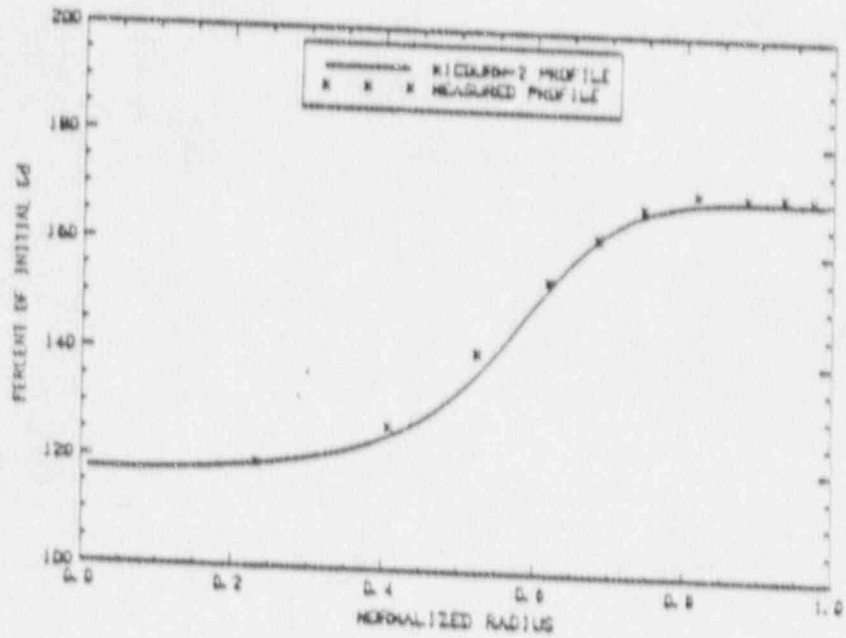

FIGURE 2 CALCULATED VERSUS MEASURED Gd-156 RADIAL PROFILE

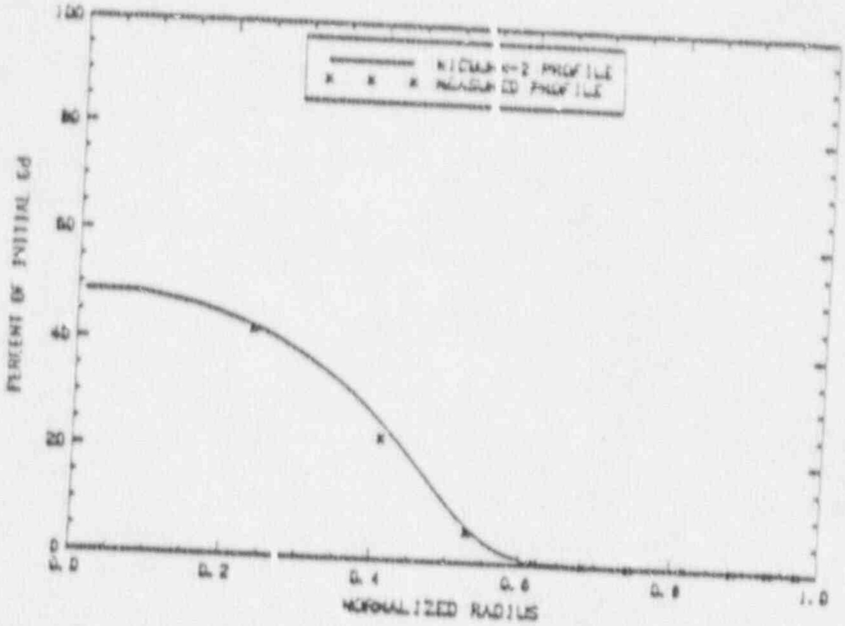

FIGURE 3 CALCULATED VERSUS MEASURED Gd-157 RADIAL PROFILE

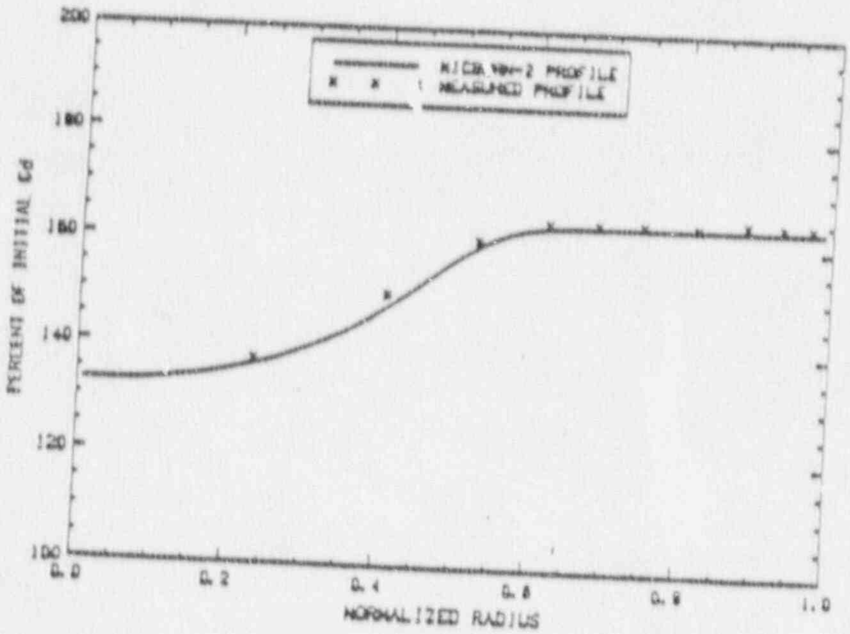

FIGURE 4 CALCU VERSUS MEASURED Gd-158 RADIAL PROFILE

MATERIAL PROPERTIES

The production of gadolinia-bearing absorber fuel pellets requires the attainment of a solid solution of Gd_2O_3 in the UO_2 matrix during fabrication. ANF has succeeded in producing solid solution Gd_2O_3-UO_2 fuel pellets at concentration levels exceeding 10 w/o gadolinia with production scale equipment.

The solid solution of Gd_2O_3 in the UO_2 matrix affects both the thermal conductivity and the melting point of the pellet. Thermal conductivity measurements performed on ANF-fabricated absorber pellets have shown that the thermal conductivity of the Gd_2O_3-UO_2 pellet decreases with increasing gadolinia concentration. The largest incremental reduction in thermal conductivity occurs for low gadolinia concentrations and is more pronounced at temperatures in the 400°C and 1600°C range. To compensate for the reduction in thermal conductivity, the power generation in the gadolinia-bearing rods is reduced by using lower U-235 enrichments than in the non-absorber fuel rods in the reload.

APPLICATION OF GADOLINIA-BEARING FUEL IN HB ROBINSON UNIT 2

Prior to Cycle 9, reload designs for HB Robinson Unit 2 were based on annual cycles and utilized conventional out-in-in fuel management plans. However, before the end of Cycle 8, concerns arose regarding reactor vessel pressurized thermal shock, which led to a program to substantially reduce the vessel fluence at critical weld locations. The vessel fluence concern was compounded by rapidly deteriorating steam generators. As a result of these perturbations on the operating plans, the Cycle 9 core was redesigned utilizing aggressive low leakage fuel management to reduce the vessel flux at the critical weld locations by a factor of about 2, while minimizing the impact on the Cycle 9 energy capability.

The Cycle 9 core was redesigned incorporating 208 gadolinia-bearing fuel rods containing 4 w/o concentration of gadolinia distributed among 24 fuel assemblies. The gadolinia served the dual purpose of controlling the power distribution and reducing the beginning of cycle temperature coefficient.

Concurrent with the finalization of the revised design, 28 of the already delivered assemblies were returned to ANF, modified to include gadolinia-bearing fuel rods (demonstrating the advantage of the easily removable upper tie plate), and shipped back to HB Robinson Unit 2. The core was loaded as planned, operated successfully, and achieved the desired cycle design goals.

Subsequent reload designs for HB Robinson Unit 2, Cycles 10, 11 and 12, have been further optimized from the standpoint of minimizing the core radial leakage. Specially designed assemblies were inserted on the core edge and the gadolinia assembly designs have been further optimized, with respect to the number and locations of the gadolinia-bearing rods within the assembly and the distribution of the gadolinia-bearing assemblies in the core, to control the radial power distribution. The gadolinia concentration level has also been increased in order to accommodate extended fuel cycles and higher fuel burnups while maintaining the aggressive low radial leakage fuel management. As an illustration, the Cycle 12 core (June 1987 startup) contains 40 fresh, 40 once-burnt, and 33 twice-burnt gadolinia-bearing assemblies with a total of 936 gadolinia-bearing rods. The assembly designs vary from as few as two gadolinia-bearing rods per assembly to a maximum of 12 rods per assembly. The gadolinia concentrations in the core range from 4 w/o to 10 w/o where the latter is loaded in eight assemblies each of which contain four rods of 10 w/o gadolinia and eight rods of 6 w/o gadolinia. Figure 5 illustrates the Cycle 12 core loading for HB Robinson Unit 2.

Figure 6 shows the comparison between calculated and measured data for soluble boron concentration as a function of exposure for HB Robinson Unit 2 Cycle 11 core. Similarly, Figure 7 shows the agreement between calculated and measured radial power distribution for the same core. As discussed earlier, accurate design predictions are maintained in cores containing gadolinia.

The HB Robinson Unit 2 cores are designed to maximize the utilization of $F_{\Delta H}$ margin with the ultimate goal of having no fresh fuel loaded on the core periphery. This has been accomplished by increasing the $F_{\Delta H}$ limit for the plant by optimizing licensing analysis and by carefully tailoring the gadolinia assembly designs to effectively yield a flat $F_{\Delta H}$ behavior as a function of cycle burnup. At the same time uranium utilization has been improved by more aggressive low leakage fuel management patterns and higher discharge burnups for the fuel. In order to satisfy these goals it has been necessary to utilize gadolinia concentrations up to and including 10 w/o, which is key to the successful development of fuel management schemes for extended fuel cycles of 18-24 months.

	H	G	F	E	D	C	B	A
8	2-A	1-C	0-A	2-B	2-A	0-A	1-D	PLSA
9	1-C	1-D	2-A	1-C	1-A		0-D	PLSA
10	0-A	2-A		0-B	2-A	1-B	0-C	
11	2-B	1-C	0-B			0-E	0-F	
12	2-A	1-A	2-A		1-C	2-B		
13	0-A		1-B	0-E	2-A			
14	1-D	0-D	0-C	0-F				
	PLSA	PLSA						

GADOLINIA-BEARING ASSEMBLIES

Assembly Type	Number of Assemblies	Cycles of Irradiation	Gd_2O_3 w/o	Gd_2O_3 Rods
0-A	8	0	4,6	8,4
0-B	8	0	6,10	8,4
0-C	8	0	4	4
0-D	8	0	4	7
0-E	8	0	4	12
1-A	8	[illegible]	4	4
1-B	8	[illegible]	4	8
1-C	16	[illegible]	4	12
1-D	8	1	4	12
2-A	21	2	4	8
2-B	8	2	4	8

FIGURE 5
HB ROBINSON UNIT 2 CYCLE 12 CORE CONFIGURATION

CONCLUSIONS

Advanced Nuclear Fuels Corporation has accumulated extensive experience with the use of gadolinia-bearing fuel rods in PWRs. Over 5,300 gadolinia-bearing fuel rods with gadolinia concentrations ranging from 1 w/o to 10 w/o have been irradiated in PWRs and assembly average burnups up to 50,000 MWd/MTU have been achieved. The performance of cores and assemblies incorporating gadolinia has been satisfactory, and their neutronics behavior can be predicted with high accuracy. Poolside examinations of urania and gadolinia-bearing fuel rods at high burnups indicate that the mechanical behavior of gadolinia absorber rods is to be fully satisfactory.

COMPARISON OF VIM AND CASMO-3 FOR BWR AND PWR ASSEMBLIES

Presented by

Malte Edenius

Studsvik of America, Inc.

CASMO USER'S GROUP MEETING

MINNEAPOLIS, MINNESOTA

JULY 14–15, 1988

MONTE CARLO/CASMO-3 BENCHMARK PROBLEMS

In a cooperative effort between Studsvik and Argonne National Laboratory, a series of lattice problems was developed with the goal of testing CASMO-3 against the VIM continuous energy Monte Carlo code with ENDF/B-5 data. The lattices are well-specified numerical problems which start from pin cell geometries and build in complexity to heterogeneous and heavily-poisoned BWR and PWR assemblies. The problems are modeled in octant geometry with reflective boundary conditions at assembly surfaces.

BWR cases include an 8X8 bundle with 0, 4 or 8 Gd rods and 0% or 70% void. BWR control rod cases (one with B_4C absorber pins and one with hafnium absorber pins) were performed for the no Gd assembly at zero void. The control rod was modeled in detail with 1/2 assembly geometry used (diagonal symmetry).

PWR cases are modeled in a 3X3 pin cell geometry with fuel pin (uniform pin cell lattice), Ag-In-Cd or Hf rod in the center position.

The VIM calculations were performed by Ed Fujita and Rich Lell of Argonne National Laboratory.

BWR CASES 1 AND 2: NO GADOLINIA RODS, 0 AND 70% VOID

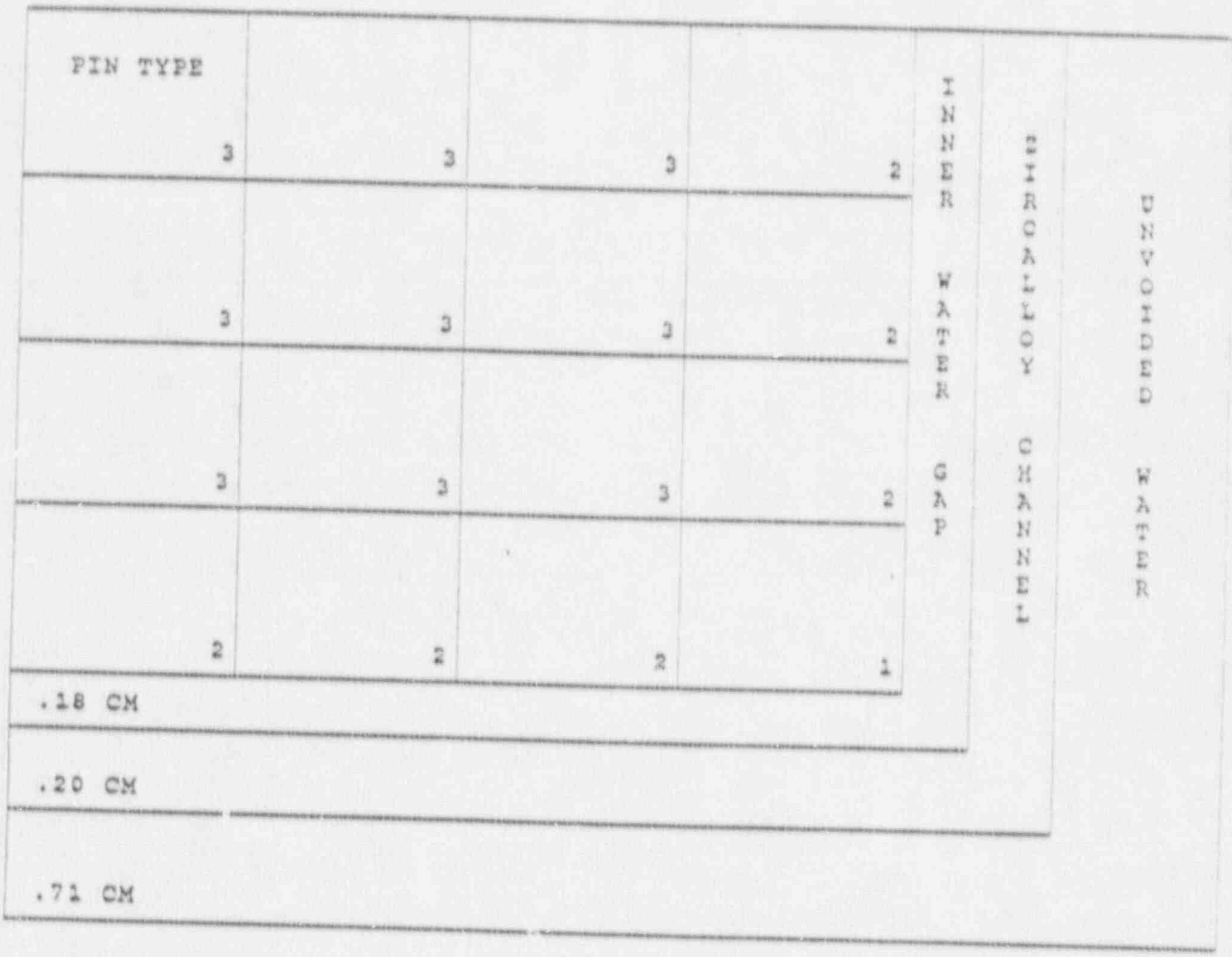

FUEL PIN RADIUS 0.52 CM

OUTER RADIUS OF CAN 0.62 CM

SQUARE LATTICE PITCH 1.63 CM

PIN TYP 1: 0% enr.
2: [illegible]% enr.
3: 3.0% enr.
4: 3.0% enr. + 6.0% Gd_2O_3

BWR CASES 3 AND 4: 4 GADOLINIA RODS, 0 AND 70% VOID

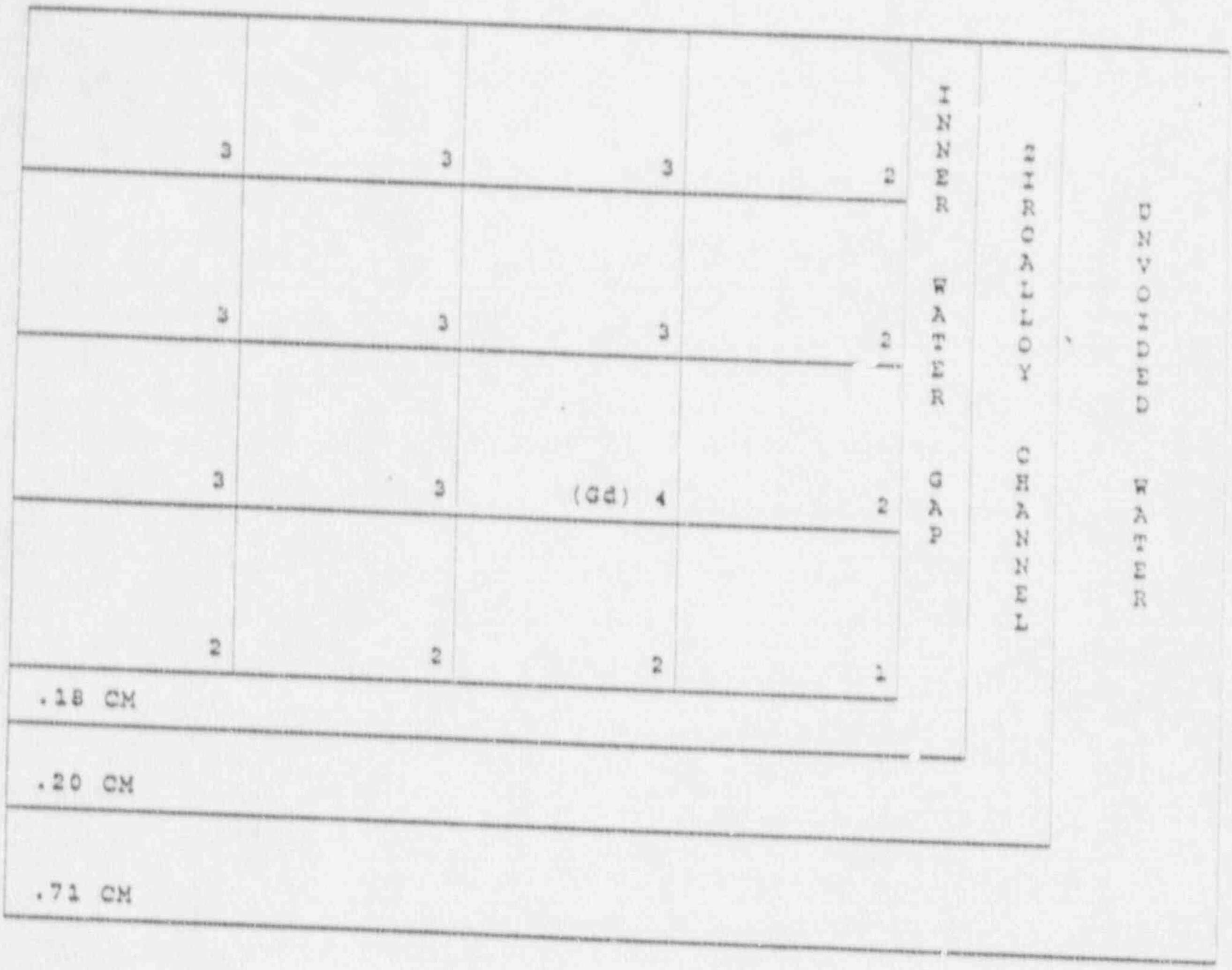

FUEL PIN RADIUS 0.52 CM

OUTER RADIUS OF CAN 0.62 CM

SQUARE LATTICE PITCH 1.63 CM

PIN TYP 1: 1.8% enr.
2: 2.4% enr.
3: 3.0% enr.
4: 3.0% enr. + 6.0% Gd_2O_3

VIM/CAS/880701

BWR CASES 5 AND 6: 8 GADOLINIA RODS, 0 AND 70% VOID

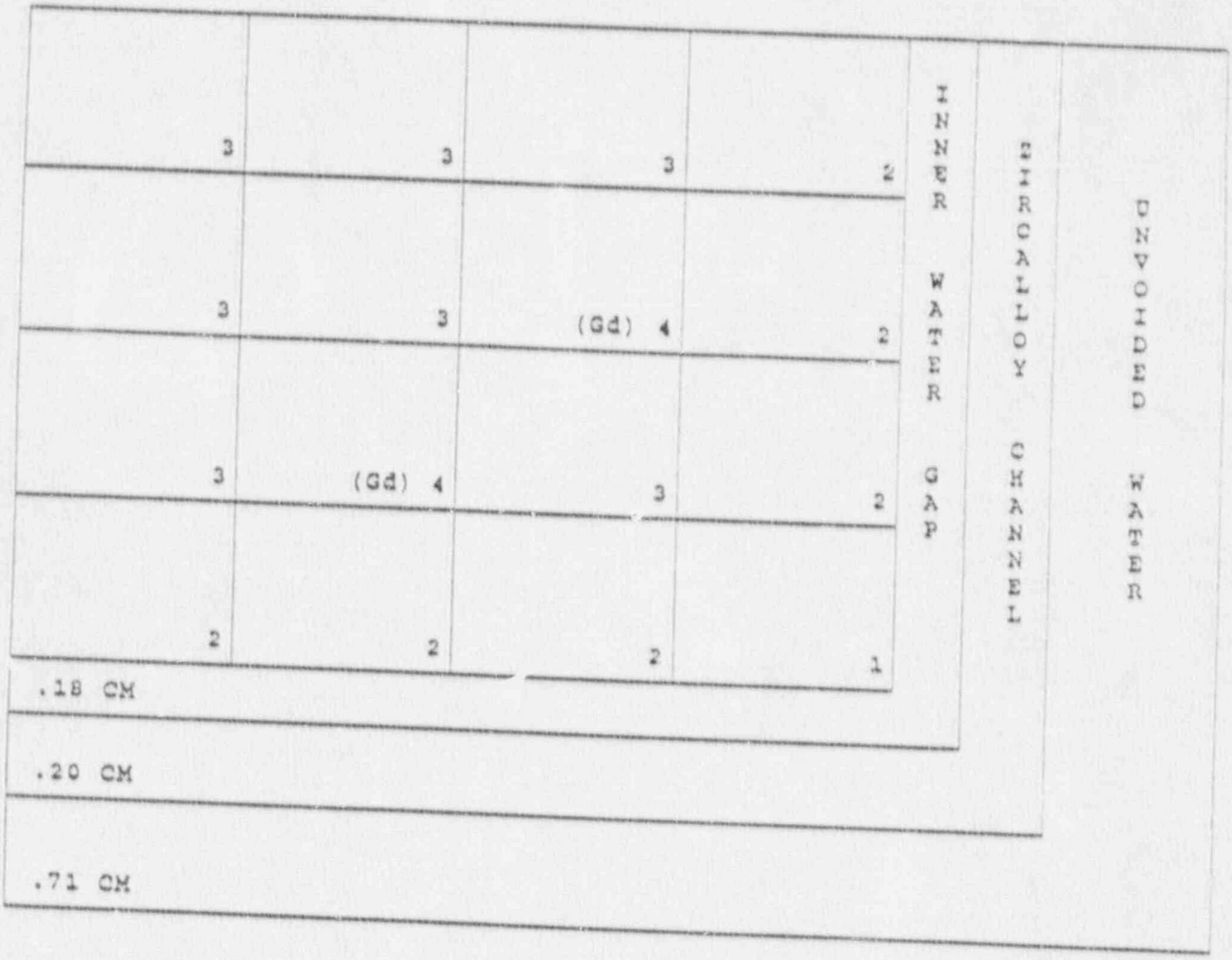

FUEL PIN RADIUS 0.52 CM

OUTER RADIUS OF CAN 0.62 CM

SQUARE LATTICE PITCH 1.63 CM

PIN TYP 1: 1.8% enr.
2: 2.4% enr.
3: 3.0% enr.
4: 3.0% enr. + 6.0% Gd_2O_3

B_4C CONTROL BLADE MODEL, GE TYPE(EPRI NP-240)

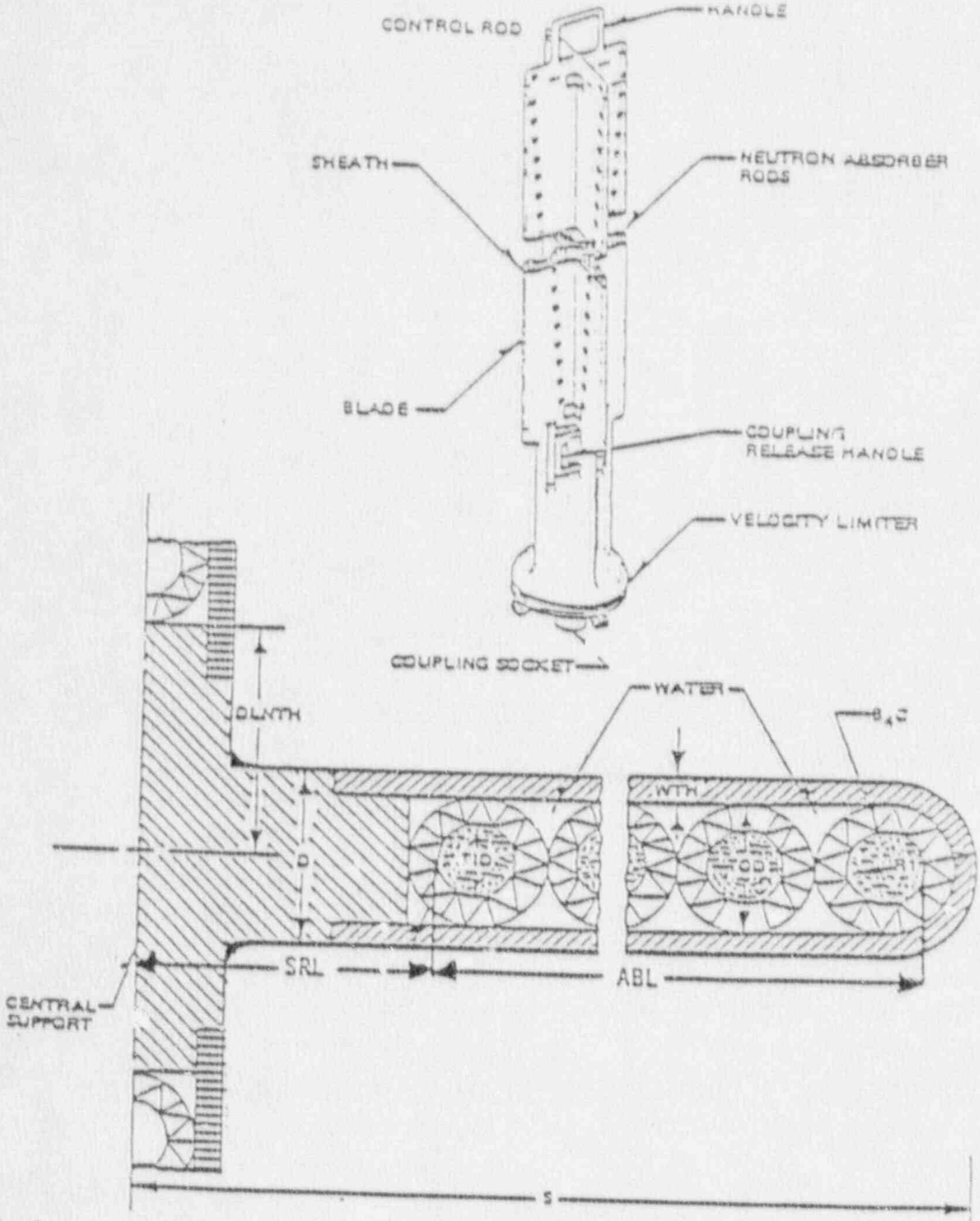

(cm)		
12.38	S	CONTROL BLADE SPAN
0.792	D	CONTROL BLADE FULL THICKNESS
1.985	DLNTH	DEAD LENGTH, i.e., CENTRAL STRUCTURE LENGTH
0.3506	TID	TUBE i.d.
0.478	TOD	TUBE o.d.
0.142	WTH	SHEATH THICKNESS
.0	NBKT	NUMBER OF BLANK TUBES ADJACENT TO CENTRAL STRUCTURE PER WING

PWR CASES 8a AND 8b: CONTROL ROD

PIN TYPE 3	3	3
3	ABSORBER 12 or 13	3
3	3	3

FUEL PIN RADIUS	0.52 CM	PIN TYP 1:	1.8% enr.
OUTER RADIUS OF CAN	0.62 CM	2:	2.4% enr.
SQUARE LATTICE PITCH	1.63 CM	3:	3.0% enr.
		4:	3.0% enr.+6.0% Gd_2O_3
		12:	Ag-In-Cd
		13:	Hafnium

DESCRIPTION OF CALCULATIONAL MODELS

VIM

EXACT GEOMETRIC REPRESENTATION

CONTINUOUS ENERGY MODEL

ENDF/B-5 DATA

100,000 HISTORIES

CASMO-3

VERSION 4.3

LIBRARY J1

70 ENERGY GROUPS

FUNDAMENTAL MODE WITH ZERO BUCKLING
(i.e. SAME CONDITIONS AS VIM)

STANDARD INPUT
- 1 MESH/PIN CELL
- 7 2-D GROUPS
- ETCETERA

COMPARISON OF VIM AND CASMO-3

EIGENVALUES

CASE	DESCRIPTION	VIM	CASMO-3	C3-VIM(pcm)
	BWR			
1	0% Void, No GAD	1.32322±0.00353	1.32354	24
2	70% Void, No GAD	1.27909±0.00397	1.28036	99
3	0% Void, 4 GAD	1.14002±0.00235	1.13612	-390
4	70% Void, 4 GAD	1.06825±0.00240	1.07077	252
5	0% Void, 8 GAD	1.01009±0.00248	1.01137	128
	70% Void, 8 GAD	0.95368±0.00268	0.95200	-168
7a	0% Void, B_4C Rod	1.07427±0.00335	1.07966	533
7b	0% Void, Hf Rod	1.11175±0.00345	1.11398	201
	PWR			
8	Pin Cell	1.38866±0.00363	1.38830	- 26
8a	Hf Control Rod	0.95404±0.00255	0.95629	236
8b	Ag-In-Cd Control Rod	0.95045±0.00285	0.95377	349

VIM/CAS/880701

COMPARISON OF VIM AND CASMO-3

Gd ABSORPTION

CASE	ENERGY GROUP	Gd-155 abs			Gd-157 abs		
		VIM	C3	C3-VIM(%)	VIM	C3	C3-VIM(%)
CASE 3	1	.00588	.00550	- 6.5	.00299	.00315	+ 5.4
0% VOID	2	.01836	.01907	+ 3.8	.08468	.08676	+ 2.4
4 GAD	TOTAL	.02423	.02457	+ 1.4	.08767	.08991	+ 2.6
CASE 4	1	.00877	.00854	- 2.6	.00484	.00498	+ 2.8
70% VOID	2	.01968	.02020	+ 2.6	.09055	.09155	+ 1.1
4 GAD	TOTAL	.02845	.02874	+ 1.0	.09539	.09653	+ 1.2
CASE 5	1	.01088	.01082	- 0.6	.00576	.00624	+ 8.3
0% VOID	2	.03055	.03091	+ 1.2	.1407	.1403	- 0.3
8 GAD	TOTAL	.04143	.04173	+ 0.7	.1465	.1465	+ 0.0
CASE 6	1	.01658	.01644	- 0.9	.00910	.00965	+ 6.0
70% VOID	2	.03025	.03071	+ 1.5	.1392	.1387	- 0.4
8 GAD	TOTAL	.04683	.04715	+ 0.7	.1483	.1484	+ 0.0

VIM 1σ uncertainty: gr 1 = 3.5%
2 = 1.5%
Total = 1.5%

VIM/CAS/880701

POWER DISTRIBUTION CASE 1: 0% VOID, NO GAD

.780 (1.3) .799 2.4 3	.842 (1.5) .835 -0.8 3	.960 (1.1) .948 -1.3 3	1.021 (1.2) 1.038 1.7 2			
.828 (1.4) .835 0.C 3	.866 (1.2) .871 0.6 3	.993 (1.2) .985 -0.8 3	1.082 (1.1) 1.074 -0.7 2	7	5	7
.923 (1.2) .948 2.7 3	.999 (1.4) .985 -1.4 3	1.098 (1.4) 1.099 0.1 3	1.168 (0.9) 1.174 0.5 2			
1.034 (1.2) 1.038 0.4 2	1.068 (1.4) 1.074 0.6 2	1.202 (1.2) 1.174 -2.3 2	1.137 (0.8) 1.108 -2.6 1			

VIM	(1σ%)
C3	
Diff.%	
	Type

POWER DISTRIBUTION CASE 2: 70% VOID, NO GAD

.766 (1.4) .767 0.1 3	.812 (1.1) .818 0.7 3	.939 (1.3) .948 1.0 3	1.015 (1.1) 1.017 0.2 2			
.817 (1.1) .818 0.1 3	.874 (1.0) .86[illegible] -0.6 3	.990 (0.9) 1.002 1.2 3	1.064 (0.9) 1.068 0.4 2	7	5	7
.922 (1.3) .948 2.8 3	1.018 (1.0) 1.002 -1.6 3	1.141 (1.0) 1.136 -0.4 3	1.189 (0.8) 1.191 0.2 2			
1.011 (1.4) 1.017 0.6 2	1.074 (1.2) 1.068 -0.6 2	1.214 (1.1) 1.191 -1.9 2	1.157 (1.0) 1.123 -2.9 1			

VIM	(1σ%)
C3	
Diff.%	
	Type

VIM/CAS/880701

POWER DISTRIBUTION CASE 3: 0% VOID, 4 GAD

.902 (1.5) .900 -0.2 3	.904 (1.2) .925 2.3 3	1.032 (1.3) 1.035 0.3 3	1.130 (0.8) 1.150 1.8 2			
.928 (1.0) .925 -0.3 3	.911 (1.3) .914 0.3 3	.968 (1.2) .952 -1.7 3	1.154 (1.1) 1.144 -0.9 2	7	5	7
1.019 (1.3) 1.035 1.6 3	.974 (0.9) .952 -2.3 3	.220 (0.8) .218 -0.9 (Gd) 4	1.196 (1.0) 1.179 -1.4 2			
1.134 (1.2) 1.150 1.4 2	1.137 (1.1) 1.144 0.6 2	1.190 (1.2) 1.179 -0.9 2	1.200 (1.1) 1.185 -1.3 1			

VIM	(1σ%)
C3	
Diff.%	
	Type

POWER DISTRIBUTION CASE 4: 70% VOID, 4 GAD

.809 (1.3) .827 2.2 3	.861 (1.0) .876 1.7 3	1.001 (1.0) 1.013 1.2 3	1.086 (0.8) 1.110 2.2 2			
.874 (1.4) .876 0.2 3	.892 (1.3) .897 0.6 3	.980 (1.0) .982 0.2 3	1.128 (1.0) 1.138 0.9 2	7	5	7
1.028 (0.9) 1.013 -1.5 3	.981 (0.7) .982 0.1 3	.348 (0.7) .344 -1.1 (Gd) 4	1.250 (1.1) 1.230 -1.6 2			
1.112 (1.1) 1.110 -0.2 2	1.130 (0.9) 1.138 1.6 2	1.260 (1.1) 1.230 -2.4 2	1.261 (1.1) 1.218 -3.4 1			

VIM	(1σ%)
C3	
Diff.%	
	Type

POWER DISTRIBUTION CASE 5: 0% VOID, 8 GAD

.907 (1.8) .915 0.9 3	.901 (1.2) .903 0.2 3	.999 (1.3) .973 -2.6 3	1.177 (1.3) 1.208 2.6 2			
.895 (1.1) .903 0.9 3	.784 (1.5) .777 -0.9 3	.241 (0.8) .238 -1.2 (Gd) 4	1.205 (1.1) 1.199 -0.5 2	7	5	7
.960 (1.7) .973 1.4 3	.241 (1.2) .238 -1.2 (Gd) 4	1.101 (1.0) 1.083 -1.6 3	1.394 (1.3) 1.396 0.1 2			
1.182 (1.3) 1.208 2.2 2	1.218 (1.1) 1.199 -1.6 2	1.408 (1.1) 1.396 -0.9 2	1.388 (1.3) 1.377 -0.8 1			

VIM	(1σ%)
C3	
Diff.%	
	Type

POWER DISTRIBUTION CASE 6: 70% VOID, 8 GAD

.800 (1.4) .807 0.9 3	.828 (1.2) .837 1.1 3	.966 (1.2) .963 -0.3 3	1.138 (1.3) 1.155 1.5 2			
.825 (1.3) .837 1.5 3	.791 (1.4) .785 -0.8 3	.369 (0.7) .370 0.3 (Gd) 4	1.201 (0.9) 1.194 -0.6 2	7	5	7
.968 (1.1) .963 -0.5 3	.371 (0.9) .370 -0.3 (Gd) 4	1.204 (1.0) 1.174 -0.8 3	1.415 (0.9) 1.402 -0.9 2			
1.158 (1.2) 1.155 -0.3 2	1.191 (0.9) 1.194 0.3 2	1.388 (1.1) 1.402 1.0 2	1.388 (1.2) 1.373 -1.1 1			

VIM	(1σ%)
C3	
Diff.%	
	Type

POWER DISTRIBUTION CASE 7a: 0% VOID, BORON CONTROL ROD

.373 (4.5) .401 7.5 1							
.476 (2.5) .507 6.5 2	.657 (3.4) .674 2.6 3						
.523 (2.1) .519 -0.8 2	.722 (3.2) .715 -1.0 3	.764 (2.7) .772 1.0 3					
.558 (1.8) .545 -2.3 2	.767 (1.7) .757 -1.3 3	.816 (2.4) .820 0.5 3	.872 (2.6) .872 0.0 3				
.576 (2.2) .593 3.0 2	.806 (2.3) .814 1.0 3	.880 (2.2) .876 -0.5 3	.943 (1.8) .927 -1.7 3	.968 (2.3) .981 1.3 3			
.689 (2.0) .692 0.4 2	.925 (2.3) .913 -1.3 3	.989 (1.8) .963 -2.6 3	1.019 (1.9) 1.009 -1.0 3	1.104 (1.4) 1.059 -4.1 3	1.173 (2.4) 1.136 -3.2 3		
.911 (2.1) .946 3.8 2	1.111 (2.0) 1.127 1.4 3	1.161 (1.9) 1.148 -1.1 3	1.188 (1.8) 1.183 -0.4 3	1.245 (1.3) 1.232 -1.0 3	1.303 (1.7) 1.311 0.6 3	1.468 (2.3) 1.496 1.9 3	
1.129 (2.2) 1.102 -2.4 1	1.284 (1.5) 1.301 1.3 2	1.282 (1.3) 1.290 0.6 2	1.305 (1.4) 1.316 0.8 2	1.365 (1.5) 1.362 -0.2 2	1.422 (1.3) 1.440 1.3 2	1.595 (1.5) 1.600 0.3 2	1.538 (2.0) 1.529 -0.6 1

VIM (1σ%) C3 Diff.% Type

POWER DISTRIBUTION CASE 7b: 0% VOID, HAFNIUM CONTROL ROD

.442 (3.3) .460 4.1 1							
.568 (1.9) .574 1.1 2	.755 (2.8) .727 -3.7 3						
.590 (1.9) .581 -1.5 2	.766 (2.2) .754 -1.6 3	.805 (2.8) .792 -1.6 3					
.610 (2.0) .604 -1.0 2	.810 (2.0) .788 -2.7 3	.842 (2.1) .830 -1.4 3	.881 (2.3) .868 -1.5 3				
.634 (2.0) .650 2.5 2	.845 (2.0) .838 -0.8 3	.898 (1.4) .876 -2.5 3	.913 (2.0) .914 0.1 3	.977 (2.7) .958 -1.9 3			
.733 (2.3) .747 1.9 2	.926 (1.1) .930 0.4 3	.973 (2.2) .956 -1.7 3	.990 (2.2) .988 -0.2 3	1.000 (1.2) 1.029 2.9 3	1.036 (2.3) 1.098 6.0 3		
.990 (1.9) .988 -0.2 2	1.123 (1.5) 1.131 0.4 3	1.126 (2.0) 1.130 0.4 3	1.110 (1.5) 1.152 3.8 3	1.163 (1.7) 1.192 2.5 3	1.281 (1.4) 1.263 -1.4 3	1.433 (2.5) 1.436 0.2 3	
1.111 (0.9) 1.115 0.4 1	1.303 (1.3) 1.291 -0.9 2	1.270 (1.3) 1.264 -0.5 2	1.254 (1.3) 1.278 1.9 2	1.297 (1.6) 1.315 1.4 2	1.358 (1.7) 1.384 1.9 2	1.573 (1.6) 1.535 -2.4 2	1.553 (1.7) 1.464 -5.7 1

VIM (1σ%) C3 Diff.% Type

VIM/CAS/880701

CASE 8a: PWR Ag-In-Cd CONTROL ROD

1.032 (1.3) 1.021 -1.1 3	.965 (1.0) .979 1.5 3	1.022 (1.0) 1.021 -0.1 3
.979 (1.1) .979 0.0 3	12	.976 (1.0) .979 0.3 3
1.019 (0.9) 1.021 0.2 3	.980 (0.9) .979 -0.1 3	1.026 (0.9) 1.021 -0.5 3

CASE 8b: PWR Hf CONTROL ROD

1.024 (1.0) 1.017 -0.7 3	.990 (0.9) .983 -0.7 3	1.030 (1.1) 1.017 -1.3 3
.963 (0.9) .983 2.1 3	13	.973 (1.1) .983 1.0 3
1.024 (1.0) 1.017 -0.7 3	.985 (0.8) .983 -0.2 3	1.012 (1.2) 1.017 0.5 3

SUMMARY OF CASMO-3/VIM COMPARISON

'VERAGE DISCREPANCY FOR K_{inf} IN UNRODDED BWR BUNDLES:

CASMO3 – VIM

0 % void	−79 ± 170 pcm
70 % void	+61 ± 170 pcm

DISCREPANCY IN ABSORBER REACTIVITY WORTH:

CASMO3 – VIM

GADOLINIA	0 % void	+1.0 ± 2 %
	70 % void	+0.1 ± 2 %
CRD	Boron rod	−2.1 ± 2 %
	Hafnium rod	−1.0 ± 2 %
CCR	AgInCd rod	−0.6 ± 1.4 %
	Hafnium rod	−0.9 ± 1.4 %

DISCREPANCY IN Gd–155 OR Gd–157 ABSORPTION:

CASMO3 – VIM

0 % void	+1.2 ± 1 %
70 % void	+0.7 ± 1 %

AVERAGE DISCREPANCIES IN POWER DISTRIBUTION FOR:

CASMO3 – VIM

Gd rods	−0.7 %
Rods adjacent to Gd rods	−0.9 %
Rods adjacent to water gaps	+0.1 %
Corner rods	−2.0 %
Along gap with cruciform control rod	+1.1 %

No trends in power distributions versus void.

IK/CAS/880701

CONCLUSIONS

* EXCELLENT AGREEMENT BETWEEN CASMO-3 AND VIM

* NO TREND OF SIGNIFICANCE TO BWR OR PWR ANALYSIS WAS OBSERVED

Transactions ANS, Vol. 49, Boston, June 1985.

2. Benchmarking of the Gamma-TIP Calculation in CASMO Against the Hatch BWR.

Malte Edenius, Peter J. Rashid, David M. Ver Planck (Studsvik USA), Odelli Ozer (EPRI)

METHODOLOGY

A gamma transport calculation has been developed for the CASMO code[1,2] under the sponsorship of the Electric Power Research Institute (EPRI). Gamma sources from capture, fission, and inelastic scattering are calculated for all regions in CASMO and a gamma transport calculation is carried out using a two-dimensional heterogeneous collision probability routine, CPM-HET. This method allows the two-dimensional calculation to be done with explicit representation of the fuel rods, i.e., the fuel rods that have large gamma cross sections are not smeared with the coolant, which is almost transparent to gamma rays.

The gamma-ray cross sections used with CASMO are based on the CLOSEUP/SCALE library[3,4] and contain data in 18 energy groups. Delayed gamma production is treated

TABLE I

CASMO Benchmarking to SAM-CE

CASE	SAM-CE (with 1σ errors)	CA	DIFF. (%)
Pin Cell Gamma Fluxes			
Cold, 1995 ppm B, 0 MWd/kg	2.10 ± 1.5%	2	+0.1
Hot, 0 ppm B, 0 MWd/kg	2.17 ± 1.5%	2	+1.5
Hot, 0 ppm B, 40 MWd/kg	2.72 ± 1.5%	2	+1.6
8x8 BWR Detector Responses			
0% void, no Gd	.280 ± 2.7%	.1	+4.3
40% , "	.285 ± 2.5%	.1	+1.7
70% , "	.293 ± 2.2%	.2	0
40% , control rod	.353 ± 2.6%	.2	1.0
40% , 6 Gd rods	.271 ± 2.9%	.2	+1.7

using the Los Alamos sum-of-exponentials representation.[3] For calculational efficiency, a condensed gamma library with 10 energy groups was developed. It was found that the detector responses calculated with the 10-group library agree to within 0.5% of 18-group calculations.

MONTE CARLO BENCHMARKING

The gamma calculation in CASMO was first benchmarked against SAM-CE Monte Carlo calculations with ENDF/B-V data performed by Brookhaven National Laboratory.[6] Results are summarized in Table I. The pin cell cases are coupled neutronics-gamma calculations and are mainly a test of the gamma sources because the gamma transport effect is small in a pin cell. In the boiling water reactor (BWR) cases, SAM-CE used precalculated gamma sources from CASMO so that these cases are a test of the gamma transport calculation only. The benchmarks show good agreement both for the gamma source and the gamma transport calculations

HATCH BENCHMARKING

The benchmarking has now been extended[7,8] to operating data for the Hatch Unit 1 BWR. End of cycle (EOC) 3 was chosen for the benchmark because extensive ^{140}La gamma-scan data (one-eighth core three-dimensional measured power distribution) are available at this state point.

Calculated gamma-sensitive traveling in-core probe (gamma-TIP) responses were compared to measured data using the SIMULATE three-dimensional nodal code[10] with two-group cross sections and gamma detector functions generated by CASMO as input. The gamma detector function is the calculated ratio between detector response and power in a neighboring assembly. This ratio is calculated in CASMO versus exposure, void, control rod, etc. and is input to SIMULATE.

The purpose of the benchmark is to compare the measured gamma-TIP with the SIMULATE calculated gamma-TIP using the measured gamma-scan power distribution and CASMO calculated TIP responses as input to SIMULATE.

Starting from beginning of cycle 3, a Haling calculation to EOC 3 was done to obtain the EOC burnup and void history distribution. Control rods were then inserted to their EOC positions to obtain the EOC equilibrium ^{140}La number densities. Comparing the calculated ^{140}La concentrations with calculated power distributions, a three-dimensional distribution of correction factors was derived. The measured power distribution was then determined by multiplying the measured ^{140}La distributions by the calculated correction factors (this is a small correction, typically <2%). Internormalization factors for the different bundle types were also applied as suggested in Ref. 8.

Finally, the measured power distribution was used as input to SIMULATE at EOC 3 and the calculated TIP responses were compared to the measured TIP responses.

The core contains 13 TIPs, which are surrounded by gamma-scanned bundles. Two TIPs were excluded from our benchmark because the measured results seem to have been influenced by a misalignment and are inconsistent with data for symmetric TIP locations. Table II shows the measured and calculated average axial distribution and the integrated radial distribution of the gamma-TIP responses normalized to unity for the subset of accepted TIP data points. The TIPs include five locations with an adjacent control rod (TIP XY 2045,

TABLE II

Measured and Calculated Gamma-TIP Responses for Hatch, EOC 3

Axial Position*	Measured Mean	Calculated Mean	Mean Difference
123	.833	.839	.006
99	1.064	1.058	-.006
75	1.086	1.080	-.006
63	1.087	1.081	-.006
51	1.077	1.070	-.007
39	.983	.989	.006
27	.869	.882	.013
Radial TIP-XY[b]	**Measured Mean**	**Calculated Mean**	**Mean Difference**
437	.708	.704	-.004
2021	1.084	1.108	.024
2045	1.152	1.133	-.019
2829	1.062	1.076	.014
2837	.983	1.001	.018
2845	1.163	1.138	-.025
3629	.999	1.006	.007
3637	1.079	1.092	.013
3645	1.117	1.098	-.019
4437	1.112	1.090	-.022
4445	.542	.554	.012

*Inches from bottom of fuel. The 11 TIPs are integrated radially to give an average axial distribution.
[b]Integrated axially to give an average radial distribution.

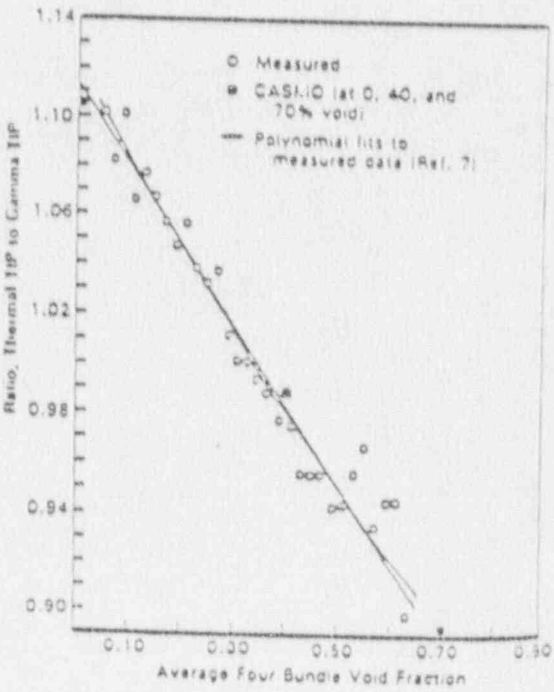

Fig. 1. Measured and calculated neutron-TIP/gamma-TIP ratios for Hatch, Cycle 1, 9356 MWd/t.

2527, 2537, 2845, and 3629). Void fractions vary from 0 to 70% and exposures from 5 to 20 MWd/kg in the surrounding fuel. The CASMO-SIMULATE results show no trend versus void, burnup, fuel type, or presence of control rod. The root-mean-square error for all nodes is 2.6%, which is within the one-sigma experimental uncertainty.

We also compared the measured[7] and calculated void dependence of the neutron-TIP/gamma-TIP ratio close to EOC 1 (Fig. 1). The TIP response is insensitive to void history and exposure in the narrow interval of interest at EOC 1. We therefore assumed exposure to be equal to the average exposure and void history to be equal to instantaneous void and calculated the void dependence of the neutron-TIP/gamma-TIP ratio directly from the CASMO results for the initial bundle type. The normalization used is arbitrary but we conclude that the measured and calculated void dependencies are in very good agreement.

CONCLUSIONS

In summary, the various benchmarks against Monte Carlo calculations and operating BWR data show that gamma detector calculations using the integral transport theory model in CASMO yield accurate results for a marginal extra computer cost and without the need for auxiliary codes.

1. A. AHLIN, M. EDENIUS, H. HAGGBLOM, "CASMO User's Manual," AE-RF-76-4158, Studsvik (1978).
2. A. AHLIN, M. EDENIUS, S. SUK, D. R. HARRIS, O. OZER, "Integral Transport Computation of In-Core Gamma Effects with CASMO/CPM," *Trans. Am. Nucl. Soc.*, 47, 434 (1984).
3. M. WESTFALL, Private Communications; see also J. A. BUCHOLZ, "SCALE: A Modular Code System for Performing Standardized Computer Analyses for Licensing Evaluations," NUREG/CR-0200, U.S. Nuclear Regulatory Commission (1980).
4. S. D. SUK, "Development of Efficient Methods for Prediction of In-Core Gamma Effects," thesis, Rensselaer Polytechnic Institute (Dec. 1984).
5. R. J. LABAUVE, T. R. ENGLAND, D. C. GEORGE, M. G. STAMATELATOS, "The Application of a Library of Processed ENDF/B-IV Fission-Product Aggregate Decay Data in the Calculation of Decay-Energy Spectra," LA-7483-MS, Los Alamos National Lab. (1978).
6. P. ROSE, E. SMITH, Brookhaven National Lab., Private Communication.
7. K. W. BURKE, "Special TIP Detector Measurements at Edwin I. Hatch Nuclear Plant Unit 1 Prior to End of Cycle 1," EPRI NP-540, Electric Power Research Institute (1977).
8. G. L. HOLLOWAY, J. E. FAWKS, B. W. CRAWFORD, "Core Design and Operating Data for Cycles 2 and 3 of Hatch 1," EPRI NP-2106, Electric Power Research Institute (1984).
9. H. D. KOSANKE, M. C. GREGORY, J. T. HA, B. W. CRAWFORD, "Gamma Scan Measurements at Edwin I. Hatch Nuclear Plant Unit 1 Following Cycle 3," EPRI NP-2105, Electric Power Research Institute (1983).
10. D. M. VER PLANCK, "SIMULATE-E: A Nodal Core Analysis Program for Light Water Reactors," NP 2792 CCM (1983).

Transactions ANS, Vol. 47, Washington, November 1984.

7. Integral Transport Computation of In-Core Gamma Effects with CASMO/CPM, *A. Ahlin, M. Edenius (Studsvik USA), S. Suk, D. R. Harris (RPI), O. Ozer (EPRI)*

INTRODUCTION

There are several applications for gamma transport calculations in power reactors, e.g., to determine gamma detector response, gamma redistribution of power, and boiling water reactor (BWR) bypass heating. Calculational tools exist for such analyses, in particular Monte Carlo codes that track neutrons and gammas together. Such methods are, however, unpractical and expensive to use for the numerous calculations needed in the design and support of power reactors.

The KENO-IV multigroup Monte Carlo code has also been used to determine Green's functions[1] for individual fuel pins, which then are combined with power shapes calculated by the standard reactor physics programs. For example, CASMO-2E, an extended version of the CASMO-2 program,[2] allows the gamma detector response to be calculated using input Green's functions.

METHODOLOGY

An alternative method to calculate the gamma detector response has been developed for CASMO (Ref. 3) and CPM (Ref. 4) under sponsorship of the Electric Power Research Institute (EPRI). Gamma sources from capture, fission, and inelastic scattering are calculated for all regions in CASMO/CPM, and a gamma transport calculation based on the two-dimensional heterogeneous collision probability routine CPM-HET is used. This eliminates the need for separate costly Monte Carlo calculations to determine rod-to-detector Green's functions.

CPM-HET was developed by Studsvik for the CPM program and is available in a special EPRI-CPM version for the neutron transport calculation. In CPM-HET, canning and coolant are homogenized but fuel is not smeared. This method was chosen for the gamma transport problem because the fuel rods are almost black for gamma rays and the water is transparent. It is difficult to determine adequate pin cell homogenized cross sections for this type of strongly heterogeneous configuration, and CPM-HET seems to be an efficient method to solve the gamma transport calculation. Other transport methods like P_n or S_n theory are unpractical for assembly calculations with discrete representation of the fuel.

GAMMA DATA

The gamma transport calculation is carried out in 18 energy groups using gamma-ray cross sections based on the CLOSEUP/SCALE library.[5] Delayed gamma production is treated using the Los Alamos sums-of-exponentials representation.[6]

Gamma rays scatter principally in-core by Compton scattering, which is quite anisotropic at energies above a few tenths of a megaelectron volt. Hence, a gamma-ray transport correction must be applied to the P_0 scattering representation used in CPM-HET. For the practical case of many energy groups, it is useful to distinguish diagonal, outflow, and inflow transport corrections.[7] Let $\Sigma_{j,g\to g'}$ represent the j'th order Legendre component of the scattering cross section from gamma group g to group g'. The diagonal P_1 transport correction consists of subtraction of the in-group scattering $\Sigma_{1,g\to g}$ from the total cross section in group g and from $\Sigma_{0,g\to g}$. The outflow transport correction subtracts

$$\sum_{g'} \Sigma_{1,g\to g'}$$

in the same way, and the inflow transport cross section subtracts

$$\sum_{g'} \Sigma_{1,g'\to g} .$$

The applicability of P_1 transport corrections for gamma transport in-core has been studied using discrete ordinate calculations for a BWR. Figure 1 shows DOT results for a mid-life steady-state gamma source spectrum emitted uniformly and isotropically on a plane at $X = 0$ in homogenized BWR material. The energy deposition effect computed using various gamma-ray scattering treatments is presented relative to P_3 scattering as reference. Several gamma-ray transport corrections were found that give reasonable results for distances up to ~10 to 15 cm from the source (sources at larger distances are negligible in in-core calculations). Both the outflow and intermediate corrections, e.g.,

$$\sum_{g'=g}^{g+1} \Sigma_{1,g\to g'} ,$$

labeled "2G diagonal P_0," seem to be adequate.

TABLE I

Gamma Flux and Detector Response for an 8 x 8 BWR with 40% Void

GROUP	UPPER ENERGY BOUNDARY (MEV)	DETECTOR RESPONSE				REL. DETECTOR RESPONSE (%)	
		SAM-CE	UNCERTAINTY	CASMO	DIFF (%)	SAM-CE	CASMO
1	10.0	0.	****	.2444E-04	*******	.000	.009
2	8.0	.5198E-03	56.7	.1516E-02	191.8	.187	.541
3	6.5	.8736E-02	19.2	.7169E-02	-17.9	3.064	2.559
4	5.0	.1310E-01	16.5	.1229E-01	-6.2	4.596	4.388
5	4.0	.2523E-01	9.4	.2604E-01	3.2	8.850	9.294
6	3.0	.2033E-01	8.6	.2207E-01	8.6	7.129	7.877
7	2.5	.4411E-01	7.6	.4187E-01	-5.1	15.473	14.944
8	2.0	.2521E-01	6.2	.2689E-01	6.5	8.843	9.597
9	1.66	.2939E-01	5.6	.2945E-01	.2	10.307	10.511
10	1.33	.3146E-01	5.8	.3189E-01	1.4	11.034	11.384
11	1.0	.2121E-01	6.6	.1918E-01	-9.6	7.440	6.845
12	0.8	.2118E-01	6.8	.1881E-01	-11.2	7.427	6.715
13	0.6	.2208E-01	6.6	.1998E-01	-9.5	7.744	7.132
14	0.4	.6124E-02	14.0	.7534E-02	23.0	2.148	2.689
15	0.3	.8876E-02	13.0	.8042E-02	-9.4	3.113	2.871
16	0.2	.6515E-02	24.1	.5827E-02	-10.4	2.285	2.083
17	0.1	.1039E-02	99.9	.1362E-02	31.1	.364	.486
18	0.05	0.	****	.2108E-03	******	.000	.075
TOTAL		.2851E+00	2.5	.2802E+00	-1.7	100.000	100.000

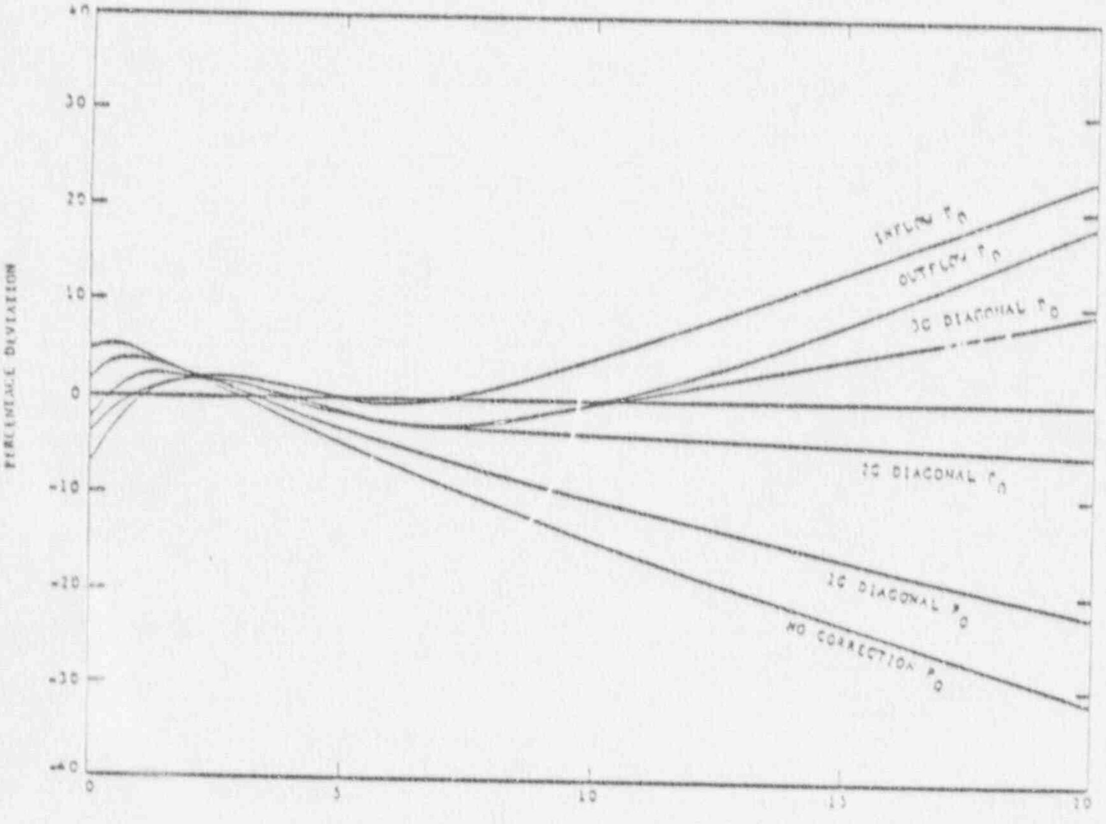

Fig. 1. Percentage deviation from P_1 gamma energy deposition rate as a function of the distance from the isotropic plane source in a homogenized BWR.

BENCHMARKING

The CASMO/CPM gamma detector calculation is being benchmarked against SAM-CE Monte Carlo calculations carried out at Brookhaven National Laboratory.[8] The SAM-CE gamma transport calculations were made using prompt gamma sources calculated by CASMO. Thus, we avoid any inconsistencies that might exist in the neutronic part of the calculation in the two codes, and the comparison is a test of the ability of the CPM-HET routine in CASMO/CPM to calculate the gamma flux.

Table I shows results for a BWR assembly using the outflow transport correction. There is a significant statistical uncertainty in the SAM-CE results, which were edited for the 18 energy groups. The 1σ error in SAM-CE is 5 to 10% in the most important energy range and the uncertainty in the total detector response is ≈3%. The CASMO code predicted the response within the 1σ uncertainty for most of the important energy groups.

Further benchmark calculations against Monte Carlo and operating data were planned for Fall 1984.

---

1. M. J. HEBERT, D. R. HARRIS, D. M. KAPITZ, E. E. PILAT, "Monte Carlo Analysis of BWR Bypass Heating, Gamma TIP Response, and Gamma Redistribution Factors," *Proc. Topl. Mtg. Advances in Reactor Physics and Core Thermal Hydraulics*, NUREG/CP-0034, p. 914, U.S. Nuclear Regulatory Commission.

2. A. AHLIN, M. EDENIUS, "CASMO-2 for Generation of Effective PDQ Cross Sections," *Trans. Am. Nucl. Soc.*, 41, 611 (1982).

3. A. AHLIN, M. EDENIUS, H. HAGGBLOM, "CASMO User's Manual," AE-RF-76-4158, Studsvik (1978).

4. A. AHLIN, M. EDENIUS, "ARMP System Documentation," Part II, Chap. 6, EPRI CCM-1, Electric Power Research Institute (1977).

5. M. WESTFALL, Private Communication; see also J. A. BUCHOLZ, "SCALE: A Modular Code System for Performing Standardized Computer Analyses for Licensing Evaluations," NUREG/CR-0200, U.S. Nuclear Regulatory Commission (1980).

6. R. J. LABAUVE, T. R. ENGLAND, D. C. GEORGE, M. G. STAMATELATOS, "The Application of a Library of Processed ENDF/B-IV Fission-Product Aggregate Decay Data in the Calculation of Decay-Energy Spectra," LA-7483-MS, Los Alamos National Lab. (1978).

7. D. R. HARRIS, "Unified Theory of Multigroup Transport Cross Sections," *Trans. Am. Nucl. Soc.*, 15, 958 (1972).

8. P. ROSE, E. SMITH, Brookhaven National Lab., Private Communication.

ADVANCED NUCLEAR FUELS *CORPORATION*

2101 HORN RAPIDS ROAD, PO BOX 130, RICHLAND, WA 99352-0130
(509) 375-8100 TELEX: 15-2876

July 20, 1990
RAC:083:90

Dr. Lambros Lois
Reactor Systems Branch
Division of Engineering and System Technology
Office of Nuclear Reactor Regulation
U. S. Nuclear Regulatory Commission
Washington, D.C. 20555

Dear Dr. Lois:

Subject: TIP ASYMMETRY UNCERTAINTY

Ref: 1. Letter, R. A. Copeland (ANF) to Director NRR (NRC), "Submittal of MICROBURN-B," dated March 8, 1989, (RAC:010:89).
2. Letter, R. A. Copeland (ANF) to R. C. Jones (NRC), "Responses to NRC Questions on CASMO-3G/MICROBURN-B," dated March 16, 1990, (RAC:022:90).

As we discussed in our telephone conversation on July 20, 1990, this letter is being written to confirm that the TIP Symmetry Uncertainty value of 6.0% will be used in the determination of the radial bundle power uncertainty for MICROBURN-B (Reference 1). This value will be used for both the C lattice and D lattice plants. This TIP Symmetry Uncertainty is the same value used to determine the radial bundle power uncertainty for the currently approved XTGBWR methodology. The other uncertainties identified in the response to Question 26 of Reference 2 that are unaffected by the TIP Symmetry Uncertainty remain the same.

Please consider the information in this letter to be proprietary to ANF. The affidavit supplied with the original submittal (Reference 3) provides the necessary information as required by 10 CFR 2.790(b) to support the withholding of this letter from public disclosure.

If there are questions, or if I can be of further help, please contact me.

Sincerely,

Bob Copeland

R. A. Copeland, Manager
Reload Licensing

XN-NF-80-19(NP)(A)
Volume 1
Supplement 3

XN-NF-80-19(NP)(A)
Volume 1
Supplement 3
Appendix F

XN-NF-80-19(NP)(A)
Supplement 4

Issue Date: 11/30/90

ADVANCED NUCLEAR FUELS METHODOLOGY FOR BOILING WATER REACTORS

<u>Distribution</u>

RA Copeland/US NRC (15)